



Theory of equilibration and  
aging in colloidal fluids of  
non-spherical interacting  
particles.

by

Ernesto Carlos Cortés Morales

---

Advisor:

Dr. Magdaleno Medina Noyola

September 27, 2018



# Contents

<b>1</b>	<b>Introduction</b>	<b>1</b>
<b>2</b>	<b>General Concepts.</b>	<b>7</b>
2.1	Review of the Self Consistent Generalized Langevin Equation Theory . . . . .	8
2.1.1	Historical review of the theory . . . . .	8
2.1.2	SCGLE for liquids of Brownian spherical interacting particles . . . . .	9
2.2	SCGLE theory for the dynamics of Brownian liquids of non-spherically interacting particles . . . . .	11
2.2.1	The generalized Langevin equation (GLE) formalism. . . . .	11
2.2.2	Collective description of the translational and orientational degrees of freedom. . . . .	13
2.2.3	Summary of the <i>equilibrium</i> SCGLE equations. . . . .	14
2.3	Dynamical properties of a liquid of dipolar hard spheres: Dynamically arrested diagram . . . . .	16
2.3.1	Asymptotic limit for SCGLE equations . . . . .	17
2.3.2	The dipolar hard sphere fluid . . . . .	18
<b>3</b>	<b>Non-equilibrium extension to the Self Consistent Generalized Langevin Equation Theory</b>	<b>21</b>
3.1	Non-stationary Onsager-Machlup Theory . . . . .	22
3.2	Evolution of the Non-stationary Structure Factor . . . . .	25
<b>4</b>	<b>Equilibration and aging processes for interacting Dipoles with Random Fixed Positions</b>	<b>31</b>
4.1	An illustrative example. . . . .	31
4.2	Slow Dynamics and Spin Glass transitions of a classical and disordered Heisenberg system . . . . .	33
4.3	Equilibration of the System of Interacting Dipoles with Random Fixed Positions . . . . .	34
4.4	Aging of the System of Interacting Dipoles with Random Fixed Positions . . . . .	37
4.5	Crossover from equilibration to aging: Determination of the dynamical arrested diagram . . . . .	40

---

<b>5</b>	<b>Non equilibrium phase diagrams of liquids of non-spherical interacting particles.</b>	<b>45</b>
5.1	Mathematical and numerical methodologies . . . . .	46
5.1.1	Formal solution of Eq. (3.19) . . . . .	46
5.1.2	Trajectory $(u_T(t_w), u_R(t_w))$ on the plane $(u_T, u_R)$ : three possible scenarios . . . . .	48
5.2	Illustrative solutions of the NE-SCLGE Equations. . . . .	51
5.2.1	Quenching and crushing the DHS model. . . . .	51
5.2.2	Dynamic arrest diagram of the DHS model. . . . .	53
5.3	Nonequilibrium kinetics of structural and dynamical relaxation. . . . .	54
<b>6</b>	<b>Applying the non equilibrium SCGLE approach to a model of a liquid of "Janus-like" interacting particles</b>	<b>59</b>
6.1	Detecting dynamic arrest transition for attractive angle-dependent potential. . . . .	59
6.2	The structure factors $S_{lm}(k; u_\alpha)$ , $S_{lm}^a(k)$ below the instability transition line . . . . .	64
<b>7</b>	<b>Conclusions</b>	<b>67</b>
	<b>Bibliography</b>	<b>69</b>

# Introduction

---

One of the fundamental topics that arise in the study of amorphous solid materials is the dynamical arrest state that occurs in these systems during their process of solidification. This feature is presented in numerous systems, such as gels and glasses, which are essential in many technologically specialized materials. Taking into account the literature, we can find a variety of studies, ranging from experiments, numerical simulations, and theoretical models [1,2], all with the goal of characterizing the specific mechanism involved in the dynamic arrest. As a result, two remarkable and important features emerge as universal fingerprints of these materials, namely, their inability to reach thermodynamic equilibrium within experimental times and the fact that their final properties will depend on the preparation protocol.

Among the variety of systems studied in the field of amorphous materials, colloidal amorphous solids constitute a particularly relevant category, of enormous fundamental and practical relevance in industrial sectors such as food, oil, and plastics, and as nano/micro-electronic devices for modern technologies. All these systems are formations of colloidal particles of (sub)micrometer dimensions, and provide a rich functionality (optical activity, mechanical strength, different types of magnetism, conductivity, etc.), already being a source (and increasingly becoming prominent) for advanced functional materials. It has been shown that homogeneous nano/micro particles exhibit a rich phase behavior and are able to develop amorphous structures reminiscent of atomic or molecular packing. Also, these kind of particles possess an important feature that we will study in detail in the next chapters: in order to determine the dynamical properties of a colloidal suspension it is necessary to know the full description of the translational and orientational diffusion processes when the particles are interacting among themselves through non-spherical pair potentials. Such geometrical asymmetry has long been known to be a key factor in designing molecules, supramolecular formations (e.g., surfactants, liquid crystals), or block co-polymers to enable self-assembly processes into solution-based aggregates, such as micelles, vesicles, polymersomes or sophisticated block co-polymers, as well as liquid crystalline bulk phases [3].

One of the most simple study cases of systems of particles with anisotropic interactions we can analyse is the one formed by colloidal particles that interact among themselves through a dipolar potential. There is a large number of experimental works, numerical simulations, and theoretical models of dipolar colloidal systems, of which various relevant physical properties are studied, for example, their phase diagrams such as the one presented in Figure. 1.1. From this complex phase diagram, a variety of assembled mesostructures can be seen, including crystals of unusual symmetry, gels with open network structures, particle chains and, depending on the dipole moments and particle sizes for mixtures of dipolar colloids, single-species interpenetrating networks of crosslinked chains, mixed interpenetrating networks with block-like structures, and random orientation of the particles or networks of crosslinked chains of one species sheathed by particles of the other species can be formed, just as it is observed in the snapshots (c-f) in Fig. 1.1.

Thus, the variety of structures of the systems of dipolar colloids mentioned above are used to model real systems of great technological and scientific interest, such as the so-called "Janus" particles (JPs), which are unique among the variety of nano/micro objects because they provide asymmetry and can thus generate drastically different chemical or physical properties as well as directionality within a single particle (represented pictorially in Fig 1.2). The broken symmetry offers efficient and distinctive means to target complex self-assembled materials and realize the emergence of properties inconceivable for homogeneous particles or symmetric interacting particles. Because the above properties, historically these kind of particles were named after the two-faced Roman deity Janus, and the term was first used to describe fictional spherical particles having one hemisphere hydrophilic and the other hydrophobic. Nowadays, the term is used to describe a special type of nanoparticles whose surfaces have two or more distinct physical properties. The first researcher to realize the potential and significance of such particles was the Nobel Laureate and French physicist Pierre-Giles de Gennes, who addressed this class of particles in his Nobel lecture in 1991 [5].

From the previous examples, we learn that the existence of exotic phases in the models of Janus particles are the result of the necessary consideration of both translational and orientational degrees of freedom. Observing the formation of a certain type of orientational gel it is reminiscent of the case of spherically symmetric attractive potentials, such as the particle systems with Lennard Jones type interaction. Under equilibrium conditions, it is expected that in certain thermodynamic states, and given the existence of the spinodal region, the system will be separated into two states, gas and liquid. However,

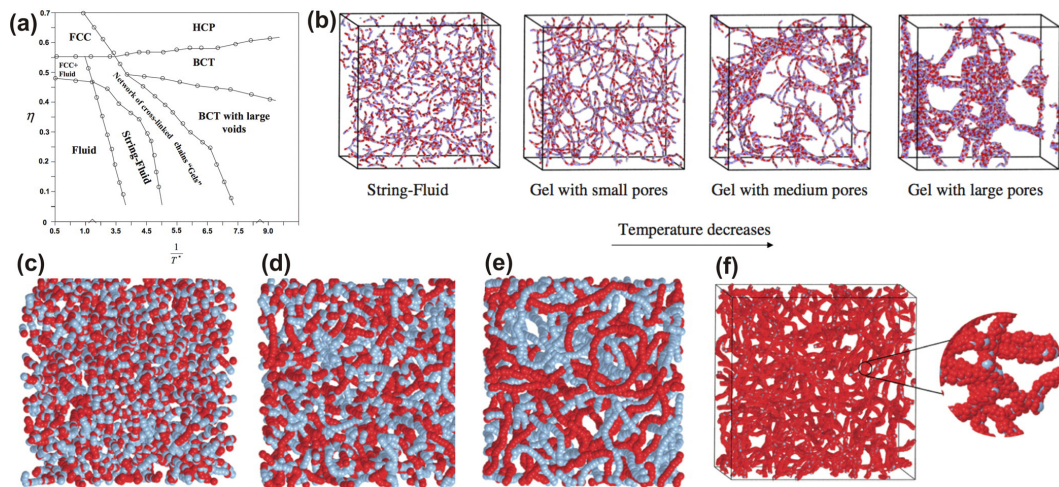


Figure 1.1: Self-assembly and phase behavior of dipolar Janus particles (JP) (a,b) and binary systems of dipolar colloids (c-f). (a) Phase diagram of dipolar Janus colloids in the packing fraction  $\eta$  vs  $T^{-1}$  plane. (b) Snapshot showing the transition from fluid to gel-like open network at  $\eta = 0.1$  as the temperature decreases, from left to right: 0.21, 0.19, 0.17, 0.15. In the bottom row, snapshots of a binary mixture of dipolar colloids are shown with percolated networks of crosslinked chains (gel): (c) Red and blue particles of slightly different size but with the same dipole momenta arranged randomly along chains upon sudden quenches from a higher temperature. (d) Red and blue particles of slightly different size but with the same dipole moment arranged in blocks along chains when the system is undergoing a slow temperature quench. See Ref. [4]

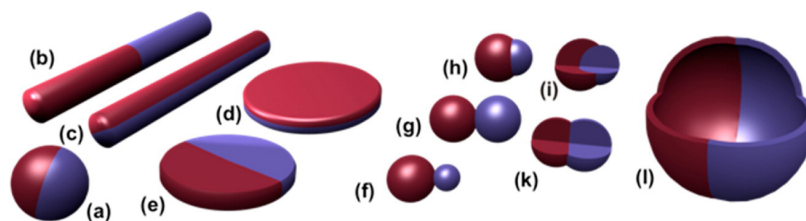


Figure 1.2: Janus particles with the following morphologies: (a) spheres, (b) and (c), two types of cylinders, and (d) and (e) disc-shaped. The next are several dumbbell-shaped particles with (f) asymmetric or snowman shape, (g) and (k) symmetric appearance, (h) attached nodes and (i) eccentric encapsulation; (l) is known as a Janus vesicle or capsule. See Ref. [3]

as shown in various experiments and simulations, if the system is brought under a suddenly temperature quench within its spinodal region, the gas-liquid separation will not take place and will remain stagnant in the formation of an amorphous solid, meaning either a physical gel, or a porous glass, depending on how low the temperature at which the system was taken. Different theoretical approaches have been used to predict this phenomenology. One of the successful theoretical framework, is the Self-Consistent Generalized Langevin Equation (SCGLE) theory in its *non equilibrium* extension. Later we will describe the historical review and the technical details of this theory, but we want to briefly show the results for the non-equilibrium processes involved in the spinodal decomposition of suddenly and deeply quenched simple fluids, as reported by Olais et al. [6]. The main result of their research is the dynamic arrest diagram shown in Fig. 1.3. The first main feature of the predicted phase diagram of attractive hard spheres is the continuity of region **III**, corresponding to the glass phase below and to the right of the curve  $T_0(\phi)$ , which contains the high-packing/ high-temperature "repulsive" glasses and the low-packing/low-temperature "attractive" glasses. For low volume fractions  $\phi$ , this liquid-glass transition penetrates the unstable region of the gas-liquid coexistence as a glass-gel transition, with the gel phase constituting region **II** of the diagram. Finally, this study associates the formation of gels with the early arrest of the growing spatial heterogeneities and its temperature dependence, described by the Cahn-Hilliard-Cook (CHC) classical linear theory of spinodal decomposition which has been shown to be a particular limit of the *non equilibrium* SCGLE theory. The previous analysis results in the recognition that indeed shallow quenches lead to full phase separation, whereas deeper quenches lead to the formation of gels.

The literature mentioned above makes one wonders if, for example the formation of complex gels in the phase diagrams of the Janus systems summarized in the Fig 1.1, are a consequence of an out-of-equilibrium phenomena, and if they can be studied with a model derived from first principles. With these questions in mind, the work described in this thesis gave rise to a theoretical tool that considers conditions of non-equilibrium in systems whose particles are non-spherically interacting: these are the focus of the present work and are being the first approach to more complex systems, such as the aforementioned Janus particles, to name only one kind of complex systems.

This thesis is then structured as follows: in chapter 2 we establish the previous works and the foundations of the development of the SCGLE theory, with specially attention on the variant of the theory that treats *non spherical*-kind of potentials, showing as an example the asymptotical dynamical properties of a liquid of interacting dipolar hard spheres. The main result of this work is

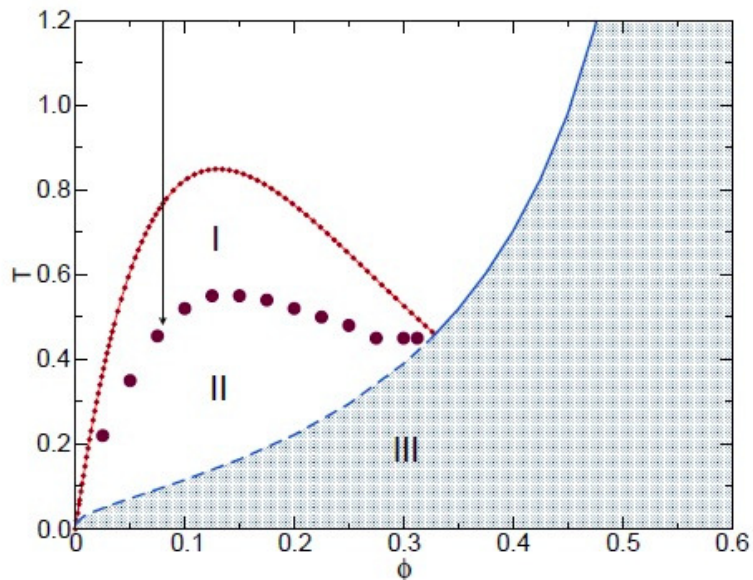


Figure 1.3: Summary of the non-equilibrium volume fraction  $\phi$ -vs- $T$  phase diagram predicted in Ref. [6] for a hard sphere system (HS) with an attractive Yukawa interaction liquid. At high temperatures and densities, compressing or cooling this system drives it through the transition (blue solid line) to states of non equilibrium repulsive glasses. At intermediate and low densities and temperatures the NE-SCGLE theory predicts that (i) the spinodal line  $T_s(\phi)$  (red dashed line) is a frontier between equilibrium and non-ergodic states, (ii) that the liquid-glass transition line penetrates inside the spinodal region as a glass-glass transition line (dashed blue line), (iii) that between these two dynamic arrest lines there exists a crossover temperature  $T_0(\phi)$  (circles), above which the unstable homogeneous liquid fully phase separates (region **I**), and below which it forms gels (region **II**), and (iv) that below the composed (solid and dashed) blue line there exists a continuous region of porous repulsive glasses (region **III**).

presented in chapter 3, which contains the theoretical framework of the **non equilibrium** extension of the non spherical SCGLE theory starting with the Onsager-Machlup abstract formalism that is later applied to a liquid of non-spherical interacting particles via the local density and general equations are obtained for the time-dependent structure factor in the case when we perform in the system a suddenly instantaneous temperature quench. We continue in chapter 4 applying the derived formalism to describe the slow orientational dynamics as well the equilibration and aging of a system of classical dipolar hard-spheres with quenched positional disorder near to its "spin-glass" transitions. In order to describe the classical dipolar system we explore in detail the full translational and rotational non equilibrium self-consistent equations in chapter 5, and the numerical methodology for their solutions. In chapter 6 a system of angle-dependent attractive interacting colloidal particles is analysed, in order to get a phase diagram of "Janus-like" colloidal particles, using the non equilibrium theory developed in previous chapters. Finally, this work is closed with the final thoughts and main conclusions, as well as future work in chapter 7.

# General Concepts.

---

## Contents

---

<b>2.1</b>	<b>Review of the Self Consistent Generalized Langevin Equation Theory . . . . .</b>	<b>8</b>
2.1.1	Historical review of the theory . . . . .	8
2.1.2	SCGLE for liquids of Brownian spherical interacting particles . . . . .	9
<b>2.2</b>	<b>SCGLE theory for the dynamics of Brownian liquids of non-spherically interacting particles . . . . .</b>	<b>11</b>
2.2.1	The generalized Langevin equation (GLE) formalism. . . . .	11
2.2.2	Collective description of the translational and orientational degrees of freedom. . . . .	13
2.2.3	Summary of the <i>equilibrium</i> SCGLE equations. . . . .	14
<b>2.3</b>	<b>Dynamical properties of a liquid of dipolar hard spheres: Dynamically arrested diagram . . . . .</b>	<b>16</b>
2.3.1	Asymptotic limit for SCGLE equations . . . . .	17
2.3.2	The dipolar hard sphere fluid . . . . .	18

---

In this chapter, we present an overview of the most general aspects concerning the theoretical approach which describes the *equilibrium* collective and self dynamics of colloidal suspensions conformed by particles interacting through non-spherical potentials. The relevant physical properties are defined, and the appropriate language to be employed is introduced in the description and characterization of the structural and dynamical properties of non-spherical colloidal fluids. We refer the reader to several articles with original references and we will assume a minimum basic background in liquids theory in order to ease (some times by direct comparison) the comprehension of the discourse presented here.

## 2.1 Review of the Self Consistent Generalized Langevin Equation Theory

### 2.1.1 Historical review of the theory

A current open problem in the soft matter field is the search of a satisfactory model for the microscopic description of complex colloid dynamics, while retaining a general formalism practical enough to make only some approximations and to take into account some microscopic parameters of physical significance.

The last 30 years have seen several important theoretical developments for many particular systems and boundary conditions of said systems. Of special importance are the theories where diffusion phenomena are measured, via the Brownian motion of individual particles in the colloidal suspensions; this is known as self-diffusion phenomena. There are also collective diffusion experiments where the relaxation of the local concentration fluctuations are measured, usually via some generalized diffusion coefficient, i. e. the van Hove function  $G(r, t)$  of the colloidal Brownian fluid, or its Fourier transform, the intermediate scattering function  $F(k, t)$  which contains all of the dynamic information of the fluid in equilibrium. For this reason, a complete theoretical model that describes dynamical properties should aim to the correct calculation and understanding of the scattering function.

This work will focus on the dynamic properties of a system formed by  $N$  non-spherical interacting particles in the abstract framework now known as the Self-Consistent Generalized Langevin Equation theory (SCGLE): its first version was detailed in the work of L. Yeomans-Reina and M. Medina-Noyola, published in 2001. Before this work, several steps were made in order to reach a full working form of the theory by the same research group, led by M. Medina-Noyola and detailed in the timeline 2.1. In the following years, improvements have been made, as well as applications to several physical colloidal systems with a variety of dynamical properties and even a non-equilibrium version of the SCGLE theory. The advances relevant to this work are pictured in 2.1; however, considerable literature has been published regarding the SCGLE theory that is out of the scope of the present work and hence will not be mentioned.

**2.1.2 SCGLE for liquids of Brownian spherical interacting particles**

The SCGLE theory is a framework that allows for the calculation of  $F(k, t)$  and the self diffusion coefficient  $F_s(k, t)$ , given that the effective interaction pair potential between particles  $u(r)$  is known, as well as any of its static structural properties, such as the static structure factor  $S(k)$  or the radial distribution function  $g(r)$ . This allows for the application of the theory to a wide number of simple and complex system.

In its first version (2002), the SCGLE theory was applied numerically to describe the collective dynamics of the two dimensional repulsive Yukawa Brownian fluid: Brownian dynamic simulations were performed to compare with the theoretical predictions for the intermediate scattering function  $F(k, t)$  and the self-scattering function  $F_s(k, t)$ ; the results show a good agreement between theory and simulations [7].

The following step in the development of the SCGLE theory was the extension of the calculation of dynamic properties to colloidal mixtures (2005), since the mono-disperse case is a very idealized condition rarely found in natural circumstances. The applications of colloidal mixtures are everywhere: in industrial, natural and chemical processes. It was then a straightforward direction to go for the theory: to propose a description of the intermediate and long-time properties of colloidal mixtures. Once the exact memory-function expressions for the partial intermediate scattering function of a colloidal mixture were derived, the Langevin equation approach was used, while noting that in this particular work, hydrodynamic interactions were not taken into account, and it is not applicable to hard-sphere potentials due to the restrictions used here of continuous pairwise interactions. This model is then applied to a binary mixture of Brownian particles interacting through a hard-core pair potential plus a repulsive Yukawa tail [8]. Comparisons are made of the intermediate and self scattering functions between the mono-disperse system and the functions for each component of the mixture, with good agreements.

In 2007, the SCGLE model was found to predict the phenomena of dynamic arrest in disperse colloidal systems, similar to the well-known Mode Coupling Theory (MCT) developed for that specific purpose. The full numerical solution of the SCGLE provides a route to the location of the fluid-glass transition in the space of the macroscopic parameters of the system, given that the inter particle forces (i.e., their potential of interaction) are known. This is useful for the development of criteria to predict wheter a system in any

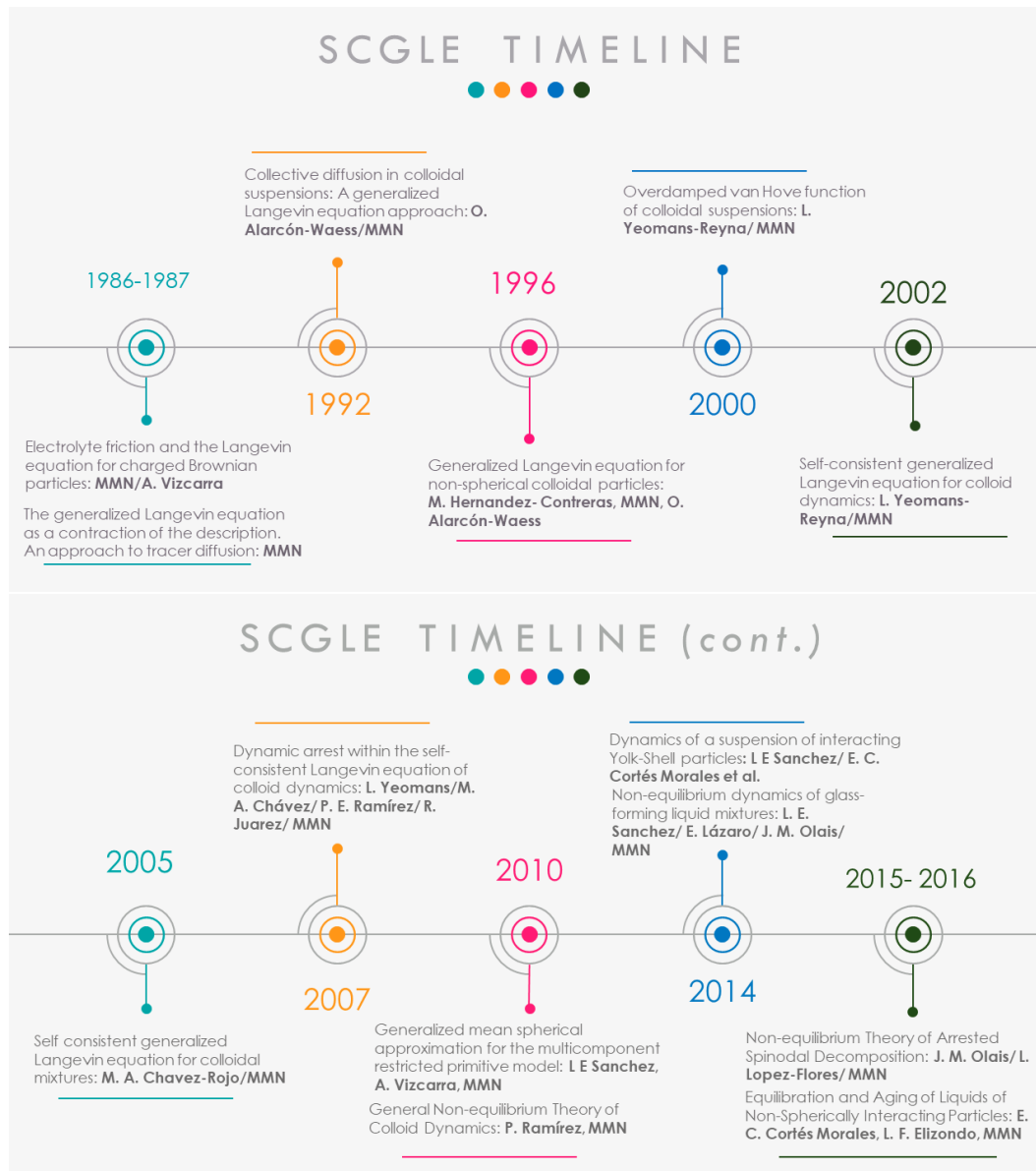


Figure 2.1: A timeline by year, authors and titles of research papers of significance to this thesis work.

given macroscopic conditions, will reach an ergodic or a dynamically-arrested state. Predictions are made with this model for the hard sphere system with the Percus Yevick approximation for the static structure factor  $S(k)$  and for the charged sphere system modelled via a repulsive screened Coulomb potential in the HNC (hypernetted chain) approximation. The results are in good agreement with the experimental data available [9].

So far, our review has covered only systems of HS particles, so the SCGLE equations are written for any radially symmetric system in the equilibrium. In the following section we will see the details of the non-equilibrium version of the SCGLE theory and its application to the non-spherical case of a system of interacting particles.

## **2.2 SCGLE theory for the dynamics of Brownian liquids of non-spherically interacting particles**

In this section we briefly describe the extension of the equilibrium SCGLE theory to the description of the dynamics of liquids formed by non-spherical particles, firstly developed by Elizondo-Aguilera et al. [10]. We will briefly review the generalized Langevin equation as a general and fundamental formalism, then define the main properties involved in the description of the dynamics of liquids formed by non-spherical particles, and then will summarize the time-evolution equations that result from this application of the GLE formalism, and which constitute the essence of the equilibrium SCGLE theory. After this review, we shall proceed in the next section to develop the extension of the SCGLE theory to the case with non-equilibrium conditions.

### **2.2.1 The generalized Langevin equation (GLE) formalism.**

The GLE formalism describes the dynamics of the thermal fluctuations  $\delta a_i(t)$  ( $\equiv a_i(t) - a_i^{eq}$ ) of the instantaneous value of the macroscopic variables  $a_i(t)$  ( $i = 1, 2, \dots, \nu$ ), around their equilibrium value  $a_i^{eq}$ . It has the structure of a general linear stochastic equation with additive noise for the vector  $\delta \mathbf{a}(t) =$

$[\delta a_1(t), \delta a_2(t), \dots, \delta a_\nu(t)]^\dagger$  (with the dagger indicating transpose), namely,

$$\frac{d\delta\mathbf{a}(t)}{dt} = -\omega\chi^{-1}\delta\mathbf{a}(t) - \int_0^t L(t-t')\chi^{-1}\delta\mathbf{a}(t')dt' + \mathbf{f}(t). \quad (2.1)$$

In this equation,  $\chi$  is the matrix of static correlations,  $\chi_{ij} \equiv \langle \delta a_i(0)\delta a_j^*(0) \rangle$ ,  $\omega$  is an antihermitian matrix,  $\omega_{ij} = -\omega_{ji}^* \equiv \langle \delta \dot{a}_i(0)\delta a_j^*(0) \rangle$  (with  $\langle \dots \rangle$  denoting the average over the initial values  $\delta\mathbf{a}(0)$ ). The matrix  $L(t)$  is determined by the fluctuation-dissipation relation  $L_{ij}(t) = \overline{f_i(t)f_j^*(0)}$ , where  $f_i(t)$  is the  $i$ th component of the vector of random forces  $\mathbf{f}(t)$  and the overline denotes the average over the realizations of  $\mathbf{f}(t)$ . Besides the selection rules imposed by these symmetry properties of the matrices  $\chi$ ,  $\omega$ , and  $L(t)$ , other selection rules may be imposed by other symmetry conditions. As shown in [11], if the variables  $a_i(t)$  have a definite parity upon time reversal,  $a_i(-t) = \lambda_i a_i(t)$  with  $\lambda_i = 1$  or  $-1$ , then  $\omega_{ij} = -\lambda_i \lambda_j \omega_{ij}$  and  $L_{ij}(t) = \lambda_i \lambda_j L_{ij}(t)$ .

Widely used in the early description of thermal fluctuations in simple liquids [12, 13], the generalized Langevin equation (GLE) was strongly associated with the Zwanzig-Mori projection operator formalism [14–16]. This association, however, obscures the fact that in reality the mathematical structure of the GLE is not a consequence of the hamiltonian basis of its Zwanzig-Mori's derivation, nor its validity is restricted to the description of fluctuations around the thermodynamic equilibrium state (as Zwanzig-Mori's derivation is). Instead, it is not difficult to discover [11] that the mathematical attribute of stationarity is a necessary and sufficient condition for the stochastic time-evolution equation of the fluctuations to have the structure of Eq.(2.1). Such an alternative point of view originates from the Onsager and Machlup theory of thermal fluctuations [17, 18] which also extends the fundamental (mathematical and physical) framework underlying Langevin's proposal of his celebrated equation [19].

The Onsager and Machlup theory constitutes a general model of equilibrium fluctuations. Including memory effects in this model is the phenomenological route to the generalized Langevin equation formalism [13]. One important feature in this line of reasoning is its remarkable flexibility. Thus, since the essence of this formalism is the mathematical condition of stationarity [11], and not necessarily the physical condition of thermodynamic equilibrium, it is in principle applicable to describe non-equilibrium stationary states ( $SS$ ) of matter, as illustrated in the following section. In this section, however, we only consider its application to conventional equilibrium conditions.

### 2.2.2 Collective description of the translational and orientational degrees of freedom.

Let us start by considering a liquid formed by  $N$  identical non-spherical colloidal particles in a volume  $V$  [10], each having a mass  $m$  and an inertia tensor  $\mathbf{I}$ . The translational degrees of freedom are described by the vectors  $\mathbf{r}^N \equiv (\mathbf{r}_1, \dots, \mathbf{r}_N)$  and  $\mathbf{p}^N \equiv (\mathbf{p}_1, \dots, \mathbf{p}_N)$ , where  $\mathbf{r}_n$  denotes the center-of-mass position vector of the  $n$ th-particle and  $\mathbf{p}_n \equiv m d\mathbf{r}_n/dt = m\mathbf{v}_n(t)$  is the associated linear momentum. Similarly, the orientational degrees of freedom are described by the abstract vectors  $\mathbf{\Omega}^N \equiv (\mathbf{\Omega}_1, \dots, \mathbf{\Omega}_N)$  and  $\mathbf{L}^N \equiv (\mathbf{L}_1, \dots, \mathbf{L}_N)$ , where  $\mathbf{\Omega}_n$  denotes the Euler angles which specify the orientation of the  $n$ th molecule, and  $\mathbf{L}_n = \mathbf{I}(\mathbf{\Omega}_n)\boldsymbol{\omega}_n$  is the corresponding angular momentum, so that  $\boldsymbol{\omega}_n$  denotes the angular velocity. Let us now assume that the potential energy  $U(\mathbf{r}^N, \mathbf{\Omega}^N)$  of the interparticle interactions is pairwise additive, i.e., that

$$U(\mathbf{r}^N, \mathbf{\Omega}^N) = \sum_{n,n'=1}^N u(\mathbf{r}_n, \mathbf{r}_{n'}; \mathbf{\Omega}_n, \mathbf{\Omega}_{n'}), \quad (2.2)$$

where  $u(\mathbf{r}_n, \mathbf{r}_{n'}; \mathbf{\Omega}_n, \mathbf{\Omega}_{n'})$  is the interaction potential between particles  $n$  and  $n'$ . In the particular case of axially-symmetric particles, that we bear in mind here, the third Euler angle is redundant, hence  $\mathbf{\Omega}_n = \mathbf{\Omega}_n(\theta_n, \phi_n)$ .

The most basic observable in terms of which we want to describe the dynamical properties of a non-spherical colloidal system is the time dependent microscopic one-particle density

$$n(\mathbf{r}, \mathbf{\Omega}; t) \equiv (1/\sqrt{N}) \sum_{n=1}^N \delta(\mathbf{r} - \mathbf{r}_n(t)) \delta(\mathbf{\Omega} - \mathbf{\Omega}_n(t)). \quad (2.3)$$

Given that the angular dependent function  $\mathbf{\Omega} = \mathbf{\Omega}(\theta, \phi)$ , any function  $f(\mathbf{r}, \mathbf{\Omega})$  can be expanded with respect to plane waves and spherical harmonics as

$$f(\mathbf{r}, \mathbf{\Omega}) = \frac{1}{V} \frac{1}{\sqrt{4\pi}} \int d\mathbf{k} \sum_{lm} (i)^l f_{lm}(\mathbf{k}) e^{-i\mathbf{k}\cdot\mathbf{r}} Y_{lm}^*(\mathbf{\Omega}) \quad (2.4)$$

where

$$f_{lm}(\mathbf{k}) = \sqrt{4\pi} i^l \int_V d\mathbf{r} \int d\mathbf{\Omega} f(\mathbf{r}, \mathbf{\Omega}) e^{-i\mathbf{k}\cdot\mathbf{r}} Y_{lm}(\mathbf{\Omega}). \quad (2.5)$$

Thus, using Eq. (2.3) in (2.4) and (2.5), we may define the *so-called* tensorial density modes

$$n_{lm}(\mathbf{k}, t) = \sqrt{\frac{4\pi}{N}} i^l \sum_{n=1}^N e^{i\mathbf{k}\cdot\mathbf{r}_n(t)} Y_{lm}(\mathbf{\Omega}_n(t)), \quad (2.6)$$

and hence, we can define the following two-time correlation functions,

$$\begin{aligned} F_{lm;l'm'}(\mathbf{k}, \tau; t) &\equiv \langle \delta n_{lm}^*(\mathbf{k}, t + \tau) \delta n_{l'm'}(\mathbf{k}, t) \rangle \\ &= \frac{4\pi}{N} i^{l-l'} \sum_{n \neq n'}^N \left\langle e^{i\mathbf{k} \cdot [\mathbf{r}_n(t+\tau) - \mathbf{r}_{n'}(t)]} Y_{lm}^*(\boldsymbol{\Omega}_n(t + \tau)) Y_{l'm'}(\boldsymbol{\Omega}_{n'}(t)) \right\rangle, \end{aligned} \quad (2.7)$$

where  $\delta n_{lm}(\mathbf{k}, t) \equiv n_{lm}(\mathbf{k}, t) - \langle n_{lm}(\mathbf{k}, t) \rangle$ .

We also define for completeness the self components

$$n_{lm}^S(\mathbf{k}, t) \equiv \sqrt{4\pi} i^l e^{i\mathbf{k} \cdot \mathbf{r}_T(t)} Y_{lm}(\boldsymbol{\Omega}_T(t)), \quad (2.8)$$

and the corresponding two-time correlation functions

$$\begin{aligned} F_{lm;l'm'}^S(\mathbf{k}, \tau; t) &\equiv \langle n_{lm}^{S*}(\mathbf{k}, t + \tau) n_{l'm'}^S(\mathbf{k}, t) \rangle \\ &= 4\pi i^{l-l'} \left\langle e^{i\mathbf{k} \cdot [\mathbf{r}_T(t+\tau) - \mathbf{r}_T(t)]} Y_{lm}(\boldsymbol{\Omega}_T(t + \tau)) Y_{l'm'}(\boldsymbol{\Omega}_T(t)) \right\rangle, \end{aligned} \quad (2.9)$$

where  $\mathbf{r}_T(t)$  denotes the position of the center of mass of *any* of the particles at time  $t$  and  $\boldsymbol{\Omega}_T(t)$  describes its orientation. As indicated before, we will refer to  $\tau$  as the delay (or *correlation*) time, whereas for  $t$  we will refer to the *evolution* time.

The equal-time value of these correlation functions are  $F_{lm;l'm'}(\mathbf{k}, \tau = 0; t) = S_{lm;l'm'}(\mathbf{k}; t)$  and  $F_{lm;l'm'}^S(\mathbf{k}, \tau = 0; t) = 1$  where  $S_{lm;l'm'}(\mathbf{k}; t)$  are the tensorial components of the static structure factor  $S(\mathbf{k}, \boldsymbol{\Omega}, \boldsymbol{\Omega}'; t)$ . Of course, the dependence of these quantities on the evolution time  $t$  is only relevant if the state of the system is non-stationary. Under the condition of thermodynamic equilibrium,  $F_{lm;l'm'}(\mathbf{k}, \tau; t)$ ,  $F_{lm;l'm'}^S(\mathbf{k}, \tau; t)$ , and  $S_{lm;l'm'}(\mathbf{k}; t)$  cannot depend on  $t$ , and we should denote them as  $F_{lm;l'm'}^{(eq)}(\mathbf{k}, \tau)$ ,  $F_{lm;l'm'}^{S(eq)}(\mathbf{k}, \tau)$ , and  $S_{lm;l'm'}^{(eq)}(\mathbf{k})$ .

### 2.2.3 Summary of the *equilibrium* SCGLE equations.

Applying the GLE formalism described in subsection 2.2.1, to the dynamical variables  $n_{lm}(\mathbf{k}, t)$  and  $n_{lm}^S(\mathbf{k}, t)$  defined in Subsection 2.2.2, one can derive exact memory function equations for  $F_{lm;l'm'}^{(eq)}(\mathbf{k}, \tau)$  and  $F_{lm;l'm'}^{S(eq)}(\mathbf{k}, \tau)$  [10]; These memory function equations require the independent determination of the corresponding self and collective memory functions. In a manner similar to the spherical case, the simple Vineyard-like approximate closure relations for these

memory functions convert the originally exact equations into a closed self-consistent system of approximate equations for these dynamic properties [10]. The resulting approximate system of equations constitute the extension to liquids of particles interacting through non-spherical pair potentials, of the *equilibrium* SCGLE theory of the dynamic properties of liquids of spherical particles. These extended equations only involve an external input the corresponding projections  $S_{lm;l'm'}^{(eq)}(\mathbf{k})$  of the *equilibrium* static structure factor. Although for the rest of this section we shall only refer to these equilibrium structural properties, for notational convenience in the rest of this work we shall not write the label (*eq*).

Let us thus summarize the set of self-consistent equations that constitute the *equilibrium* SCGLE theory for a Brownian liquid of axially-symmetric non spherical particles. In the simplest version of our theory (we refer the reader to Ref. [10] for details), these equations involve only the diagonal elements  $F_{lm}(\mathbf{k}, \tau) \equiv F_{lm;lm}(\mathbf{k}, \tau)$  and  $F_{lm}^S(\mathbf{k}, \tau) \equiv F_{lm;lm}^S(\mathbf{k}, \tau)$ , and are written in terms of the corresponding Laplace transforms  $F_{lm}(\mathbf{k}, z)$  and  $F_{lm}^S(\mathbf{k}, z)$  as

$$F_{lm}(k, z) = \frac{S_{lm}(k)}{z + \frac{k^2 D_T^0 S_{lm}^{-1}(k)}{1 + \Delta\zeta_T^*(z)\lambda_T^{(lm)}(k)} + \frac{l(l+1)D_R^0 S_{lm}^{-1}(k)}{1 + \Delta\zeta_R^*(z)\lambda_R^{(lm)}(k)}} \quad (2.10)$$

and

$$F_{lm}^S(k, z) = \frac{1}{z + \frac{k^2 D_T^0}{1 + \Delta\zeta_T^*(z)\lambda_T^{(lm)}(k)} + \frac{l(l+1)D_R^0}{1 + \Delta\zeta_R^*(z)\lambda_R^{(lm)}(k)}}. \quad (2.11)$$

In equations (??),  $D_R^0$  is the rotational free-diffusion coefficient, and  $D_T^0$  is the center-of-mass translational free-diffusion coefficient, whereas the functions  $\lambda_T^{(lm)}(k)$  and  $\lambda_R^{(lm)}(k)$  are defined as  $\lambda_T^{(lm)}(k) = 1/[1 + (k/k_c)^2]$  and  $\lambda_R^{(lm)}(k) = 1$ , where  $k_c = \alpha \times k_{max}$ , with  $k_{max}$  being the position of the main peak of  $S_{00}(k)$  and  $\alpha = 1.305$ . This ensures that for radially-symmetric interactions, we recover the original theory describing liquids of soft and hard spheres [20].

On the other hand, within the well defined approximations discussed in appendix A of Ref [10], the functions  $\Delta\zeta_\alpha^*(\tau)$  ( $\alpha = T, R$ ) may be written as

$$\Delta\zeta_T^*(\tau) = \frac{1}{3} \frac{D_T^0}{(2\pi)^{3n}} \int d\mathbf{k} k^2 \sum_l [2l+1] [1 - S_{l0}^{-1}(k)]^2 F_{l0}^S(k; \tau) F_{l0}(k; \tau) \quad (2.12)$$

and

$$\Delta\zeta_R^*(\tau) = \frac{1}{2} \frac{D_R^0}{(2\pi)^3} \frac{n}{4} \frac{1}{(4\pi)^2} \int d\mathbf{k} \sum_{l,m} [2l+1] h_{l0}^2(k) [A_{l;0m}]^2 [S_{lm}^{-1}(k)]^2 \quad (2.13)$$

$$\times F_{lm}^S(k; \tau) F_{lm}(k; \tau)$$

where  $h_{lm}(k)$  denotes the diagonal  $k$ -frame projections of the total correlation function  $h(\mathbf{k}, \boldsymbol{\Omega}, \boldsymbol{\Omega}')$ , i.e.,  $h_{lm}(k)$  is related to  $S_{lm}(k)$  by  $S_{lm}(k) = 1 + (n/4\pi)h_{lm}(k)$ , and  $n = N/V$  is the number density. Finally,  $A_{l;mm'} \equiv [C_{lm}^+ \delta_{m+1,m'} + C_{lm}^- \delta_{m-1,m'}]$  and  $C_{lm}^\pm \equiv \sqrt{(l \mp m)(l \pm m + 1)}$ .

Let us mention that, in order to obtain the closed set of eqs. (2.10)-(2.13) involving the functions  $F_{lm}(k, \tau)$ ,  $F_{lm}^S(k, \tau)$ ,  $\Delta\zeta_T^*(\tau)$  and  $\Delta\zeta_R^*(\tau)$ , we have introduced simple first-order Vineyard-like approximations, connecting the collective and self memory kernels for both translational and rotational dynamics (see eq. 42 in Ref. [10]). In turn, the functions  $\Delta\zeta_T^*(\tau)$  and  $\Delta\zeta_R^*(\tau)$  are, respectively, the translational and rotational memory kernels for the tracer diffusion, which can also be obtained within the GLE formalism [21]. For the main details in determining eqs. (2.12) and (2.13) the reader is referred to the appendix of Ref. [10] and the references therein.

Thus, equations (2.10)-(2.13) constitute the equilibrium non spherical version of the SCGLE theory, whose solution provides the full time-evolution of the dynamic correlation functions  $F_{lm}(k; \tau)$  and  $F_{lm}^S(k; \tau)$  and of the memory functions  $\Delta\zeta_\alpha^*(\tau)$ .

## 2.3 Dynamical properties of a liquid of dipolar hard spheres: Dynamically arrested diagram

The complete solution of the self-consistent system of equations discussed above provides the full wave-vector and time dependence of the generalized correlators  $F_{lm}(k; t)$  and  $F_{lm}^S(k; t)$ . Thus, a detailed description of the slow dynamics of a given system may be realized by solving Eqs. (2.10)-(2.13) for every relevant value of  $l$  and  $m$  (in many cases, as in the example described below, the values for  $l$  and  $m$  are restricted due to symmetry considerations imposed by the system itself). Under some circumstances, however, one may only be interested in identifying and locating the regions of the different ergodic or non ergodic phases involving the translational and orientational de-

degrees of freedom of our system in its state space. For this purpose it is possible to derive from the full SCGLE equations the so-called bifurcation equations which allow us to obtain the dynamic arrest diagram in a similar fashion as in the spherical case. In this chapter we first derive these bifurcation equations and we then apply them to a particular system, namely, a dipolar hard sphere fluid. The idea is only to illustrate the applicability of our theory in a simple but non-trivial exercise, that can be contrasted with the corresponding results previously obtained by MCT [22].

### 2.3.1 Asymptotic limit for SCGLE equations

Equations (2.10)-(2.13) described in the previous section may be numerically solved using standard methods once the projections  $S_{lm}(k)$  of the static structure factor are provided. Under some circumstances, however, one may be only be interested in identifying and locating the regions in state space that correspond to the various possible ergodic or non ergodic phases involving the translational and orientational degrees of freedom of a given system. For this purpose it is possible to derive from the full SCGLE equations the so-called bifurcation equations, i.e., the equations for the long-time stationary solutions of equations (2.10)-(2.13). These are written in terms of the non-ergodicity parameters defined as

$$f_{lm}(k) \equiv \lim_{\tau \rightarrow \infty} \frac{F_{lm}(k; \tau)}{S_{lm}(k)}, \quad (2.14)$$

$$f_{lm}^S(k) \equiv \lim_{\tau \rightarrow \infty} F_{lm}^S(k; \tau), \quad (2.15)$$

and

$$\Delta\zeta_\alpha^{*(\infty)} \equiv \lim_{\tau \rightarrow \infty} \Delta\zeta_\alpha^*(\tau), \quad (2.16)$$

with  $\alpha = T, R$ . The simplest manner to determine these asymptotic solutions is to take the long-time limit of equations (2.10)-(2.13), leading to a system of coupled equations for  $f_{lm}(k)$ ,  $f_{lm}^S(k)$ , and  $\Delta\zeta_\alpha^{*(\infty)}$ .

It is not difficult to show that the resulting equations can be written as

$$f_{lm}(k) = \frac{[S_{lm}(k)] \lambda_T^{(lm)}(k) \lambda_R^{(lm)}(k)}{S_{lm}(k) \lambda_T^{(lm)}(k) \lambda_R^{(lm)}(k) + k^2 \gamma_T \lambda_R^{(lm)}(k) + l(l+1) \gamma_R \lambda_T^{(lm)}(k)} \quad (2.17)$$

and

$$f_{lm}^S(k) = \frac{\lambda_T^{(lm)}(k) \lambda_R^{(lm)}(k)}{\lambda_T^{(lm)}(k) \lambda_R^{(lm)}(k) + k^2 \gamma_T \lambda_R^{(lm)}(k) + l(l+1) \gamma_R \lambda_T^{(lm)}(k)}, \quad (2.18)$$

where the dynamic order parameters  $\gamma_T$  and  $\gamma_R$ , are defined as

$$\gamma_\alpha \equiv \frac{D_\alpha^0}{\Delta\zeta_\alpha^{*(\infty)}}, \quad (2.19)$$

are determined from the solution of

$$\frac{1}{\gamma_T} = \frac{1}{6\pi^2 n} \int_0^\infty dk k^4 \sum_l [2l+1] [1 - S_{l0}^{-1}(k)]^2 S_{l0}(k) f_{l0}^S(k) f_{l0}(k), \quad (2.20)$$

and

$$\frac{1}{\gamma_R} = \frac{1}{16\pi^2 n} \int_0^\infty dk k^2 \sum_{lm} [2l+1] [S_{l0}(k) - 1]^2 S_{lm}^{-1}(k) f_{lm}^S(k) f_{lm}(k) A_{l;0m}^2. \quad (2.21)$$

As discussed in Ref. [10], fully ergodic states are described by the condition that the non-ergodicity parameters (i.e.,  $f_{lm}(k)$ ,  $f_{lm}^S(k)$ , and  $\Delta\zeta_\alpha^{*(\infty)}$ ) are all zero and hence, the dynamic order parameters  $\gamma_T$  and  $\gamma_R$  are both infinite. Any other possible solution for these bifurcation equations indicate total or partial loss of ergodicity. Thus,  $\gamma_T$  and  $\gamma_R$  finite indicate full dynamic arrest whereas  $\gamma_T$  finite and  $\gamma_R = \infty$  correspond to the mixed state in which the translational degrees of freedom are dynamically arrested but not the orientational degrees of freedom.

### 2.3.2 The dipolar hard sphere fluid

As a simple illustration on the use of the bifurcation equations (Eqs. (2.20) - (2.21)) to determine a dynamic arrest diagram, let us these equations for a particular system, namely, a monodisperse fluid of dipolar hard spheres (DHS). This system consists of  $N$ -identical hard spheres with diameter  $d$  and dipolar momentum  $\boldsymbol{\mu}_n$ , where  $|\boldsymbol{\mu}_n| = \mu$  for all  $n$ . Besides the hardcore interaction, the pairwise potential also includes a dipolar term given by

$$U_{dip}(\mathbf{r}^N, \boldsymbol{\Omega}^N) = \mu^2 \sum_{n \neq n'} |\mathbf{r}_n - \mathbf{r}_{n'}|^{-5} [(\mathbf{r}_n - \mathbf{r}_{n'})^2 (\mathbf{e}_n \cdot \mathbf{e}_{n'}) - 3((\mathbf{r}_n - \mathbf{r}_{n'}) \cdot \mathbf{e}_n)((\mathbf{r}_n - \mathbf{r}_{n'}) \cdot \mathbf{e}_{n'})], \quad (2.22)$$

where the unit vector  $\mathbf{e}_n \equiv \boldsymbol{\mu}_n/\mu$  pointing in the direction of the dipole  $\boldsymbol{\mu}_n$  describes the orientation of the  $n$ th particle, also denoted as  $\boldsymbol{\Omega}_n$ .

In Ref. [23], the external determination of the static structure factor  $S(\mathbf{k}, \boldsymbol{\Omega}, \boldsymbol{\Omega}')$ , was provided by Wertheim's solution using the Mean Spherical Approximation (MSA). The details of the determination of the resulting structure factor,

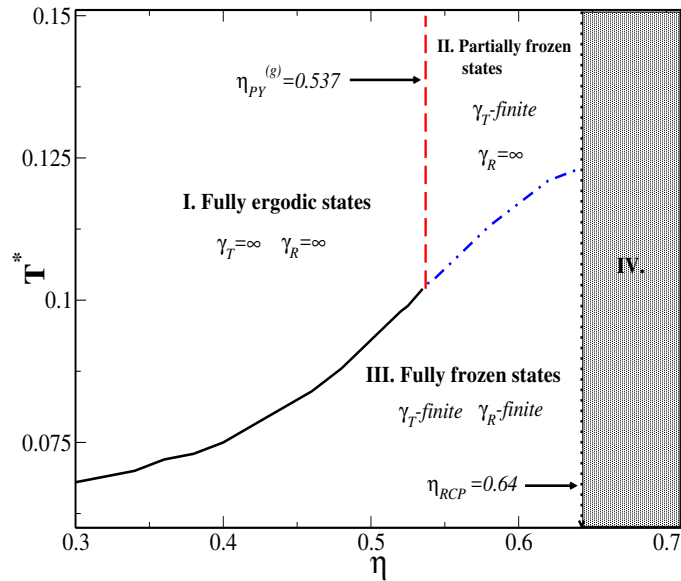


Figure 2.2: Phase diagram for the liquid and glassy states of the dipolar hard-sphere system. The corresponding translational arrest lines (dashed blue) match at a volume fraction  $\eta \approx 0.51$  calibrating the parameter  $\alpha$  for the interpolating function  $\lambda_T^{lm}(k)$  to the value  $\alpha = 1.941$ .

whose only non zero projections are  $S_{00}(k)$ ,  $S_{10}(k)$  and  $S_{11}(k)$ , can be consulted in appendix E of reference [22]. This information, evaluated at a given point  $(\eta, T^*)$  in the phase space spanned by the volume fraction  $\eta \equiv \frac{\pi}{6}nd^3$  and the scaled temperature  $T^* \equiv d^3/\mu^2\beta$ , was then employed in Eqs. (2.20) - (2.21), whose solution are the values  $\gamma_T(\eta, T^*)$  and  $\gamma_R(\eta, T^*)$  of the dynamic order parameters at that state point, which determine the expected dynamic state of the system at that particular state point  $(\eta, T^*)$ . Scanning in this manner the full state space, in Ref. [10] the regions of fully ergodic, fully arrested, and dynamically mixed states were determined.

The results of these calculations are summarized in the dynamic arrest diagram of Fig. 4.5, where the state space can be partitioned in four distinct regions depending on the packing fraction and on the scaled temperature. There is a fluid fully-ergodic region (I) delimited by two different phase boundaries. Thus, fixing a point in this region, the control parameters may be modified to induce two type of transitions. One of these transitions drives the system into a mixed state (II) where the translational degrees of freedom (TDF) freeze, whereas orientational degrees of freedom (ODF) remain ergodic (notice that this transition occurs at a volume fraction  $\eta_{PY}^{(g)} = 0.537$  which coincides with

the SCGLE prediction for the glass transition of the hard sphere fluid using the Percus Yevick approximation). Another possibility may be observed, for example, by lowering the temperature. This drive the system into a fully non-ergodic phase (**II**), where both TDF and ODF freezes in a glassy state. Finally, another type of transition is observed by fixing a different point in the mixed region (**II**). The ODF can also be freezed by lowering the temperature. Finally, we notice that we have used the packing fraction  $\eta_{rcp} = 0.64$  of the random close packing as a *cutoff* to exclude the non-physical scenarios, the region (**IV**).

In conclusion, the tools developed by Elizondo *et al* [10] were capable of accurately describe the *equilibrium* scenario of translational and rotational dynamics of Brownian liquids formed by particles that interact through non-spherically symmetric pairwise potentials. However, one of the expectations stated in [10] was to describe aging phenomena on systems involving non-spherically symmetric interactions, as being done for liquids formed by spherical particles. What follows in the next Chapter is the realization of that idea that was the main result of my Doctoral period.

# Non-equilibrium extension to the Self Consistent Generalized Langevin Equation Theory

---

## Contents

---

<b>3.1</b>	<b>Non-stationary Onsager-Machlup Theory . . . . .</b>	<b>22</b>
<b>3.2</b>	<b>Evolution of the Non-stationary Structure Factor . . .</b>	<b>25</b>

---

This Chapter contains the first original contribution of this thesis. As explained in the previous chapter the equilibrium version of the SCGLE theory and its applications to the dipolar hard-spheres fluid was derived in Ref. [10] and in the PhD. thesis of Luis Fernando Elizondo. Here we develop the extension of such the non-spherical SCGLE theory to non equilibrium conditions.

In the previous chapter, a quick review of the main aspects in the SCGLE theory of liquids was given, with emphasis in the interactions between a system of non-spherical particles; this review is the basis for the full detailed theoretical description of a non-stationary, irreversible and non equilibrium process which is characteristic of systems that exhibit glassy dynamics, and one of such characteristic behaviour that we wish to focus on, is the property of aging [24].

In this section we will outline, firstly the principal concepts and derivations of the equations that constitute the non equilibrium version of the SCGLE formalism, and secondly the theory applied to glass-forming liquids of non-spherical particles. This specific formalism shall be referred from now on as the non equilibrium generalized Langevin equation theory (NE-SCGLE).

The formalism known as SCGLE has been extended, as mentioned above, to provide a bridge between the states of ergodic equilibration to non equilibrium aging. The details have been reported extensively in the relevant litera-

ture, so here we will review the main details with emphasis in the information required for our non-spherical system.

### 3.1 Non-stationary Onsager-Machlup Theory

The phenomenological route to the generalized Langevin equation formalism is the Onsager-Machlup general model of fluctuations [13], which summarizes the dynamics of a continuous stochastic process (stochastic or random process refers to a mathematical abstraction defined as a collection of variables randomly changing over time). The Onsager-Machlup theory is used to define a probability density for any stochastic process, in analogy with the Lagrangian of a dynamic system: this theory was developed first by Lars Onsager and S. Machlup in 1953.

In addition to the general model of fluctuations, the inclusion of memory effects is also part of the SCGLE formalism, which by taking this effect into account, adds to its flexibility of said formalism in order to accurately describe non equilibrium processes.

The starting point of the generalized Langevin equation formalism is the mathematical condition of stationarity [11], which means not only the thermodynamic equilibrium physical condition, but also non-equilibrium stationary states. By following this line of thought, and in order to model a non-stationary stochastic process as a sequence of stationary processes [24], the Onsager theory of thermal fluctuations and irreversible processes was developed [17, 18, 25, 26].

To summarize the previous statements regarding the non equilibrium version of Onsager's formalism:

1. The mean value  $\bar{\mathbf{a}}(t)$  of the vector  $\mathbf{a}(t) = [a_1(t), a_2(t), \dots, a_\nu(t)]^\dagger$  constituted by the  $\nu$  macroscopic variables that describe the state of the system is the solution of some generally non-linear equation, represented by

$$\frac{d\bar{\mathbf{a}}(t)}{dt} = \mathcal{R}[\bar{\mathbf{a}}(t)], \quad (3.1)$$

whose linear version in the vicinity of a stationary state  $\bar{\mathbf{a}}^{ss}$  (i.e.,  $\mathcal{R}[\bar{\mathbf{a}}^{ss}] = 0$ ) reads

$$\frac{d\Delta\bar{\mathbf{a}}(t)}{dt} = -\mathcal{L}[\bar{\mathbf{a}}^{ss}] \cdot \mathcal{E}[\bar{\mathbf{a}}^{ss}] \cdot \Delta\bar{\mathbf{a}}(t), \quad (3.2)$$

with  $\Delta\bar{\mathbf{a}}(t) \equiv \bar{\mathbf{a}}(t) - \bar{\mathbf{a}}^{ss}$ .

2. The relaxation equation for the  $\nu \times \nu$  covariance matrix  $\sigma(t) \equiv \overline{\delta\mathbf{a}(t)\delta\mathbf{a}^\dagger(t)}$  of the non-stationary fluctuations  $\delta\mathbf{a}(t) \equiv \mathbf{a}(t) - \bar{\mathbf{a}}(t)$  can be written as [24]

$$\frac{d\sigma(t)}{dt} = -\mathcal{L}[\bar{\mathbf{a}}(t)] \cdot \mathcal{E}[\bar{\mathbf{a}}(t)] \cdot \sigma(t) \quad (3.3)$$

$$- \sigma(t) \cdot \mathcal{E}[\bar{\mathbf{a}}(t)] \cdot \mathcal{L}^\dagger[\bar{\mathbf{a}}(t)] + (\mathcal{L}[\bar{\mathbf{a}}(t)] + \mathcal{L}^\dagger[\bar{\mathbf{a}}(t)]).$$

3. In addition, the non-equilibrium version of Onsager's formalism introduces the globally non-stationary (but locally stationary) extension [24] of the generalized Langevin equation for the stochastic variables  $\delta a_i(t + \tau) \equiv a_i(t + \tau) - \bar{a}_i(t)$  [24],

$$\begin{aligned} \frac{\partial \delta\mathbf{a}(t + \tau)}{\partial \tau} &= -\omega[\bar{\mathbf{a}}(t)] \cdot \sigma^{-1}(t) \cdot \delta\mathbf{a}(t + \tau) \\ &\quad - \int_0^\tau d\tau' \gamma[\tau - \tau'; \bar{\mathbf{a}}(t)] \cdot \sigma^{-1}(t) \cdot \delta\mathbf{a}(t + \tau') + \mathbf{f}(t + \tau), \end{aligned} \quad (3.4)$$

where the random term  $\mathbf{f}(t + \tau)$  has zero mean and two-time correlation function given by the fluctuation-dissipation relation  $\langle \mathbf{f}(t + \tau)\mathbf{f}(t + \tau') \rangle = \gamma[\tau - \tau'; \bar{\mathbf{a}}(t)]$ . From this equation one derives the time-evolution equation for the non-stationary time-correlation matrix  $C(\tau; t) \equiv \overline{\delta\mathbf{a}(t + \tau)\delta\mathbf{a}^\dagger(t)}$ , reading

$$\begin{aligned} \frac{\partial C(\tau; t)}{\partial \tau} &= -\omega[\bar{\mathbf{a}}(t)] \cdot \sigma^{-1}(t) \cdot C(\tau; t) \\ &\quad - \int_0^\tau d\tau' \gamma[\tau - \tau'; \bar{\mathbf{a}}(t)] \cdot \sigma^{-1}(t) \cdot C(\tau'; t), \end{aligned} \quad (3.5)$$

whose initial condition is  $C(\tau = 0; t) = \sigma(t)$ .

Regarding the second point, the equations  $\mathcal{L}[\mathbf{a}]$  is a  $\nu \times \nu$  "kinetic" matrix, defined in terms of  $\mathcal{R}[\mathbf{a}]$  as  $\mathcal{L}[\mathbf{a}] \equiv -(\partial\mathcal{R}[\mathbf{a}]/\partial\mathbf{a}) \cdot \mathcal{E}^{-1}[\mathbf{a}]$ , whereas  $\mathcal{E}[\mathbf{a}]$  is the  $\nu \times \nu$  thermodynamic ("stability") matrix, defined as

$$\mathcal{E}_{ij}[\mathbf{a}] \equiv -\frac{1}{k_B} \left( \frac{\partial^2 S[\mathbf{a}]}{\partial a_i \partial a_j} \right) = - \left( \frac{\partial F_i[\mathbf{a}]}{\partial a_j} \right) \quad (i, j = 1, 2, \dots, \nu), \quad (3.6)$$

with  $S[\mathbf{a}]$  being the entropy and  $F_j[\mathbf{a}] \equiv k_B^{-1} (\partial S[\mathbf{a}]/\partial a_j)$  the conjugate intensive variable associated with  $a_j$ . The function  $S = S[\mathbf{a}]$ , which assigns a value of the entropy  $S$  to any possible state point  $\mathbf{a}$  in the phase space of the system, is the fundamental thermodynamic relation [27], and constitutes the most important and fundamental external input of the non-equilibrium theory. The previous equations, however, do not explicitly require the function  $S = S[\mathbf{a}]$ , but only its second derivatives defining the stability matrix  $\mathcal{E}[\mathbf{a}]$ . The most important property of the matrix  $\mathcal{E}[\mathbf{a}]$  is that its inverse is the covariance of the *equilibrium* fluctuations, i.e.,

$$\mathcal{E}[\bar{\mathbf{a}}^{eq}] \cdot \sigma^{eq} = I, \quad (3.7)$$

with  $\sigma_{ij}^{eq} \equiv \overline{\delta a_i \delta a_j^{eq}}$ , where the average is calculated by using the already known probability distribution  $P^{eq}[\mathbf{a}]$  of the equilibrium ensemble.

In reference to the third statement in the Onsager formalism, the equations  $\omega[\mathbf{a}]$  represents conservative (being either mechanical, geometrical or streaming) relaxation processes, and it is simply the antisymmetric part of  $\mathcal{L}[\mathbf{a}]$ , i.e.,  $\omega[\mathbf{a}] = (\mathcal{L}[\mathbf{a}] - \mathcal{L}^\dagger[\mathbf{a}])/2$ . The memory function  $\gamma[\tau; \bar{\mathbf{a}}(t)]$ , on the other hand, summarizes the effects of all the complex dissipative irreversible processes taking place in the system.

By taking the Laplace transform (LT) of eq. (3.5) in order to integrate out the variable  $\tau$  in favour of the variable  $z$ , this equation is rewritten as

$$C(z; t) = \{z\mathbf{I} + \mathbf{L}[z; \bar{\mathbf{a}}(t)] \cdot \sigma^{-1}(t)\}^{-1} \cdot C(\tau = 0; t) \quad (3.8)$$

with  $\mathbf{L}[z; \bar{\mathbf{a}}(t)]$  being the LT of

$$\mathbf{L}[\tau; \bar{\mathbf{a}}(t)] \equiv 2\delta(\tau)\omega[\bar{\mathbf{a}}(t)] + \gamma[\tau; \bar{\mathbf{a}}(t)]. \quad (3.9)$$

To avoid confusion, let us mention that the quantity  $\mathbf{L}[z; \bar{\mathbf{a}}(t)]$  previously defined is not an angular momentum, despite of the notation. The phenomenological “kinetic” matrix  $\mathcal{L}[\bar{\mathbf{a}}(t)]$  appearing in Eq. (3.3), can be expressed now as a function of this quantity  $\mathbf{L}[z; \bar{\mathbf{a}}(t)]$ , which is understood as a generalized kinetic matrix from the Green-Kubo theory.

$$\mathcal{L}[\bar{\mathbf{a}}(t)] = \mathbf{L}[z = 0; \bar{\mathbf{a}}(t)] \equiv \omega[\bar{\mathbf{a}}(t)] + \int_0^\infty d\tau \gamma[\tau; \bar{\mathbf{a}}(t)], \quad (3.10)$$

which extends to non-equilibrium conditions the Kubo formula (also known as Green-Kubo formula). Let us recall that the Kubo formula is an equation expressing the linear response of any observable quantity, due to a time-dependent perturbation: applications include charge and spin susceptibilities

of electron systems due to external electric or magnetic fields, as well as a response to external mechanical forces or vibrations.

In our system of interest, the precise determination of  $\gamma[\tau; \mathbf{a}]$  is not always possible, except for a few specific systems or in certain limiting cases; hence, for the rest of the systems we must resort to some approximations, that will take the mathematical form of a closure relation which will describe  $\gamma[\tau; \bar{\mathbf{a}}(t)]$  in terms of the two-time correlation matrix  $C(\tau; t)$ . From this consideration, a self consistent equation system will arise to be solved explicitly for a given example in the following section.

## 3.2 Evolution of the Non-stationary Structure Factor

The abstractions in the Onsager-Machlup theory can be applied to the description of our interest: namely, the non-equilibrium diffusive processes inside colloidal dispersions. In order to do so, we will first start identifying the following general state variables:  $a_i = a_{(r, \Omega)} \equiv N_{(r, \Omega)} / \Delta V$  defined as the number concentration of  $N$  particles with orientation  $\Omega$  in the  $r$ th cell of an imaginary partitioning of the volume occupied by the liquid in  $C$  cells of volume  $\Delta V$ . In the continuum limit, the components of the state vector  $\mathbf{a}(t)$  will become the microscopic local concentration profile  $n(\mathbf{r}, \Omega; t)$  defined in Eq. (2.3), and the *fundamental thermodynamic relation*  $S = S[\mathbf{a}]$  (which assigns a value of the entropy  $S$  to any point  $\mathbf{a}$  of the thermodynamic state space [27]) becomes the functional dependence  $S = S[\mathbf{n}]$  of the entropy (or equivalently, of the free energy) on the local concentration profile  $n(\mathbf{r}, \Omega; t)$ .

Using this identification in Eqs. (3.1) and (3.3) leads to the time evolution equations for the mean value  $\bar{n}(\mathbf{r}, \Omega; t)$ , and for the covariance  $\sigma(\mathbf{r}, \Omega; \mathbf{r}'\Omega'; t) \equiv \overline{\delta n(\mathbf{r}, \Omega; t) \delta n(\mathbf{r}', \Omega'; t)}$  of the fluctuations  $\delta n(\mathbf{r}, \Omega; t) = n(\mathbf{r}, \Omega; t) - \bar{n}(\mathbf{r}, \Omega; t)$  of the local concentration profile  $n(\mathbf{r}, \Omega; t)$ . These two equations are the non-spherical extensions of Eqs. (3.6) and (3.8) in reference [24], which form a coupled set between two translational and rotational local mobility functions,  $b^T(\mathbf{r}, \Omega; t)$  and  $b^R(\mathbf{r}, \Omega; t)$ , and can be also written as functions of the two-time correlation function  $C(\mathbf{r}, \Omega; \mathbf{r}'\Omega'; t, t') \equiv \overline{\delta n(\mathbf{r}, \Omega; t) \delta n(\mathbf{r}', \Omega'; t')}$  via an approximation.

The complete set of well-defined approximations made on the memory function  $C(\mathbf{r}, \Omega; \mathbf{r}'\Omega'; t, t')$  extended to the system of non-spherical particles like the ones described in reference [24] in the context of spherical particles, results in the aforementioned NE-SCGLE theory.

The general NE-SCGLE and its main equations applied in general to many systems have been extensively discussed elsewhere, so instead we will focus on explaining the intricacies of such equations in the particular phenomena of liquids composed of non spherical particles that form glasses, due to being subjected to a controlled descent in temperature, while constraining the non spherical particles to remain homogeneous and isotropic, as well as with a fixed number density  $\bar{n}$ .

Thus, rather than solving the time-evolution equation for  $\bar{n}(\mathbf{r}, \mathbf{\Omega}; t)$ , we have that  $\bar{n}(\mathbf{r}, \mathbf{\Omega}; t) = \bar{n}$  now becomes a control parameter. As a result, we only have to solve the time-evolution equation for the covariance  $\sigma(\mathbf{r}, \mathbf{\Omega}; \mathbf{r}'\mathbf{\Omega}'; t) = \sigma(\mathbf{r}-\mathbf{r}', \mathbf{\Omega}, \mathbf{\Omega}'; t)$ . Furthermore, let us only consider the simplest cooling protocol, namely, the instantaneous temperature quench at  $t = 0$  from an arbitrary initial temperature  $T_i$  to a final value  $T_f$ .

At this point we notice that it is actually more practical to identify the abstract vector of state variables  $\mathbf{a}(t) = [a_1(t), a_2(t), \dots, a_\nu(t)]^\dagger$  not with the local concentration  $\bar{n}(\mathbf{r}, \mathbf{\Omega}; t)$  itself, but with *just one* of its tensorial modes, so that  $\mathbf{a}(t) = [a_1(t)]$ , with  $a_1 \equiv n_{lm}(\mathbf{k}, t)$ , defined in Eq.(2.6).

Under the above stated conditions, the corresponding non-stationary covariance  $\sigma(t)$  is just a scalar, denoted by  $S_{lm}(k, t)$ , and defined as

$$\sigma(t) = S_{lm}(k, t) \equiv \overline{\delta n_{lm}^*(\mathbf{k}, t) \delta n_{lm}(\mathbf{k}, t)}, \quad (3.11)$$

with  $\delta n_{lm}(\mathbf{k}, t) \equiv n_{lm}(\mathbf{k}, t) - \overline{n_{lm}(\mathbf{k}, t)}$ . In other words,  $S_{lm}(k, t)$  is a diagonal element of the matrix  $S_{lm, l'm'}(k, t) \equiv \overline{\delta n_{lm}^*(\mathbf{k}, t) \delta n_{l'm'}(\mathbf{k}, t)}$ , and the time-evolution equation of  $S_{lm}(k, t)$  now follows from identifying all the elements of Eq. (3.3) with those already known.

The first of such elements is the thermodynamic matrix  $\mathcal{E}[\mathbf{a}]$ , which in this case is also a scalar quantity denoted as  $\mathcal{E}_{lm}[n_{lm}(\mathbf{k})]$ ; this quantity is defined in terms of the second derivative of the entropy  $S[n_{lm}(\mathbf{k})]$  (in a contracted description in which the only explicit macroscopic variable is  $n_{lm}(\mathbf{k})$ ) as

$$\mathcal{E}_{lm}[n_{lm}(\mathbf{k})] \equiv -\frac{1}{k_B} \left( \frac{d^2 S[n_{lm}(\mathbf{k})]}{dn_{lm}^2(\mathbf{k})} \right). \quad (3.12)$$

According to Eq. (3.7), this thermodynamic property is precisely the inverse of the equilibrium value of  $S_{lm}^{eq}(k) \equiv \overline{\delta n_{lm}^*(\mathbf{k}) \delta n_{lm}(\mathbf{k})}^{eq}$  of  $S_{lm}(k, t)$ ,

$$\mathcal{E}_{lm}[n_{lm}(\mathbf{k})] = 1/S_{lm}^{eq}(k). \quad (3.13)$$

We will notice now that  $\mathcal{E}_{lm}[n_{lm}(\mathbf{k})]$  is not just the diagonal element of the matrix  $\mathcal{E}_{lm,\nu'm'}[n]$ , defined in terms of the second partial derivative of the entropy  $S[n]$ <sup>a</sup> as

$$\mathcal{E}_{lm,\nu'm'}[n] \equiv -\frac{1}{k_B} \left( \frac{\partial^2 S[n]}{\partial n_{lm}(\mathbf{k}) \partial n_{\nu'm'}(\mathbf{k})} \right). \quad (3.14)$$

but this element is, according again to Eq. (3.7), rather the full equilibrium covariance  $S_{lm,\nu'm'}^{eq}(k) \equiv \overline{\delta n_{lm}^*(\mathbf{k}) \delta n_{\nu'm'}(\mathbf{k})}^{eq}$ , whose diagonal elements  $S_{lm}^{eq}(k)$  do determine  $\mathcal{E}_{lm}[n_{lm}(\mathbf{k})]$ , according to Eq. (3.13). We shall mention, additionally, that  $\mathcal{E}_{lm}[n_{lm}(\mathbf{k})]$  is also a functional of the spatially non-uniform local temperature field  $T(\mathbf{r})$ . To indicate this dependence more explicitly we denote the thermodynamic matrix as  $\mathcal{E}_{lm}[n_{lm}(\mathbf{k}); T]$ . In the present analysis, however, we will impose the constraint that at any instant the system is thermally uniform,  $T(\mathbf{r}) = T$ , and instantaneously adjusted to the reservoir temperature  $T$ , which will then be a (possibly time-dependent) control parameter  $T(t)$ .

The second element of Eq. (3.3) that we must identify is the kinetic matrix  $\mathcal{L}[\mathbf{a}]$ . For this, let us first compare the equilibrium version of Eq. (3.8), namely,

$$C(z) = \{z\mathbf{I} + \mathbf{L}[z; \bar{\mathbf{a}}] \cdot \sigma^{-1}\}^{-1} \cdot \sigma, \quad (3.15)$$

with the particular case in Eq. (2.10), in which the scalars  $F_{lm}(k, z)$  and  $S_{lm}(k)$  correspond, respectively, to  $C(z)$  and  $\sigma$ . This comparison allows us to identify  $\mathbf{L}[z; \bar{\mathbf{a}}]$  with the scalar

$$\left[ \frac{k^2 D_T^0}{1 + \Delta\zeta_T^*(z) \lambda_T^{(lm)}(k)} + \frac{l(l+1) D_R^0}{1 + \Delta\zeta_R^*(z) \lambda_R^{(lm)}(k)} \right]. \quad (3.16)$$

Extending this identification to non-stationary conditions, we have that

$$\mathbf{L}[z; \bar{\mathbf{a}}(t)] = \left[ \frac{k^2 D_T^0}{1 + \Delta\zeta_T^*(z; t) \lambda_T^{(lm)}(k; t)} + \frac{l(l+1) D_R^0}{1 + \Delta\zeta_R^*(z; t) \lambda_R^{(lm)}(k; t)} \right], \quad (3.17)$$

where the functions  $\lambda_R^{(lm)}(k; t)$  are defined as the unity and the functions  $\lambda_T^{(lm)}(k; t)$  as  $\lambda_T^{(lm)}(k; t) = 1/[1 + (k/k_c(t))^2]$ , where  $k_c = 1.305 \times k_{max}(t)$ , with  $k_{max}(t)$  being the position of the main peak of  $S_{00}(k; t)$ . The functions  $\Delta\zeta_T^*(z; t)$  and  $\Delta\zeta_R^*(z; t)$ , to be defined below, are the non-stationary versions of the functions  $\Delta\zeta_T^*(z)$ , and  $\Delta\zeta_R^*(z)$ .

---

<sup>a</sup>in a *non*-contracted description in which the explicit macroscopic variables are *all* the tensorial density modes  $n_{lm}(\mathbf{k})$  of the microscopic one-particle density  $n(\mathbf{r}, \mathbf{\Omega}; t)$

Since  $\mathcal{L}[\bar{\mathbf{a}}(t)] = \mathbf{L}[z = 0; \bar{\mathbf{a}}(t)]$  (see Eq. (3.10)), the general and abstract time-evolution equation in Eq. (3.3) for the non-stationary covariance becomes

$$\begin{aligned} \frac{\partial S_{lm}(k; t)}{\partial t} = & -2 \left[ \frac{k^2 D_T^0}{1 + \Delta\zeta_T^*(z = 0; t)\lambda_T^{(lm)}(k = 0; t)} + \frac{l(l+1)D_R^0}{1 + \Delta\zeta_R^*(z = 0; t)\lambda_R^{(lm)}(k = 0; t)} \right] \\ & \times [\mathcal{E}_{lm}(k, t)S_{lm}(k; t) - 1], \end{aligned} \quad (3.18)$$

where  $\mathcal{E}_{lm}(k, t) = \mathcal{E}_{lm}[n_{lm}(\mathbf{k}); T(t)]$ . In the present application to the instantaneous isochoric quench at time  $t = 0$  to a final temperature  $T_f$  and fixed bulk density  $n$ , this property is constant, i.e., for  $t > 0$  we have that  $\mathcal{E}_{lm}(k, t) = \mathcal{E}_{lm}[n_{lm}(\mathbf{k}); T_f] = \mathcal{E}_{lm}^{(f)}(k)$ . In addition, in consistency with the coarse-grained limit  $z = 0$  in  $\Delta\zeta_T^*(z = 0; t)$  and  $\Delta\zeta_R^*(z = 0; t)$ , we have also approximated  $\lambda_T^{(lm)}(k; t)$  and  $\lambda_R^{(lm)}(k; t)$  by its  $k \rightarrow 0$  limit  $\lambda_T^{(lm)}(k = 0; t)$  and  $\lambda_R^{(lm)}(k = 0; t)$ , which are unitary. Thus, the previous equation reads

$$\frac{\partial S_{lm}(k; t)}{\partial t} = -2 [k^2 D_0^T b^T(t) + l(l+1)D_0^R b^R(t)] \mathcal{E}_{lm}^{(f)}(k) [S_{lm}(k; t) - 1/\mathcal{E}_{lm}^{(f)}(k)], \quad (3.19)$$

where the translational and rotational time-dependent mobilities  $b^T(t)$  and  $b^R(t)$  are defined as

$$b^T(t) = [1 + \int_0^\infty d\tau \Delta\zeta_T^*(\tau; t)]^{-1} \quad (3.20)$$

and

$$b^R(t) = [1 + \int_0^\infty d\tau \Delta\zeta_R^*(\tau; t)]^{-1}. \quad (3.21)$$

in terms of the non-stationary  $\tau$ -dependent friction functions  $\Delta\zeta_T^*(\tau; t)$  and  $\Delta\zeta_R^*(\tau; t)$ .

In order to determine  $b^T(t)$  and  $b^R(t)$ , we adapt to non-equilibrium non-stationary conditions, the same approximations leading to Eqs. (2.12) and (2.13) for the equilibrium friction functions  $\Delta\zeta_T^*(\tau)$  and  $\Delta\zeta_R^*(\tau)$ , which in the present case lead to similar approximate expressions for  $\Delta\zeta_T^*(\tau; t)$  and  $\Delta\zeta_R^*(\tau; t)$ , namely,

$$\Delta\zeta_T^*(\tau; t) = \frac{1}{3} \frac{D_T^0}{(2\pi)^3 n} \int d\mathbf{k} k^2 \sum_l [2l+1] [1 - S_{l0}^{-1}(k; t)]^2 F_{l0}^S(k, \tau; t) F_{l0}(k, \tau; t) \quad (3.22)$$

and

$$\Delta\zeta_R^*(\tau; t) = \frac{1}{2} \frac{D_R^0}{(2\pi)^3} \frac{n}{4} \frac{1}{(4\pi)^2} \times \int d\mathbf{k} \sum_{lm} [2l+1] h_{l0}^2(k; t) [A_{l;0m}]^2 [S_{lm}^{-1}(k; t)]^2 F_{lm}^S(k, \tau; t) F_{lm}(k, \tau; t), \quad (3.23)$$

where  $F_{lm;l'm'}(\mathbf{k}, \tau; t)$  are the non-stationary,  $\tau$ -dependent correlation functions  $F_{lm;l'm'}(\mathbf{k}, \tau; t) \equiv \langle \delta n_{lm}^*(\mathbf{k}, t + \tau) \delta n_{l'm'}(\mathbf{k}, t) \rangle$ , with  $F_{lm;l'm'}^S(\mathbf{k}, \tau; t)$  being the corresponding *self* components.

In a similar manner, the time-evolution equations for  $F_{lm;l'm'}(k, \tau; t)$  and  $F_{lm;l'm'}^S(k, \tau; t)$  are written, in terms of the Laplace transforms  $F_{lm;l'm'}(k, z; t)$ ,  $F_{lm;l'm'}^S(k, z; t)$ ,  $\Delta\zeta_T^*(z; t)$ , and  $\Delta\zeta_R^*(z; t)$ , as

$$F_{lm}(k, z; t) = \frac{S_{lm}(k; t)}{z + \frac{k^2 D_T^0 S_{lm}^{-1}(k; t)}{1 + \Delta\zeta_T^*(z; t) \lambda_T^{(lm)}(k; t)} + \frac{l(l+1) D_R^0 S_{lm}^{-1}(k; t)}{1 + \Delta\zeta_R^*(z; t) \lambda_R^{(lm)}(k; t)}}, \quad (3.24)$$

$$F_{lm}^S(k, z; t) = \frac{1}{z + \frac{k^2 D_T^0}{1 + \Delta\zeta_T^*(z; t) \lambda_T^{(lm)}(k; t)} + \frac{l(l+1) D_R^0}{1 + \Delta\zeta_R^*(z; t) \lambda_R^{(lm)}(k; t)}}. \quad (3.25)$$

For any given set of thermodynamic functions  $\mathcal{E}_{lm}[n_{lm}(\mathbf{k}); T_f]$ , (3.19) to (3.25) equations, they form a closed set that gives way to the non-equilibrium properties of the system  $S_{lm}(k; t)$ ,  $F_{lm}(k, \tau; t)$ ,  $F_{lm}^S(k, \tau; t)$ , and their solution forms a complete description of the non stationary and non equilibrium structural relaxation in the process of glass forming in liquids, all of this embedded in the NE-SCGLE methodology; this is no trivial feature and more so, the only input required by the NE-SCGLE theory is the analytical form of  $\mathcal{E}_{lm}[n_{lm}(\mathbf{k}); T_f]$  and any given projected initial static structure factor  $S_{lm}(k) \equiv S_{lm}(k; t = 0)$ .

As we will see in the next chapter, the application of the theory is straightforward, and we want to explore the key features of simple systems just as the dipolar-interacting colloidal particles (Chap. 4 and 5) or attractive-angular-dependent interacting particles (Chap. 6).



# Equilibration and aging processes for interacting Dipoles with Random Fixed Positions

---

## Contents

---

4.1	An illustrative example. . . . .	31
4.2	Slow Dynamics and Spin Glass transitions of a classical and disordered Heisenberg system . . . . .	33
4.3	Equilibration of the System of Interacting Dipoles with Random Fixed Positions . . . . .	34
4.4	Aging of the System of Interacting Dipoles with Random Fixed Positions . . . . .	37
4.5	Crossover from equilibration to aging: Determination of the dynamical arrested diagram . . . . .	40

---

As a first application of the “non equilibrium” theoretical framework developed in previous chapter, we now discuss the slow dynamics near the spin glass (SG) transition [28] of a classical Heisenberg system consisting of a set of linear interacting classical dipoles with random positional disorder. This illustrative example allows us to investigate the relevant features of the orientational dynamics during the equilibration and aging processes, and it opens for discussion many relevant issues, such as the relationship between these theoretical predictions and the phenomenology of aging in real spin-glass systems.

## 4.1 An illustrative example.

Eqs. (3.19)-(3.25) describe the coupled translational and rotational dynamics of a Brownian liquid of non-spherical particles in search of thermodynamic equilibrium after a sudden quench. A thorough application to a concrete system should then exhibit the full interplay of the translational and rotational

degrees of freedom during this process. As an illustrative application here we discuss the solution of our resulting equations describing the irreversible evolution of the orientational dynamics of a system of strongly interacting dipoles with fixed but random positions subjected to a sudden temperature quench.

For this, let us recall that two important inputs of Eqs. (3.19)-(3.25), are the short-time self-diffusion coefficients  $D_T^0$  and  $D_R^0$ , which describe, respectively, the short-time Brownian motion of the center of mass and of the orientations of the particles. Hence, *arbitrarily* setting  $D_T^0 = 0$  implies that the particles are prevented from diffusing translationally in any time scale, thus remaining fixed in space. Within this simplification Eq. (3.19) reduces to

$$\frac{\partial S_{lm}(k; t)}{\partial t} = -2l(l+1)D_0^R b^R(t) \mathcal{E}_{lm}^{(f)}(k) \left[ S_{lm}(k; t) - 1/\mathcal{E}_{lm}^{(f)}(k) \right], \quad (4.1)$$

whereas Eqs. (3.24) and (3.25) now read

$$F_{lm}(k, z; t) = \frac{S_{lm}(k; t)}{z + \frac{l(l+1)D_R^0 S_{lm}^{-1}(k; t)}{1 + \Delta\zeta_R^*(z; t)\lambda_R^{(lm)}(k, t)}}, \quad (4.2)$$

and

$$F_{lm}^S(k, z; t) = \frac{1}{z + \frac{l(l+1)D_R^0}{1 + \Delta\zeta_R^*(z; t)\lambda_R^{(lm)}(k, t)}}. \quad (4.3)$$

Also, the time-dependent translational mobility satisfies  $b^T(t) = 1$ . Hence, we only need to complement Eqs. (4.1), (4.2) and (4.3) with

$$b^R(t) = \left[ 1 + \int_0^\infty d\tau \Delta\zeta_R^*(\tau; t) \right]^{-1}. \quad (4.4)$$

and

$$\Delta\zeta_R^*(\tau; t) = \frac{1}{2} \frac{D_R^0}{(2\pi)^3} \frac{n}{4} \frac{1}{(4\pi)^2} \int d\mathbf{k} \sum_{lm} [2l+1] h_{l0}^2(k; t) [A_{l;0m}]^2 [S_{lm}^{-1}(k; t)]^2 \times F_{lm}^S(k, \tau; t) F_{lm}(k, \tau; t), \quad (4.5)$$

where  $A_{l;0m} \equiv [C_{l0}^+ \delta_{1,m} + C_{l0}^- \delta_{-1,m}]$  and  $C_{l0}^\pm \equiv \sqrt{(l \mp 0)(l+1)}$ . In the following subsections we report the simplest application of these equations.

## 4.2 Slow Dynamics and Spin Glass transitions of a classical and disordered Heisenberg system

Let us consider a system formed by  $N$  identical dipolar hard spheres of diameter  $\sigma$  bearing a point dipole of magnitude  $\mu$  at their center, such that the dipolar moment of the  $n$ -th particle ( $n = 1, 2, \dots, N$ ) can be written as  $\boldsymbol{\mu}_n = \mu \hat{\boldsymbol{\mu}}_n$  where the unitary vector  $\hat{\boldsymbol{\mu}}_n$  describes its orientation. Thus, the orientational degrees of freedom of the system,  $\boldsymbol{\Omega}^N$ , are described by the set of unitary vectors  $(\hat{\boldsymbol{\mu}}_1, \hat{\boldsymbol{\mu}}_2, \dots, \hat{\boldsymbol{\mu}}_N) = \boldsymbol{\Omega}^N$ , so that the pair potential  $u(\mathbf{r}_n, \mathbf{r}_{n'}; \boldsymbol{\Omega}_n, \boldsymbol{\Omega}_{n'})$  between particles  $n$  and  $n'$  is thus the sum of the radially-symmetric hard-sphere potential  $u_{HS}(|\mathbf{r}_n - \mathbf{r}_{n'}|)$  plus the dipole-dipole interaction, given by

$$u_{dip}(\mathbf{r}_n, \mathbf{r}_{n'}; \boldsymbol{\Omega}_n, \boldsymbol{\Omega}_{n'}) = \mu^2 |\mathbf{r}_n - \mathbf{r}_{n'}|^{-5} [(\mathbf{r}_n - \mathbf{r}_{n'})^2 (\hat{\boldsymbol{\mu}}_n \cdot \hat{\boldsymbol{\mu}}_{n'}) - 3((\mathbf{r}_n - \mathbf{r}_{n'}) \cdot \hat{\boldsymbol{\mu}}_n)((\mathbf{r}_n - \mathbf{r}_{n'}) \cdot \hat{\boldsymbol{\mu}}_{n'})]. \quad (4.6)$$

The state space of this system is spanned by the number density  $n$  and the temperature  $T$ , expressed in dimensionless form as  $[n\sigma^3]$  and  $[k_B T \sigma^3 / \mu^2]$  (with  $k_B$  being Boltzmann's constant). From now on we shall denote  $[n\sigma^3]$  and  $[k_B T \sigma^3 / \mu^2]$  simply as  $n$  and  $T$ , i.e., we shall use  $\sigma$  as the unit of length, and  $\mu^2 / k_B \sigma^3$  as the unit of temperature; most frequently, however, we shall also refer to the hard-sphere volume fraction  $\phi \equiv \pi n / 6$ .

The application of the NE-SCGLE equations starts with the external determination of the thermodynamic function  $\mathcal{E}_{lm}^{(f)}(k) \equiv \mathcal{E}_{lm}(k; \phi, T_f)$ . At a given state point  $(\phi, T)$ , the function  $\mathcal{E}_{lm}(k; \phi, T)$  can be determined using the fact that its inverse is identical to the projection  $S_{lm}^{eq}(k; \phi, T)$  of the *equilibrium* static structure factor  $S^{eq}(\mathbf{k}, \boldsymbol{\mu}, \boldsymbol{\mu}')$  at that state point. In the context of the present application, this equilibrium property will be approximated by the solution of the mean spherical approximation (MSA) for the dipolar hard sphere (DHS). The details involved in the determination of the resulting equilibrium static structure factor, whose only non zero projections are  $S_{00}^{eq}(k), S_{10}^{eq}(k)$  and  $S_{11}^{eq}(k) = S_{1-1}^{eq}(k)$ , can be consulted in appendix E of reference [22]

The equilibrium projections  $S_{lm}^{eq}(k; \phi, T)$  can also be used in the so-called bifurcation equations of the equilibrium theory. These are Eqs. (2.17)-(2.21) for the non-ergodic parameters  $\gamma_T^{eq}(\phi, T)$  and  $\gamma_R^{eq}(\phi, T)$ . According to Eq.(2.19), however,  $D_T^0 = 0$  implies  $\gamma_T^{eq}(\phi, T) = 0$ , so that in the present case we must only solve Eq. (2.21) for  $\gamma_R^{eq}(\phi, T)$ . If the solution is infinite we say that the asymptotic stationary state is ergodic, and hence, that at the point  $(\phi, T)$  the system will be able to reach its thermodynamic equilibrium

state. If, on the other hand,  $\gamma_R^{eq}(\phi, T)$  turns out to be finite, the system is predicted to become dynamically arrested and thus, the long time limit of  $S_{lm}(k, t)$  will differ from the thermodynamic equilibrium value  $S_{lm}^{eq}(k; \phi, T)$ . The application of this criterion leads to the prediction that the system under consideration will equilibrate for temperatures  $T$  above a critical value  $T_c(\phi)$ , whereas the system will be dynamically arrested for temperatures below  $T_c$ . In this manner one can trace the dynamic arrest line  $T_c = T_c(\phi)$ .

We can now use the same thermodynamic function  $\mathcal{E}_{lm}^{(f)}(k) \equiv \mathcal{E}_{lm}(k; \phi, T_f)$  to go beyond the determination of the dynamic arrest line  $T_c = T_c(\phi)$  by solving the set of NE-SCGLE equations (4.1)-(4.5) to describe the rotational diffusive relaxation of our system. For this, let us notice that these equations happen to have the same mathematical structure as the NE-SCGLE equations that describe the translational diffusion of *spherical* particles (see, e.g., Eqs. (2.1)-(2.6) of Ref. [6]). Although the physical meaning of these two sets of equations is totally different, their mathematical similarity allows us to implement the same method of solution described in Ref. [29]. Thus, we do not provide further details of the numerical protocol to solve Eqs. (4.1)-(4.5), but go directly to illustrate the resulting scenario. For example, along the isochore  $\phi = 0.2$ , this procedure determines that  $T_c = T_c(\phi = 0.2) = 0.116$ .

At this point let us notice that there are two possible classes of stationary solutions of Eq. (4.1). The first class corresponds to the long-time asymptotic condition  $\lim_{t \rightarrow \infty} S_{lm}(k; t) = 1/\mathcal{E}_{lm}^{(f)}(k)$ , in which the system is able to reach the thermodynamic equilibrium condition  $S_{lm}^{eq}(k) = 1/\mathcal{E}_{lm}^{(f)}(k)$ . Equilibration is thus a sufficient condition for the stationarity of  $S_{lm}(k, t)$ . It is, however, not a *necessary* condition. Instead, according to Eq. (4.1), another sufficient condition for stationarity is that  $\lim_{t \rightarrow \infty} b_R(t) = 0$ . This is precisely the hallmark of dynamically-arrested states. In what follows we discuss the phenomenology predicted by the solution of Eqs. (4.1)-(4.5) for each of these two mutually exclusive possibilities.

### 4.3 Equilibration of the System of Interacting Dipoles with Random Fixed Positions

Let us now discuss the solution of Eqs. (4.1)-(4.5) describing the non-equilibrium response of the system to an instantaneous temperature quench. For this, we assume that the system was prepared in an equilibrium state characterized by the initial value  $S_{lm}^{(i)}(k) = S_{lm}^{(eq)}(k, \phi, T_i) = S_{lm}(k, t = 0)$ , of  $S_{lm}(k, t)$ , and that

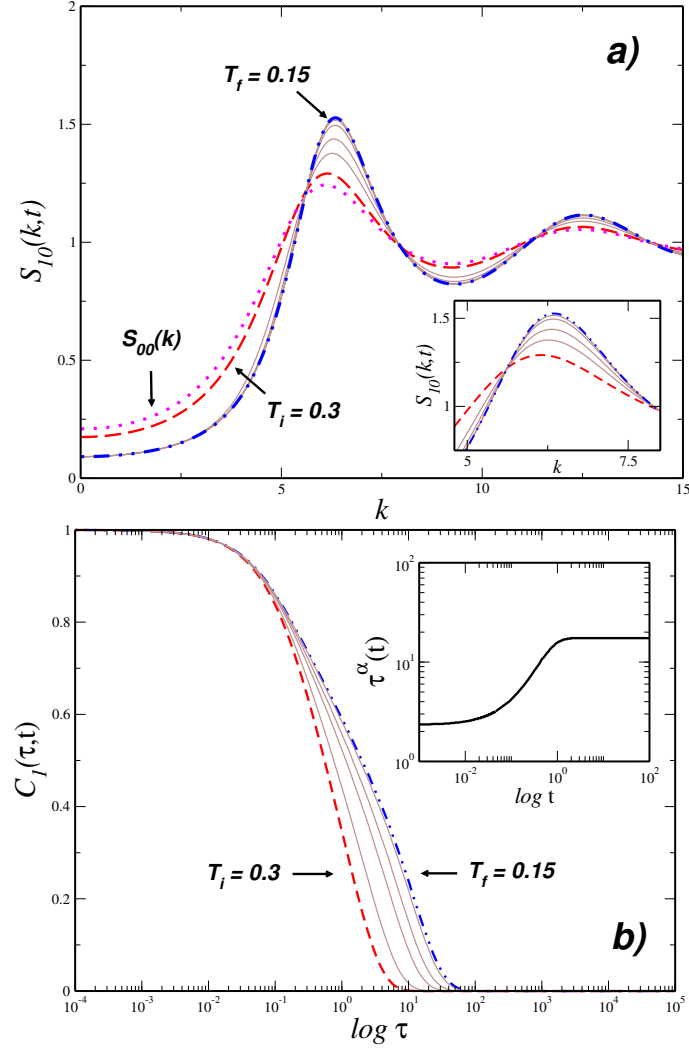


Figure 4.1: (Color online) Illustration of an equilibration process: (a) Snapshots of the time evolution of the  $l = 1, m = 0$  static structure factor projection,  $S_{10}(k, t)$ , corresponding to the isochoric quench  $T_i \rightarrow T_f$  for  $\phi = 0.2$ , with  $T_i = 0.3$  and  $T_f = 0.15$ . The (red) dashed line is the initial structure factor  $S_{10}(k, t = 0) = S_{10}^{(i)}(k)$ . The (blue) dot-dashed line is the asymptotic limit  $S_{10}(k, t \rightarrow \infty) = S_{10}^{(f)}(k) = S_{10}^{(eq)}(k)$ . The sequence of thinner (brown) solid lines in between represents  $S_{10}(k, t)$  for  $t = 0.3, 0.78, 1.42, 2.33$  and  $t \rightarrow \infty$ . For reference we also include the non-evolving component  $S_{00}(k, t) = S_{00}^{eq}(k; \phi, T_i)$ , indicated by the dotted line. (b) Snapshots of the orientational autocorrelation function  $C_1(\tau; t)$  as a function of correlation time  $\tau$  (thin brown solid lines), corresponding to the same isochoric quench and same sequence of waiting times  $t$  as in (a). The (red) dashed line represents the initial function  $C_1(\tau; t = 0) = C_1^{(eq)}(\tau; \phi, T_i)$  and the (blue) dot-dashed line is the asymptotic limit  $C_1(\tau; t \rightarrow \infty) = C_1^{(eq)}(\tau; \phi, T_f)$ . The inset plots the  $\alpha$ -relaxation time, defined as  $C_1(\tau_\alpha; t) = 1/e$ , as a function of waiting time  $t$ .

at time  $t = 0$  the temperature is instantaneously quenched to a final value  $T_f$ . Normally one expects that, as a result, the system will eventually reach full thermodynamic equilibrium, so that the long time asymptotic limit of  $S_{lm}(k, t)$  will be the equilibrium projections  $S_{lm}^{(eq)}(k; \phi, T_f)$ . Such equilibration processes are illustrated in Fig. 4.1(a) with an example in which the system was quenched from an initial equilibrium state at temperature  $T_i = 0.3$ ,  $S_{lm}(k, t = 0) = S_{lm}(k; \phi, T_i)$ , to a final temperature  $T_f = 0.15 > T_c = 0.116$ , keeping the volume fraction constant at  $\phi = 0.2$ .

Under these conditions, we should expect that the system will indeed equilibrate, so that  $S_{lm}(k, t \rightarrow \infty) = S_{lm}^{(eq)}(k; \phi, T_f)$ . This, however, will only be true for  $S_{10}(k, t)$  and  $S_{11}(k, t)$ , since, according to Eq. (4.1),  $S_{00}(k, t)$  must remain constant for  $t > 0$ , indicating that the artificially-quenched spatial structure will not evolve as a result of the temperature quench. For the same reason, Eqs. (4.2) and (4.3) imply that the normalized intermediate scattering functions  $F_{00}(k, \tau; t)/S_{00}(k; t)$  and  $F_{00}^S(k, \tau; t)$  will be unity for all positive values of the correlation time  $\tau$  and waiting time  $t$ . For reference, the structure of the frozen positions represented by  $S_{00}(k, t) = S_{00}^{(eq)}(k, \phi, T_i)$ , is displayed in Fig. 4.1(a) by the (magenta) dotted line, which clearly indicates that the fixed positions of the dipoles are strongly correlated, in contrast with a system of dipoles with purely random fixed positions, in which  $S_{00}(k, t)$  would be unity. In the same figure, the initial and final equilibrium static structure factor projections,  $S_{10}^{(i)}(k) = S_{10}^{(eq)}(k; \phi, T_i)$  and  $S_{10}^{(f)}(k) = S_{10}^{(eq)}(k; \phi, T_f)$ , are represented, respectively, by the (red) dashed and (blue) dot-dashed curves. The sequence of (brown) solid curves in between represents the evolution of  $S_{10}(k, t)$  with waiting time  $t$ , as a series of snapshots corresponding to the indicated values of  $t$ .

For each snapshot of the static structure factor projections  $S_{lm}(k, t)$ , the solution of Eqs. (4.1)-(4.5) also determines a snapshot of each of the dynamic correlation functions  $F_{lm}(k, \tau; t)$  and  $F_{lm}^S(k, \tau; t)$ . These functions are related with other more intuitive and experimentally accessible properties, such as the time-dependent autocorrelation function  $C_1(\tau; t) \equiv \langle \sum_{i=1}^N \hat{\boldsymbol{\mu}}_i(t + \tau) \cdot \hat{\boldsymbol{\mu}}_i(t) \rangle / \langle \sum_{i=1}^N \hat{\boldsymbol{\mu}}_i(t) \cdot \hat{\boldsymbol{\mu}}_i(t) \rangle$  of the normalized dipole vectors  $\hat{\boldsymbol{\mu}}_i$ . In fact, since our dynamic correlators  $F_{lm}(k, \tau; t)$  and  $F_{lm}^S(k, \tau; t)$  were assumed to be described from the intermolecular  $k$ -frame [10], one can relate them with the time-dependent autocorrelation function  $C_1(\tau; t)$  directly through the following expression [30],

$$C_1(\tau; t) = \frac{1}{3} \lim_{k \rightarrow 0} \sum_{m=-1}^1 F_{1m}^S(k, \tau; t) \quad (4.7)$$

Let us notice that, according to Eq. (4.3), the three terms in the sum on the right hand side of Eq. (4.7),  $F_{10}^S(k, \tau; t)$ ,  $F_{11}^S(k, \tau; t)$  and  $F_{1-1}^S(k, \tau; t)$ , satisfy the same equation of motion (which only depends explicitly on  $l$ ) and contribute exactly in the same manner to the  $\tau$  and  $t$  dependence of  $C_1(\tau; t)$ . Thus,  $C_1(\tau; t)$  summarizes the irreversible time evolution of the orientational dynamics, as illustrated in Fig. 4.1(b) with the snapshots corresponding to the same set of evolution times  $t$  as the snapshots of  $S_{10}(k, t)$  in Fig. 4.1(a). We observe that  $C_1(\tau; t)$  starts from its initial equilibrium value,  $C_1(\tau; t = 0) = C_1^{(eq)}(\tau; \phi, T_i)$  and quickly evolves in a waiting time  $t$  towards  $C_1(\tau; t \rightarrow \infty) = C_1^{(eq)}(k, \tau; \phi, T_f)$ . This indicates that the expected equilibrium state at  $(\phi = 0.2, T_f)$  is reached without impediment and that the orientational dynamics remain ergodic at that state point.

As mentioned before, the structure of Eqs. (4.1)-(4.5) is the same as that of the equations in [29] describing the *spherical* case. Thus, one should not be surprised that the general dynamic and kinetic scenario predicted in both cases will exhibit quite similar patterns. For example, the non-equilibrium evolution described by the sequence of snapshots of  $C_1(\tau; t)$  can be summarized by the evolution of its  $\alpha$ -relaxation time  $\tau_\alpha(t)$ , defined through the condition  $C_1(\tau_\alpha; t) = 1/e$ . In the inset of Fig. 4.1(b) we illustrate the saturation kinetics of the equilibration process in terms of the  $t$ -dependence of  $\tau_\alpha(t)$ , as determined from the sequence of snapshots of  $C_1(\tau_\alpha; t)$  displayed in the figure. Clearly, after a transient stage, in which  $\tau_\alpha(t)$  evolves from its initial value  $\tau_\alpha^{eq}(\phi, T_i)$ , it will eventually saturate to its final equilibrium value  $\tau_\alpha^{eq}(\phi, T_f)$ .

## 4.4 Aging of the System of Interacting Dipoles with Random Fixed Positions

Let us now present the NE-SCGLE description of the second class of irreversible isochoric processes, in which the system starts in an ergodic state but ends in a dynamically arrested state. For this, let us consider now the case in which the system is subjected to a sudden isochoric cooling, at fixed volume fraction  $\phi = 0.2$ , and from the same initial state as before, but this time to the final state point  $(\phi, T_f = 0.095)$  lying inside the region of dynamically arrested states (the second of the two quenches schematically indicated by

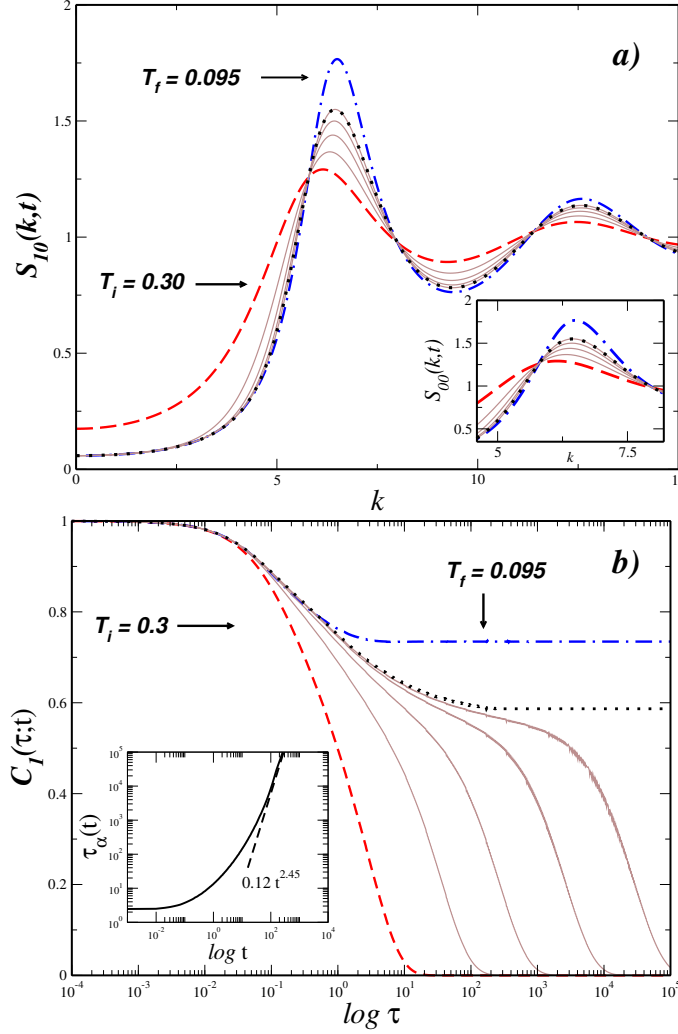


Figure 4.2: Illustration of an aging process: (a) Snapshots of the non-equilibrium time evolution of the  $l = 1, m = 0$  static structure factor projection,  $S_{10}(k, t)$ , corresponding to the isochoric quench  $T_i \rightarrow T_f$  for  $\phi = 0.2$ , with  $T_i = 0.3$  and  $T_f = 0.095$ . The (red) dashed line is the initial structure factor  $S_{10}(k, t = 0) = S_{10}^{(i)}(k)$ . The (blue) dot-dashed line is the (now inaccessible) equilibrium structure factor  $S_{10}^{(eq)}(k; \phi, T_f)$ , whereas the (black) dotted line is the predicted asymptotic limit  $S_{10}(k, t \rightarrow \infty) = S_{10}^{(a)}(k)$ . The sequence of thinner (brown) solid lines in between represents  $S_{10}(k, t)$  for  $t = 1.16, 4.264, 14.056, \text{ and } 150.61$ . (b) Snapshots of the orientational autocorrelation function  $C_1(\tau; t)$  as a function of correlation time  $\tau$  (thin brown solid lines), corresponding to the same isochoric quench and same sequence of waiting times  $t$  as in (a). The (red) dashed line represents the initial function  $C_1(\tau; t = 0) = C_1^{(eq)}(\tau; \phi, T_i)$ , the (blue) dot-dashed line is the expected (but now inaccessible) equilibrium correlation  $C_1^{(eq)}(\tau; \phi, T_f)$ , and the (black) dotted line is the predicted long- $t$  asymptotic limit,  $C_1(\tau; t \rightarrow \infty) = C_1^{(a)}(\tau)$ . The inset plots the corresponding  $\alpha$ -relaxation time as a function of waiting time  $t$ , with the (black) dashed line representing the asymptotic power law  $\tau_\alpha \propto t^{2.45}$ .

the dashed vertical arrows of Fig. (4.5).

Under such conditions, the long-time asymptotic limit of  $S_{lm}(k; t)$  will no longer be the expected equilibrium static structure factor  $S_{lm}^{(eq)}(k; \phi, T_f)$ , but another, well-defined non-stationary structure factor  $S_{lm}^{(a)}(k)$ . In Fig. 4.2(a) we illustrate this behavior with a sequence of snapshots of the non-equilibrium evolution of  $S_{10}(k; t)$  after this isochoric quench at  $\phi = 0.2$  from  $T^{(i)} = 0.3$  to  $T^{(f)} = 0.095$ . There we highlight the initial structure factor  $S_{10}^{(i)}(k) = S_{10}^{(eq)}(k; \phi, T_i)$ , represented by the (red) dashed line and the dynamically arrested long-time asymptotic limit,  $S_{10}^{(a)}(k)$ , of the non-equilibrium evolution of  $S_{10}(k; t)$ , described by the (black) dotted line. For reference, we also plot the expected, but inaccessible, equilibrium static structure factor  $S_{10}^{(eq)}(k; \phi, T_f) \neq S_{10}^{(a)}(k)$  (blue dot-dashed line).

Finally, let us illustrate how this scenario of dynamic arrest manifests itself in the non-equilibrium evolution of the dynamics. We recall that for each snapshot of the non-stationary structure factor  $S_{lm}(k; t)$ , the solution of Eqs. (4.1)-(4.5) also determines a snapshot of all the dynamic properties at the waiting time  $t$ . For example, in Fig. 4.2(b) we present the sequence of snapshots of  $C_1(\tau; t)$ , plotted as a function of correlation time  $\tau$ , that corresponds to the sequence of snapshots of  $S_{10}(k; t)$  in Fig 4.2(a). In this figure we highlight in particular the initial value  $C_1(\tau; t = 0) = C_1^{(eq)}(\tau; \phi, T_i)$  (red dashed line), the predicted non-equilibrium asymptotic limit,  $C_1^{(a)}(\tau) \equiv \lim_{t \rightarrow \infty} C_1(k, \tau; t)$  (black dotted line) and the inaccessible equilibrium value of  $C_1^{(eq)}(\tau; \phi, T_f)$  (blue dot-dashed line). Notice that, in contrast with the equilibration process, in which the long-time asymptotic solution  $C_1^{(eq)}(\tau; \phi, T_f)$  decays to zero within a finite relaxation time  $\tau_\alpha^{eq}(\phi, T_f)$ , in the present case  $C_1^{(eq)}(\tau; \phi, T_f)$  does not decay to zero, but to a finite plateau. This arrested equilibrium correlation function, however, is completely inaccessible, since now the long- $t$  asymptotic limit of  $C_1(k, \tau; t)$  is  $C_1^{(a)}(\tau)$ , which is also a dynamically arrested function, but with a different plateau than  $C_1^{(eq)}(\tau; \phi, T_f)$ .

Just like in the equilibration process, which starts at the same initial state, here we also observe that at  $t = 0$ ,  $C_1(\tau; t)$  shows no trace of dynamic arrest, and that as the waiting time  $t$  increases, the relaxation time increases as well. We can summarize this irreversible evolution of  $C_1(\tau; t)$  by exhibiting the kinetics of the  $\alpha$ -relaxation time  $\tau_\alpha(t)$  extracted from the sequence of snapshots of  $C_1(\tau_\alpha; t)$  in the same figure. This is done in the inset of fig. 4.2(b). Clearly, after the initial transient stage, in which  $\tau_\alpha(t)$  increases from its initial value  $\tau_\alpha^{eq}(\phi, T_i)$  in a similar fashion as in the equilibration case,  $\tau_\alpha(t)$  no longer satu-

rates to any finite stationary value. Instead, it increases with  $t$  without bound, and actually diverges as a power law,  $\tau_\alpha(t) \propto t^a$ , with  $a \approx 2.45$ .

Except for quantitative details, such as the specific value of this exponent, we find a remarkable general similarity between this predicted aging scenario of the dynamic arrest of our system of interacting dipoles, and the corresponding aging scenario of the structural relaxation of a soft-sphere glass-forming liquid described in Ref. [29] (compare, for example, our Fig. 4.2(b), with Fig. 12 of that reference). As mentioned before, however, our intention in this paper is not to discuss the physics behind these similarities and these scenarios, but only to present the theoretical machinery that reveals it.

## 4.5 Crossover from equilibration to aging: Determination of the dynamical arrested diagram

Of course, one could continue describing the predictions of the NE-SCGLE theory regarding the detailed evolution of each relevant structural and dynamic property of the glass-forming system along the process of equilibration or aging. At this point, however, we would like to unite the main results of the previous two sections in a single integrated scenario that provides a more vivid physical picture of the predictions of the present theory. With this intention, we have put together the results for the isochoric evolution of a characteristic dynamical property extracted from the correlation functions, i.e. the  $\alpha$ -time correlation  $\tau_\alpha(t; \eta)$  in terms of the temperature  $T$  (Fig. 4.4), and in terms of the evolution time  $t$  (Fig. 4.3). For both perspectives, we can take a better vision of what we want to show about the dynamical crossover between the two-states taking as an example an isochore  $\eta = 0.2$ , and different temperatures  $T$ . From both examples we take the first observation taking only the slope of the asymptotic limit for the  $\tau_\alpha$  functions, for the values of temperature that equilibrate going to a slope for long times, while the non equilibrium temperatures going to a power law  $\tau_\alpha(T) \approx t^a$  for  $a = 2.45$ , the same qualitative behavior presented in simple repulsive systems just like the WCA-potential system [29].

The ergodic-arrested states that were presented above in the system can be spanned with the quenches methodology taking into account that there exist a series of values of states points  $(\eta, T)$  that make effective the frontier

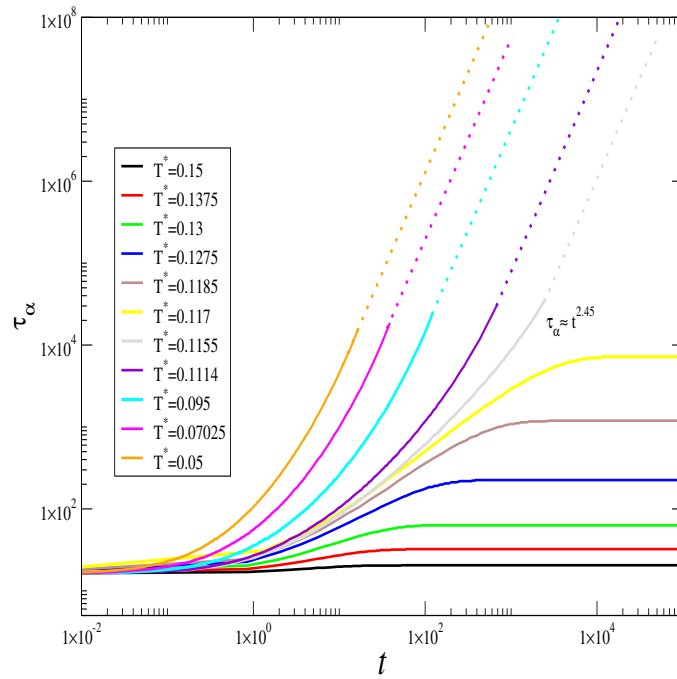


Figure 4.3: Waiting time dependence of the  $\alpha$ -relaxation time  $\tau_\alpha(t; T)$  for a sequence of evolution times after the sudden temperature quench at fixed volume fraction  $\phi$ , from an initial temperature  $T^{(i)}$  to a final temperature  $T^{(f)}$ .

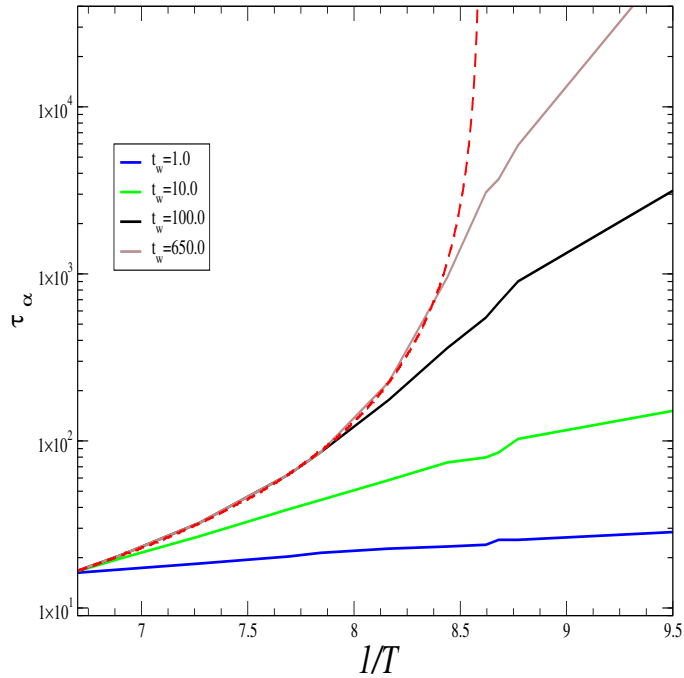


Figure 4.4: Waiting time dependence of the  $\alpha$ -relaxation time  $\tau_\alpha(t; T)$  for a sequence of fixed temperatures. The dashed line is  $\tau_\alpha^{eq}(T) \equiv \lim_{t \rightarrow \infty} \tau_\alpha(t; T)$ , which is the equilibrium  $\alpha$ -relaxation time of the hard-sphere system, predicted by the equilibrium SCGLE theory.

between both regions. If we use the quenches method for a continuum of isochores  $\eta > 0$ , and for each value of the volume fraction, we determine  $T_c$ , then we can obtain the complete dynamical arrest diagram, that for the system presented it is shown in Fig. 4.5. This algorithm for the generation of the dynamical arrested phase diagram can be applied in general for both translational and orientational degrees of freedom. In next Chapter we generalize the numerical methodology of the solution of the non equilibrium SCGLE and we apply it to the well-known dipolar hard sphere system.

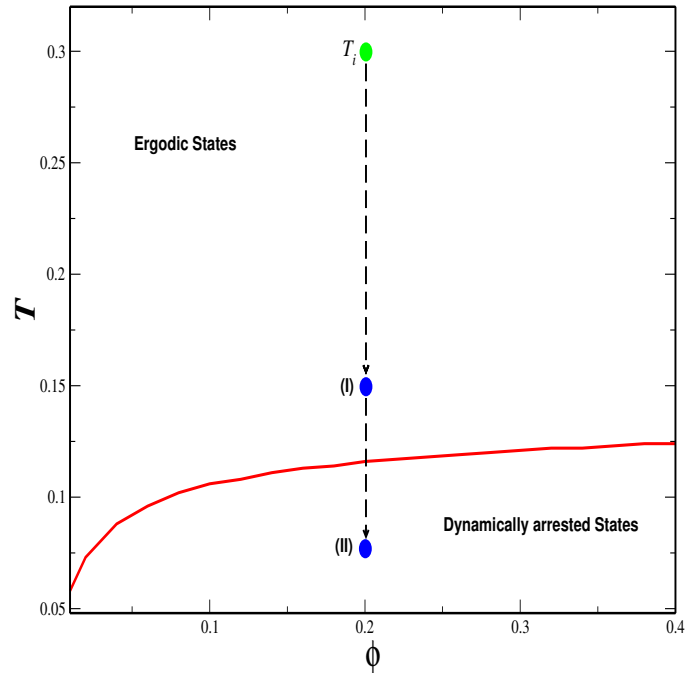


Figure 4.5: Dynamical arrest line (solid curve) in the  $(\phi, T)$  state space of the system of interacting dipoles with fixed positions. This line is the boundary between the region of ergodic states, at which the system is predicted to reach thermodynamic equilibrium, and the predicted region of dynamically arrested states. Each of the two superimposed vertical lines illustrate the quench of the system from an initial temperature  $T_i$  (green dot) to a final temperature  $T_f$  (blue dots), in one case above (I) and in the other case below (II) the dynamic arrest line.



# Non equilibrium phase diagrams of liquids of non-spherical interacting particles.

## Contents

<b>5.1</b>	<b>Mathematical and numerical methodologies . . . . .</b>	<b>46</b>
5.1.1	Formal solution of Eq. (3.19) . . . . .	46
5.1.2	Trajectory $(u_T(t_w), u_R(t_w))$ on the plane $(u_T, u_R)$ : three possible scenarios . . . . .	48
<b>5.2</b>	<b>Illustrative solutions of the NE-SCLGE Equations. . . . .</b>	<b>51</b>
5.2.1	Quenching and crushing the DHS model. . . . .	51
5.2.2	Dynamic arrest diagram of the DHS model. . . . .	53
<b>5.3</b>	<b>Nonequilibrium kinetics of structural and dynamical relaxation. . . . .</b>	<b>54</b>

As we recall in the previous chapter, we can see that the non-equilibrium non-spherical SCGLE theory can arise to us the true behavior of the dynamical properties inside the dynamical arrest region, as the aging phenomena is well described for, for example, time correlation function  $C(t, \tau)$  and the  $\alpha$ -time relaxation for the example described before, that was the liquid of dipolar hard sphere and the translational degrees of freedom were suddenly freezing. In this chapter, we loose the above restriction and we review the main features of the solution of these equations for a few elementary non-equilibrium processes that we can model with the present theory.

## 5.1 Mathematical and numerical methodologies

In this section we briefly discuss the most relevant mathematical and numerical aspects of the strategy of solution of the NE-SCGLE equations (3.19)–(3.25), illustrating some steps with the concrete examples involving the DHS model. It is important to emphasize, however, that the strategy and methods described in this Section will be applicable not only to this illustrative but specific model, but to all other systems within the wider class described by the generic pair potential in Eq. (4.7).

### 5.1.1 Formal solution of Eq. (3.19)

Let us start the description of the general methodological aspects of the solution of the NE-SCGLE equations (3.19)–(3.25) by focusing on the mathematical structure of Eq. (3.19). Defining the functions  $\alpha_{lm}(k) = 2k^2 D_T^0 \mathcal{E}_{lm}(k; T_f)$  and  $\beta_{lm}(k) = l(l+1) D_R^0 \mathcal{E}_{lm}(k; T_f)$ , it is not difficult to show that its formal solution can be written as

$$S_{lm}(k; t_w) = S_{lm}^*(k; u_T(t_w), u_R(t_w)), \quad (5.1)$$

with the function  $S_{lm}^*(k; u_T, u_R)$  given by

$$S_{lm}^*(k; u_T, u_R) = S_{lm}^{(0)}(k) e^{-(\alpha_{lm}(k)u_T + \beta_{lm}(k)u_R)} + \mathcal{E}_{lm}(k; T_f^*)^{-1} [1 - e^{-(\alpha_{lm}(k)u_T + \beta_{lm}(k)u_R)}]. \quad (5.2)$$

In these equations, the functions  $u_T(t_w)$  and  $u_R(t_w)$  play the role of the translational and rotational “material” times [29], defined as

$$u_T(t_w) = \int_0^{t_w} b^T(t'_w) dt'_w \quad (5.3)$$

and

$$u_R(t_w) = \int_0^{t_w} b^R(t'_w) dt'. \quad (5.4)$$

Let us also define the inverse functions

$$t_w(u_T, u_R) = \int_0^{u_T} \frac{du'_T}{b_T^*(u'_T, u'_R)} \quad (5.5)$$

and

$$t_w(u_T, u_R) = \int_0^{u_R} \frac{du'_R}{b_R^*(u'_T, u'_R)}, \quad (5.6)$$

where  $b_T^*(u_T, u_R) \equiv b_T(t_w(u_T, u_R))$  and  $b_R^*(u_T, u_R) \equiv b_R(t_w(u_T, u_R))$ . In order for these two expressions to yield the same value of the actual (*real!*) waiting

time  $t_w$ , it is necessary that not only their right sides coincide, but also that the differential form of this identity holds, so that the relationship

$$dt_w = \frac{du_T}{b_T^*(u_T, u_R)} = \frac{du_R}{b_R^*(u_T, u_R)}, \quad (5.7)$$

must be satisfied along the physical trajectory  $(u_T(t_w), u_R(t_w))$  in the  $(u_T, u_R)$  plane.

To generate this physical trajectory, let us use of Eqs. (5.1) and (5.2) to evaluate  $S_{lm}(k; t_w)$  at a discrete sequence of waiting times  $t_w^{(n)}$  ( $n = 0, 1, 2, \dots$ ), or equivalently, to evaluate  $S_{lm}^*(k; u_T, u_R)$  at the corresponding sequence of points  $(u_T^{(n)}, u_R^{(n)})$  in the plane  $(u_T, u_R)$ , since at each waiting time  $t_w^{(n)}$ , Eqs. (5.3) and (5.4) assign the values  $u_T^{(n)} = u_T(t_w^{(n)})$  and  $u_R^{(n)} = u_R(t_w^{(n)})$  to the material times  $u_T$  and  $u_R$ . In practice, we start by inputting the (given) initial value  $S_{lm}^{(0)}(k)$  of  $S_{lm}(k; t)$  in Eqs. (3.22)-(3.25), whose solution determines  $\Delta\zeta_T^*(\tau; t_w = 0)$  and  $\Delta\zeta_R^*(\tau; t_w = 0)$ , and through Eqs. (3.20)-(3.21), also the initial value  $(b_T^{*(0)}, b_R^{*(0)}) \equiv (b_T(0), b_R(0))$  of the sequence  $(b_T^{*(n)}, b_R^{*(n)}) \equiv (b_T(t_w^{(n)}), b_R(t_w^{(n)}))$ . This is the  $n = 0$  step of the evaluation of the sequence  $S_{lm}(k; t_w^{(n)})$ ,  $b_T(t_w^{(n)})$ ,  $b_R(t_w^{(n)})$  with  $n = 0, 1, 2, \dots$ .

In general, at any subsequent step  $n$ , corresponding to the waiting time  $t_w^{(n)}$ , we first input the value  $S_{lm}(k; t_w^{(n)})$  in Eqs. (3.20)-(3.25), whose solution determines  $b_T(t_w^{(n)})$  and  $b_R(t_w^{(n)})$ , among all the other dynamic properties at time  $t_w^{(n)}$  (or, equivalently, at the point  $(u_T^{(n)}, u_R^{(n)})$  in the plane  $(u_T, u_R)$ ). The next step starts with the arbitrary choice of a sufficiently small increment  $\Delta u_T^{(n)} \equiv u_T^{(n+1)} - u_T^{(n)}$ . Since Eq. (5.7) implies that  $\Delta t_w^{(n)} = \Delta u_T^{(n)} / b_T(t_w^{(n)}) = \Delta u_R^{(n)} / b_R(t_w^{(n)})$  this choice then determines  $\Delta u_R^{(n)} \equiv u_R^{(n+1)} - u_R^{(n)}$  and  $\Delta t_w^{(n)} \equiv t_w^{(n+1)} - t_w^{(n)}$ , thus defining also  $t_w^{(n+1)}$  and the new point  $(u_T^{(n+1)}, u_R^{(n+1)})$  along the real trajectory in the ‘‘material-time’’ plane  $(u_T, u_R)$ . The determination of  $(u_T^{(n+1)}, u_R^{(n+1)})$ , together with Eq. (5.2) allows us to evaluate  $S_{lm}^*(k; u_T^{(n+1)}, u_R^{(n+1)})$ , which we can also label as  $S_{lm}(k; t_w^{(n+1)})$ . This allows us to start the next step of the sequence, by inputting  $S_{lm}(k; t_w^{(n+1)})$  in Eqs. (3.20)-(3.25).

The full solution of the NE-SCGLE equations (3.19)-(3.25) traces the real trajectory of the point  $(u_T(t_w), u_R(t_w))$  on the plane  $(u_T, u_R)$ , as the waiting time proceeds from  $t_w = 0$  to  $t_w = \infty$ . Some general features of this real trajectory can be anticipated from the analysis of the possible long-time asymptotic limits  $b_T^{(a)} \equiv \lim_{t_w \rightarrow \infty} b_T(t_w)$  and  $b_R^{(a)} \equiv \lim_{t_w \rightarrow \infty} b_R(t_w)$  of  $b_T(t_w)$  and  $b_R(t_w)$ .

### 5.1.2 Trajectory $(u_T(t_w), u_R(t_w))$ on the plane $(u_T, u_R)$ : three possible scenarios

If both,  $b_T(t_w)$  and  $b_R(t_w)$ , reach finite values  $b_T^{(a)} = b_T^{(eq)} > 0$  and  $b_R^{(a)} = b_R^{(eq)} > 0$  within a finite time, then Eqs. (5.3) and (5.4) imply that, as  $t_w$  increases from 0 to infinity, the material times will also increase without bound,  $0 \leq u_T \leq \infty$  and  $0 \leq u_R \leq \infty$ , so that the real trajectory will start at the origin,  $(u_T, u_R) = (0, 0)$ , and will end at  $(u_T, u_R) = (\infty, \infty)$ . According to Eqs. (5.1) and (5.2), the system will then be able to reach full equilibrium, characterized by the condition  $S_{lm}(k; t \rightarrow \infty) = [\mathcal{E}_{lm}(k; T_f^*)]^{-1}$ .

If, in contrast, both asymptotic values  $u_T^{(a)}$  and  $u_R^{(a)}$  turn out to be finite, i.e.,  $\lim_{t_w \rightarrow \infty} u_T(t_w) = u_T^{(a)} < \infty$  and  $\lim_{t_w \rightarrow \infty} u_R(t_w) = u_R^{(a)} < \infty$ , the real trajectory will also start at the origin,  $(u_T, u_R) = (0, 0)$ , but now will end at the point  $(u_T, u_R) = (u_T^{(a)}, u_R^{(a)})$ . Under these conditions, according to Eq. (5.2), none of the tensorial components  $S_{lm}(k; t)$  will be able to reach its equilibrium value  $[\mathcal{E}_{lm}(k; T_f^*)]^{-1}$ , but will be trapped in a *fully arrested* (or *fully non-ergodic*) state, whose asymptotic non-equilibrium structure factor will be described by the components

$$S_{lm}^{*(a)}(k) = S_{lm}^{(0)}(k) e^{-(\alpha_{lm}(k)u_T^{(a)} + \beta_{lm}(k)u_R^{(a)})} + \mathcal{E}_{lm}(k; T_f^*)^{-1} \left[ 1 - e^{-(\alpha_{lm}(k)u_T^{(a)} + \beta_{lm}(k)u_R^{(a)})} \right]. \quad (5.8)$$

This, of course, may only occur if both mobilities vanish asymptotically, i.e., if  $b_T^{(a)} = b_R^{(a)} = 0$ .

These two asymptotic scenarios happen to appear when solving Eqs. (3.19) – (3.25) for the dipolar hard sphere fluid within the MSA thermodynamic input described in Chapter 2. Let us imagine for concreteness that this model system, assumed initially at equilibrium at the state point  $(\phi_i, T_i^*) = (0.3, 2.0)$ , is suddenly quenched to a lower final temperature  $T_f^*$ , with the volume fraction constrained to remain constant. Two quenches of this type, that differ only in the depth, are schematically indicated in the inset of Fig. 5.1 by the downward arrows I and II. In the same inset we also indicate two complementary irreversible processes, in which the system, also initially at equilibrium at the same initial state  $(\eta, T_i^*) = (0.3, 2.0)$ , is now instantaneously compressed to a higher volume fraction  $\eta_f$ , with the temperature  $T^*$  constrained to remain constant (horizontal arrows III and IV). For each of these processes, solving Eqs. (3.19)-(3.25) determines the real trajectory of the point  $(u_T(t_w), u_R(t_w))$  on the plane  $(u_T, u_R)$ , as  $t_w$  increases from 0 to infinity.

The resulting trajectories for the shallowest temperature quench (arrow I, corresponding to  $T_f^* = 0.5$ ) and for the shallowest crush (arrow III, corresponding to  $\eta_f = 0.5$ ), illustrate the most common process, namely, full

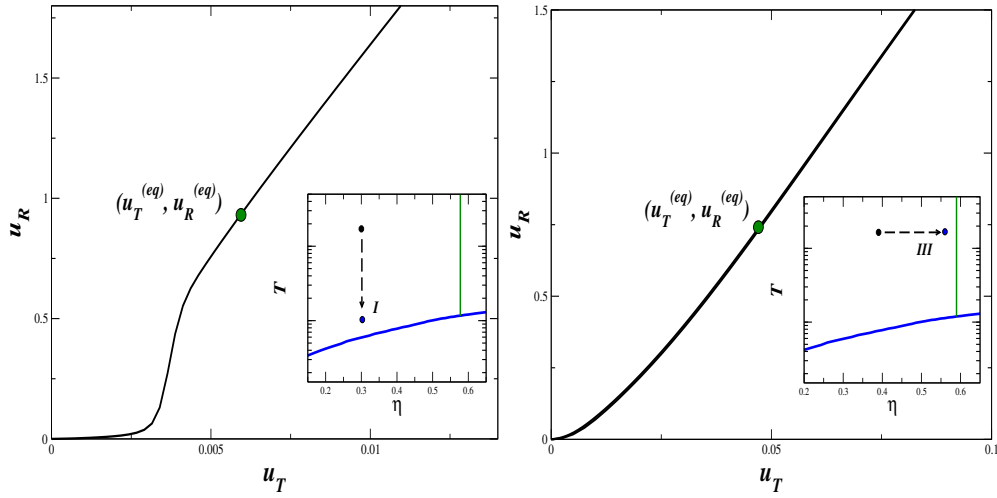


Figure 5.1: Evolution of the “material times”  $(u_T, u_R)$  (a) after a suddenly instantaneous quench of temperature from an initial temperature  $T_i = 2.0$  to a final temperature  $T_f = 0.2$  for a fixed isochores  $\eta = 0.3$ , and (b) after a suddenly instantaneous compression from an initial volume fraction  $\eta_i = 0.3$  to a final volume fraction  $\eta_f = 0.55$  for a fixed temperature  $T^* = 2.0$ . The evolution of these quantities follows the evolution of the relationship in Eq. (5.7), introducing an equally-spaced  $u_T$  grid. For instance, two limit regions can be observed: for initial values of  $u_T$ , we can approximate the  $u$  times relationship to  $u_R \approx (b_T^0/b_R^0)u_T$ , i.e. the first mobilities values immediately after performed the quench; and for long  $u_T$  times, the approximation for  $u_R \approx (b_T^{(eq)}/b_R^{(eq)})u_T$ .

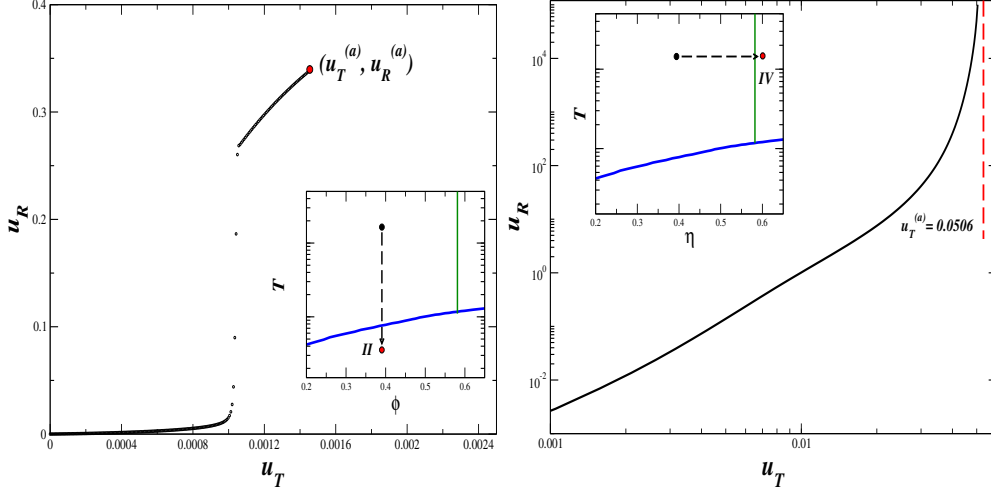


Figure 5.2: (a) Evolution of the “material times”  $(u_T, u_R)$  after a suddenly instantaneous quench of temperature from an initial temperature  $T_i = 2.0$  to a final temperature  $T_f = 0.05$  for a fixed isochore  $\eta = 0.3$ , and (b) after a suddenly instantaneous compression from an initial volume fraction  $\eta_i = 0.3$  to a final volume fraction  $\eta_f = 0.6$  for a fixed temperature  $T^* = 2.0$ . The evolution of these quantities follows the evolution of the relationship in Eq. (5.7), introducing a equally-spaced  $u_T$  grid. For instance, two limit regions can be observed: for initial values of  $u_T$ , we can approximate the  $u$  times relationship to  $u_R \approx (b_T^0/b_R^0)u_T$ , i.e. the first mobilities values immediately after performed the quench; and the for long  $u_T$  times, the approximation for  $u_R \approx (b_T^{(eq)}/b_R^{(eq)})u_T$ .

equilibration, in which both mobilities,  $b_T(t_w)$  and  $b_R(t_w)$ , reach their finite equilibrium values  $b_T^{(eq)} > 0$  and  $b_R^{(eq)} > 0$  at an exponential-like fashion, i.e., within a well-defined finite *equilibration* time  $t_w^{(eq)}$ . After this waiting time,  $u_T(t_w)$  and  $u_R(t_w)$  will increase linearly with  $t_w$  (see Eqs. (5.3) and (5.4)), so that the trajectory  $(u_T(t_w), u_R(t_w))$  will be described at long times by a straight line  $u_R \propto (b_T^{(eq)}/b_R^{(eq)})u_T$ , which will diverge to infinity at long times. These two trajectories, whose asymptotic state is an equilibrium state, are represented in Fig. 5.1.

In contrast, the trajectory corresponding to the deepest temperature quench (vertical arrow II, with  $T_f^* = 0.05$ ) is presented in Fig. 5.2 (a) and illustrates the “fully arrested” or “fully non-ergodic” scenario, in which the long time asymptotic mobilities vanish, and the asymptotic limits of  $u_T(t_w)$  and  $u_R(t_w)$  now attain the finite values  $u_T^{(a)}$  and  $u_R^{(a)}$ . Thus, the trajectory  $(u_T(t_w), u_R(t_w))$  starts at the origin, very much as in the previous case, but now ends at the point  $(u_T^{(a)}, u_R^{(a)})$  ( $= (0.015, 0.34)$  in the present example). In stark contrast

with the equilibration processes, in which the long-time asymptotic value of the mobilities are finite and are attained at an exponential-like fashion (thus defining the concept of “equilibration time”), in the present case, the vanishing of the asymptotic mobilities has profound kinetic implications. The most important is the prediction that the approach to the non-equilibrium fully non-ergodic stationary state is no longer exponential-like. Instead, it occurs at an extremely slower, power-law, fashion, as discussed below in more detail.

Besides these two possibilities (full equilibration and full dynamic arrest) one can identify still a third possibility, in which  $u_T^{(a)}$  turns out to be finite with  $u_R^{(a)}$  being infinite. This is illustrated by the deepest instantaneous crush schematically indicated by the horizontal arrow IV in Fig. 5.3, whose real trajectory, presented in Fig. 5.2 (b), is confined to the subspace  $0 \leq u_T \leq u_T^{(a)} = 0.0506$  and  $0 \leq u_R \leq u_R^{(a)} = \infty$ . In this third possibility  $b_R(t_w)$  will reach a finite asymptotic value  $b_R^{(a)} > 0$ , but  $b_T(t_w)$  will vanish asymptotically. This corresponds to a dynamically-mixed state, in which the translational degrees of freedom will become dynamically arrested, but not the orientational ones.

## 5.2 Illustrative solutions of the NE-SCLGE Equations.

Once the thermodynamic input  $\mathcal{E}_{lm}^{(f)}(k)$  of our model DHS fluid has been provided by the mean spherical approximation (MSA), we can start the numerical solution of the NE-SCGLE equations (3.19)–(3.25). In this section we review the main features of the solution of these equations for a few elementary non-equilibrium processes that we can model with the present theory.

### 5.2.1 Quenching and crushing the DHS model.

For concreteness, in the illustrative examples presented below we shall assume that the system was prepared to be initially at equilibrium at a volume fraction  $\eta_0 = 0.3$  and a temperature  $T_0 = 2.0$ . At  $t_w = 0$  this system is subjected to an instantaneous quench to a lower final temperature  $T_f$ , with the volume fraction constrained to remain constant. Two quenches of this type, that differ only in their depth, are schematically indicated in Fig. 5.3 by the dashed downward arrows I and II.

We shall also consider another idealized manipulation protocol, in which the system, also initially at equilibrium at the same initial state  $(\eta_0, T_0) = (0.3, 2.0)$ , is now instantaneously *compressed* to a higher volume fraction  $\eta_f$ , with the temperature  $T_0$  constrained to remain constant. This process, which

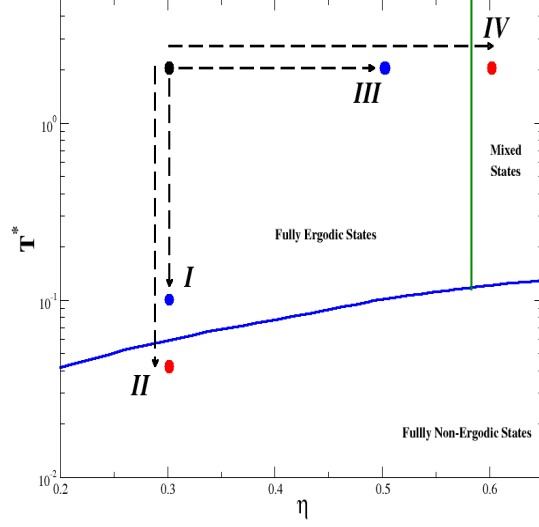


Figure 5.3: State diagram of the dipolar hard sphere fluid. The vertical arrows.

we shall refer to as instantaneous crush, is schematically represented by any of the horizontal arrows III and IV in Fig. 5.3, which then correspond to two instantaneous crushes that only differ in their final volume fraction  $\eta_f$ .

For each of these instantaneous processes, the solution of the NE-SCGLE equations (3.19)-(3.25) will describe the non-equilibrium structural relaxation of the system in terms of the irreversible evolution of the non-equilibrium properties  $S_{lm}(k; t_w)$ ,  $b^T(t_w)$ ,  $b^R(t_w)$ ,  $\Delta\zeta_T^*(\tau; t_w)$ ,  $\Delta\zeta_R^*(\tau; t_w)$ ,  $F_{lm}(k, \tau; t_w)$ , and  $F_{lm}^S(k, \tau; t_w)$  after the described thermal or mechanical instantaneous manipulation. In other words, we are assuming that for waiting times  $t_w > 0$  the system is assumed to be left unperturbed but constrained by the isochoric and isothermal conditions of the final density and temperature.

Let us point out, however, that an instantaneous quench/crush is a convenient representation of real cooling/compressing processes that occur at large cooling/compressing rates. For example, a more realistic cooling protocol could be described by  $T(t_w) = \theta(-\Delta t_w - t_w)T_0 + \theta(\Delta t_w + t_w)\theta(-t_w)[T_f - rt_w] + \theta(t_w)T_f$ , with  $r \equiv (T_0 - T_f)/\Delta t_w$  being a finite cooling rate. If the system was at equilibrium at  $T = T_0$  for  $t_w < -\Delta t_w$ , the initial condition would be  $S_{lm}(k; t_w = -\Delta t_w) = S_{lm}^{eq}(k; \eta_0, T_0) = 1/\mathcal{E}_{lm}^{(f)}(k; \eta_0, T_0)$ , and we would then have to solve the NE-SCGLE equations during the finite transient  $-\Delta t_w < t_w < 0$ , leading to a value of  $S_{lm}(k; t_w = 0)$  different from  $S_{lm}^{eq}(k; \eta_0, T_0) = 1/\mathcal{E}_{lm}^{(f)}(k; \eta_0, T_0)$ .

A fast temperature quench, however, only involves the transfer of molecular kinetic energy, which indeed may be quite fast compared with the configurational restructuring involved in the evolution of  $S_{lm}(k; t_w)$ . Thus, here we

shall neglect this slight difference in the initial value  $S_{lm}(k; t_w = 0)$ , and will use  $S_{lm}(k; t_w = 0) = S_{lm}^{eq}(k; \eta_0, T_0^*) = 1/\mathcal{E}_{lm}^{(f)}(k; \eta_0, T_0)$  as the initial condition, corresponding to the instantaneous isochoric quench. In contrast, an instantaneous crush of a liquid of hard spheres is actually a more severe idealization than the instantaneous temperature quench. However, since the examples that follow are only aimed at illustrating the mathematical and numerical strategy of solution of the NE-SCGLE Eqs. (3.19)–(3.25), here we shall also ignore the effects of the restructuring of the liquid during the transient of a finite compression rate, and will use  $S_{lm}(k; t_w = 0) = S_{lm}^{eq}(k; \eta_0, T_0) = 1/\mathcal{E}_{lm}^{(f)}(k; \eta_0, T_0)$  as the initial condition for the four processes indicated in Fig. 5.3.

### 5.2.2 Dynamic arrest diagram of the DHS model.

In Fig. 5.3 we also include for reference the *dynamic arrest diagram* (or “*non-equilibrium phase diagram*”) of the DHS system in the plane  $(\eta, T)$ . It consists of the three regions bordered by the solid lines, which are the transition lines that separate the region of equilibrium (or “ergodic”) states, from two additional regions, one of them corresponding to fully arrested states and the other one to mixed (or partially arrested) states, in which translational diffusion is arrested but rotational diffusion is not. These non-equilibrium phases were announced by the simple analysis of the possible non-equilibrium stationary solutions of Eq. (3.19) in Chapter 3.

The dynamic arrest lines reproduced in Fig. 5.3, however, were determined in 2015 by Elizondo-Aguilera et al. [10], from the *equilibrium* version of the SCGLE theory, extended to fluids formed by particles interacting through orientation-dependent pair interactions. Such an extension was also developed in the same reference. The corresponding calculation of the dynamic arrest diagram was based on the determination of the non-ergodicity parameters, which are the long- $\tau$  limits of  $\Delta\zeta_T^{*(eq)}(\tau)$ ,  $\Delta\zeta_R^{*(eq)}(\tau)$ ,  $F_{lm;l'm'}^{(eq)}(k, \tau)$ , and  $F_{lm;l'm'}^{S(eq)}(k, \tau)$ , all of which must vanish at equilibrium states. Let us emphasize here that these predictions of the equilibrium SCGLE theory are qualitatively identical to those derived long before, in 1997, using the “non-spherical” version of mode-coupling theory (MCT), by Schilling and Scheidsteger [22], as illustrated in Fig. 1 of Ref. [10]. In particular, both theories predict the existence of the same non-equilibrium phases and the same topology of their corresponding non-equilibrium phase diagram.

Being intrinsically equilibrium theories, MCT and the previously-referred SCGLE theory, cannot describe intrinsically non-equilibrium phenomena such as aging. This limitation is removed by the present non-equilibrium (or NE-SCGLE) theory. Thus, a relevant issue to clarify refers to the exact relationship between the *non-equilibrium* and the *equilibrium* versions of this theory,

and the consistency between their predicted scenarios regarding the dynamic arrested phases of the DHS model liquid. Such a relationship was immediately established in the context of the original NE-SCGLE theory proposed in 2010 by Ramírez-Geonzález and Medina-Noyola [24], which only referred to spherical particles, and it extends without change to the present “non-spherical” context.

For this we mean that the present non-equilibrium theory, represented by Eqs. (3.19)–(3.25), becomes the *equilibrium* SCGLE theory developed in Ref. [?] in the long-time limit  $t_w \rightarrow \infty$  and assuming equilibration, i.e., that  $\lim_{t_w \rightarrow \infty} S_{lm}(k; t_w) = S_{lm}^{(eq)}(k; \bar{n}, T_f) = 1/\mathcal{E}_{lm}^{(f)}(k)$ . In fact, applied to liquids formed by particles interacting through the present kind of non-spherical potentials, the referred equilibrium SCGLE theory, is represented by the set of equations (3.22)–(3.25), with  $S_{lm}(k; t)$  replaced by its equilibrium value  $S_{lm}^{(eq)}(k; \bar{n}, T_f)$ . As we shall see in the appendix, the NE-SCGLE Eqs. (3.19)–(3.25) provides a more powerful method to determine the non-equilibrium phase diagram which, of course, coincides with that in Fig. 5.3. In what follows, however, we shall also illustrate that the present NE-SCGLE theory provides a wealth of additional predictions, such as the non-equilibrium evolution of all the structural and dynamical properties involved in these equations.

### 5.3 Nonequilibrium kinetics of structural and dynamical relaxation.

This section illustrates the predictive capabilities of the NE-SCGLE theory, by describing the scenario that emerges from the full solution of the NE-SCGLE equations corresponding to the elementary instantaneous processes indicated by the four arrows in Fig. 5.3. Let us start by illustrating the irreversible evolution of the most central dynamical properties entering in these equations, namely, the  $t_w$ -dependent tensorial components  $F_{lm}(k, \tau; t_w)$  of the intermediate scattering function, explicitly coupled by Equations (3.19)–(3.25).

The predicted evolution of  $F_{lm}(k, \tau; t_w)$  after the shallow quench (arrow I of Fig. 5.3) of the DHS liquid is presented in Fig. 5.4(a),(b). This set of figures illustrates a typical process of equilibration, in which the system, initially at equilibrium at the state point  $(\eta, T_0) = (0.3, 2.0)$ , is subjected to a (shallow) instantaneous quench to another equilibrium state point, in this case with final temperature  $T_f = 0.1$ , but the same volume fraction  $\eta = 0.3$ . Thus, both functions evolve from their initial value  $F_{00}^{eq}(\eta, T_0)$  and  $F_{10}^{eq}(\eta, T_0)$  to their finite final value  $F_{00}^{eq}(\eta, T_f)$  and  $F_{10}^{eq}(\eta, T_f)$ . The kinetics of this process is quasi-exponential, with these final values fully reached after fairly well-defined equilibration times  $t_T^{eq}$  and  $t_R^{eq}$ . Then, we present the crushing process (arrow

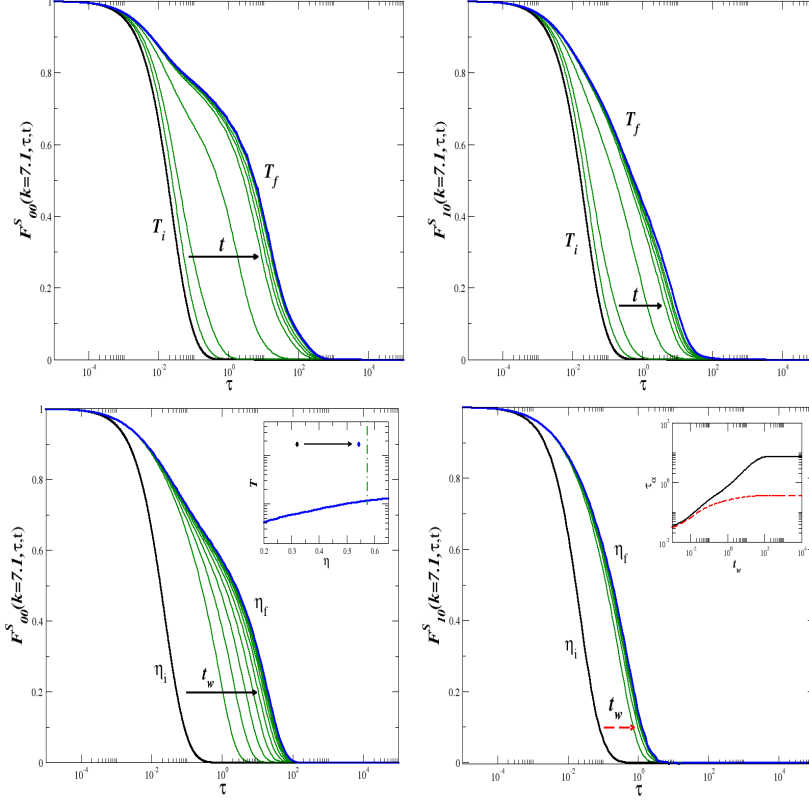


Figure 5.4: Sequence of snapshots of the projections of the intermediate scattering function  $F_{lm}^S(k, \tau; t_w)$  at  $k = 7.1$  plotted as a function of correlation time  $\tau$  for a sequence of values of the waiting time  $t_w$  ( $=0.2, 2.0, 5.0, 12, 20, 32, 60,$  and  $108$ ) after (a,b) the sudden temperature quench at fixed volume fraction  $\eta = 0.3$ , from  $T_i = 2$  to  $T_f = 0.2$ , and after (c,d) the sudden density crushing at fixed temperature  $T = 2.0$ , from  $\eta_i = 0.3$  to  $\eta_f = 0.55$ . The evolution is going from the initial state at  $t_w = 0$  (solid black lines in a) and b) to the final state  $t_w \rightarrow \infty$  (solid blue lines).

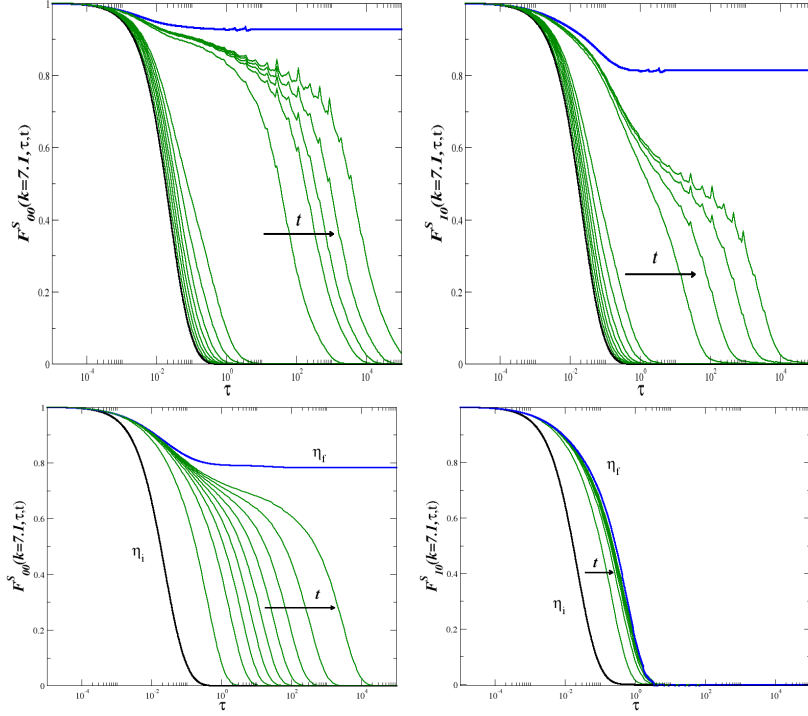


Figure 5.5: Sequence of snapshots of the projections of the intermediate scattering function  $F_{lm}^S(k, \tau; t_w)$  at  $k = 7.1$  [thin solid (green) lines] plotted as a function of correlation time  $\tau$  for a sequence of values of the waiting time  $t_w$  ( $=0.25, 5.6, 106, 400, 590,$  and  $1600$ ) after (a,b) the sudden temperature quench at fixed volume fraction  $\eta = 0.3$ , from  $T_i = 2$  to  $T_f = 0.05$ , and after (c,d) the sudden density crushing at fixed temperature  $T = 2.0$ , from  $\eta_i = 0.3$  to  $\eta_f = 0.6$ . The process start in the initial state (black solid line) and evolves until the asymptotic non equilibrium state at  $t_w \rightarrow \infty$ , that it is not actually the final equilibrium state (blue solid line). These behavior represents the aging phenomena, which is a truly *non-equilibrium* process.

II of Fig. 5.3) in Fig. 5.4(c)-(d), and both functions evolve from their initial value at equilibrium at the state point  $(\eta_0, T_0) = (0.3, 2.0)$ ,  $F_{00}^{eq}(\eta_0, T)$  and  $F_{10}^{eq}(\eta_0, T)$  to their finite final value at  $\eta_f = 0.55$  with the same temperature  $T = 2.0$ ,  $F_{00}^{eq}(\eta_f, T)$  and  $F_{10}^{eq}(\eta_f, T)$ . Both scenarios shown the equilibration process in the fashion of the evolution of “material times” ( $u_T(t_w), u_R(t_w)$ ) showed in previous sections.

On the contrary,  $F_{lm}(k, \tau; t_w)$  after the deep quench (arrow III of Fig. 5.3) of the DHS liquid presented in Fig. 5.5(a),(b) illustrates a truly “non-equilibrium” process, in which the system, initially at equilibrium at the state point  $(\eta, T_0) = (0.3, 2.0)$ , is subjected to a (deep) instantaneous quench to another equilibrium state point, in this case with final temperature  $T_f = 0.05$ ,

---

but the same volume fraction  $\eta = 0.3$ . Thus, both functions evolve from their initial value  $F_{00}^{eq}(\eta, T_0)$  and  $F_{10}^{eq}(\eta, T_0)$  but their finite final value  $F_{00}^{eq}(\eta, T_f)$  and  $F_{10}^{eq}(\eta, T_f)$  are not reaching in a finite waiting time. The kinetics of this process is now in a fashion of law-potency for waiting time, with these final values only reached after fairly well-defined equilibration times  $u_T^{(a)}$  and  $u_R^{(a)}$ . Then, we present the crushing process (arrow IV of Fig. 5.3) in Fig. 5.4(c)-(d), and both functions evolve from their initial value at equilibrium at the state point  $(\eta_0, T_0) = (0.3, 2.0)$ ,  $F_{00}^{eq}(\eta_0, T)$  and  $F_{10}^{eq}(\eta_0, T)$  to their finite final value at  $\eta_f = 0.6$  with the same temperature  $T = 2.0$ .



# Applying the non equilibrium SCGLE approach to a model of a liquid of “Janus-like” interacting particles

## Contents

6.1 Detecting dynamic arrest transition for attractive angle-dependent potential. . . . .	59
6.2 The structure factors $S_{lm}(k; u_\alpha)$ , $S_{lm}^a(k)$ below the instability transition line . . . . .	64

In this chapter, we now discuss the application of the *non equilibrium* SCGLE theory to the description of the non-equilibrium processes involved in an angular-dependent attractive potential as a model for the particular liquid of “Janus”-like colloidal particles, drawing the *non equilibrium* dynamical arrest diagram and the time-dependent non-ergodic parameters  $\gamma_T$  and  $\gamma_R$ .

## 6.1 Detecting dynamic arrest transition for attractive angle-dependent potential.

Following the previous results, we will continue using the SS potential for the simplicity of the expression and the good static information that provides for the SCGLE theory [6]. As a next step, we use a radial potential for the correlation function at (4.7) in the form  $u(r) = -\exp(-r/z)/r$ , i.e. an attractive

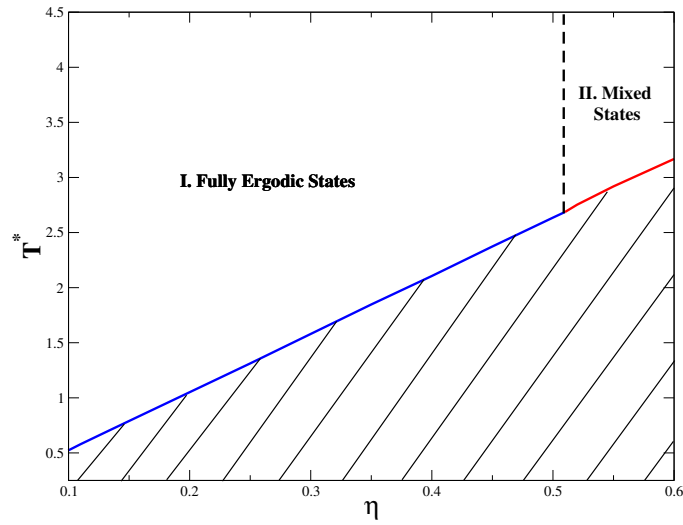


Figure 6.1: Dynamical Arrest diagram for the non spherical model fluid described calculated with the Sharma-Sharma approximation for  $\mathcal{E}_{lm}(k; \bar{n}_{lm}, T^*)$ . Just as the dynamical arrest diagram for dipolar Hard-Sphere system [10], there are three different state regions, calculated from the solution of  $\gamma_{\alpha}^{eq}(T, \phi)$  of the equilibrium “bifurcation equation” (chapter 2), but the region III for “Janus-like” particles is now an instability region and where the solution for  $\gamma_{\alpha}^{eq}(T, \phi)$  is undetermined.

Yukawa potential. We calculated the equilibrium structure factor  $S_{lm}^{eq}$  following with the calculation of the dynamical arrest diagram using the gamma function  $\gamma_{\alpha}^{eq}$ , and the correlation function in  $k$ -space via the SS approximation as

$$\beta u(k) \equiv -(4\pi/T^*) \int_1^{\infty} dr r^2 \times [\sin(kr)/(kr)] u(r), \quad (6.1)$$

We show the resulting diagram in Fig. 6.1. The manner to calculate the frontier of the different arrest regions is different in this case; the transition from the full ergodic region (I) to the shaded region (III) is marked by the divergence at  $k = 0$  of one of the structure factor components,  $S_{10}(k; T^*)$ , for temperatures below the transition curve (blue and red lines), instead of the discontinuity of  $\gamma_{\alpha}^{eq}$ , which is undetermined because of the divergence of the static structure. In order to understand this new phenomenology, we should review the systems of interacting particles by attractive potentials, such as the Lenard-Jones (LJ) potential, which were tested in the same fashion as we previously did, except that the *equilibrium* equilibrium SCGLE theory for spherically-symmetric potentials [6] was used. Inside the thermodynamic unstable (spinodal) region for these attractive systems, the thermodynamic properties such as the static structure factor  $S(k; T)$  is not determined, and as a consequence, the gamma function  $\gamma^{eq}$  is also undetermined. The authors at [6] use the *nonequilibrium* version of the SCGLE theory to provide a manner to overcome this limitation of the equilibrium theory, offering an unexpected scenario of the dynamic arrest present in the early stages of the gas-liquid phase separation. Thus, we will test the recent developed *nonequilibrium* version of the SCGLE theory for non-spherically interacting particles [?] to investigate the phenomenology that could bring us physical information for the regions at the Fig. 6.1.

For such case, we implemented the above protocol to solve the particular problem stated by the intermolecular potential defined in the Eq. (6.1), taking as a reference the equilibrium arrest diagram showed in the Fig. 6.1. From this, we considered the thermodynamical states into the isochores  $\phi < \phi_b$ , which are the volume fractions before the bifurcation point. In particular, we focus our efforts in the forward analysis in a isochore  $\eta = 0.2$ , which it will be the same for any other isochore. The methodology used is as follows: starting to choose a starting fixed point located in the full-ergodic ( $\eta = 0.2, T_i^* = 2.5$ ), then we will sequentially decrease the final temperature  $T_f^*$  in order to calculate the nonstationary structure factor

$$S_{lm}^a(k) \equiv [\mathcal{E}_{lm}(k; T_f^*)]^{-1} + \left[ S_{lm}^{(i)}(k) - [\mathcal{E}_{lm}(k; T_f^*)]^{-1} \right] e^{-(\alpha_{lm}(k)u_T^a + \beta_{lm}(k)u_R^a)}, \quad (6.2)$$

and the asymptotic values of time-dependent non ergodic parameters

$$\frac{1}{\gamma_T} = \frac{1}{6\pi^2 n} \int_0^\infty dk k^4 \sum_l [2l + 1] [1 - S_{l0}^{-1}(k)]^2 S_{l0}(k; u_\varepsilon) f_{l0}^S(k; u_\varepsilon) f_{l0}(k; u_\varepsilon), \quad (6.3)$$

and

$$\begin{aligned} \frac{1}{\gamma_R} = & \frac{1}{16\pi^2 n} \int_0^\infty dk k^2 \sum_{lm} [2l + 1] [S_{l0}(k; u_\varepsilon) - 1]^2 S_{lm}^{-1}(k; u_\varepsilon) \\ & \times f_{l0}^S(k; u_\varepsilon) f_{l0}(k; u_\varepsilon) A_{l,0,m}^2. \end{aligned} \quad (6.4)$$

We shown these in Fig. 6.2 (a)-(b) for a fixed volume fraction  $\eta = 0.2$ , after we performed a serie of instantaneous temperature quench for a initial temperature  $T_i = 2.5$ . We notice for the translational parameters  $\gamma_T^a$  a couple of features that differ drastically of what the same parameters show for the repulsive dipolar hard sphere presented in L. Elizondo work [10]. For instance, the results indicate that  $\gamma_T^a$  and  $u_T^a$  remain infinite for all temperatures above a critical temperature  $T_s$ , and that this specific temperature coincides precisely with the temperature of the thermodynamical instability showed in the "equilibrium" arrest diagram in Fig. 6.1 for the same isochore. This reveals a unexpected conclusion, namely, the blue curve besides of being the threshold of thermodynamic instability, turns to be also the threshold of non-ergodicity. Also, from  $\gamma_T^a$  coming to diverge as  $T$  approach to  $T_s$  from below determines that this transition from ergodic to non- ergodic states occurs in a continuous fashion, i.e., that it is classified as a "type A" dynamic arrest transition in MCT language. Paying attention again in the results showed in Fig. 6.1, but now at temperatures well below the instability curve, we see that the parameter  $\gamma_T^a$  exhibits a discontinuity at a lower temperature  $T = T_g$ . This discontinuity reveals the existence of still a second dynamic arrest transition, now corresponding to a glass-glass "type B" transition, in which the dynamic order parameter  $\gamma_T^a$  (and  $\gamma_R^a$ ) changes discontinuously. Repeating these calculations at other isochores, we determine both transition temperatures  $T_g$  and  $T_s$ , as a function of volume fraction. The corresponding dynamic arrest transition lines are presented in Fig. 6.3.

At first glance, some of these predictions might appear counter intuitive. Let us remind, however, that they are based only on the analysis of the dependence of the dynamic order parameter  $\gamma_T^a$  (and  $\gamma_R^a$ ) on the final temperature

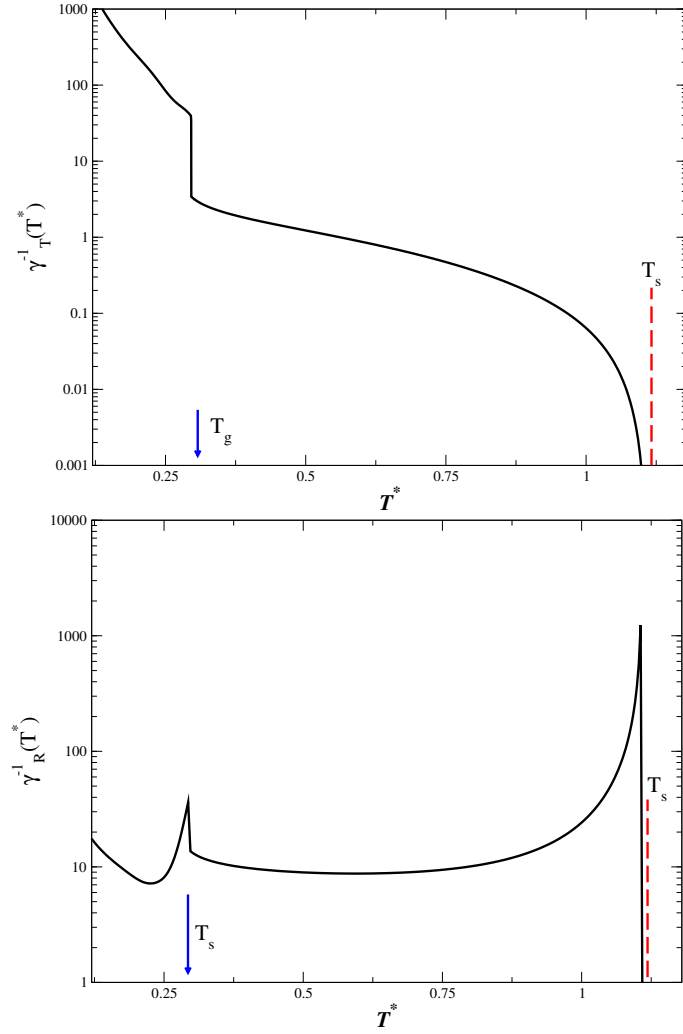


Figure 6.2: (a) Dependence of  $\gamma_T^a(T)$  and (b)  $\gamma_R^a(T)$  on the final temperature  $T_f$  of an instantaneous quench with initial temperature  $T_i = 2.5$  and fixed volume fraction  $\eta = 0.2$ . The discontinuity of the  $\gamma_\varepsilon^a(T)$  at the temperature  $T_g$ .

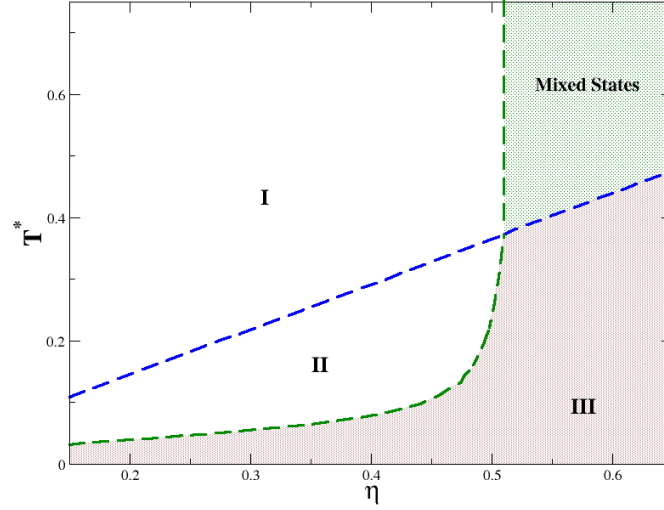


Figure 6.3: Dynamical Arrest diagram for the non-spherical model fluid described by the inter-molecular potential in Eq. (6.1), calculated with the Sharma-Sharma approximation for  $\mathcal{E}_{lm}(k; \bar{n}_{lm}, T^*)$ . The nonequilibrium solution for  $\gamma_\alpha(T, \phi)$  allows us to predict the regions **II** and **III** inside the instability region divided by a borderline, or a “glass-glass” kind transition as we observed in the spinodal region of a spherically-interacting attractive potential [6].

$T$  of the instantaneous isochoric quenches analyzed. This order parameter is a functional of the long-time asymptotic value  $S_{lm}^{(a)}(k)$  of the non-stationary structure factor  $S_{k;t}$ . These properties will be analyzed in the next section.

## 6.2 The structure factors $S_{lm}(k; u_\alpha)$ , $S_{lm}^a(k)$ below the instability transition line

Now we discuss the mechanism that allows the existence of a well-behaved non-equilibrium  $S_{10}(k; u_\alpha)$  for quenches of state points inside what we called the “orientational” spinodal region, where the uniform fluid state has become thermodynamically unstable and the equilibrium structure factor  $S_{10}^{(eq)}(k)$  does not exist. According to Eq. (6.2), the calculation of  $S_{lm}(k; u_\alpha)$  requires the value of the thermodynamic property  $\mathcal{E}_{lm}(k; T)$  for  $k > 0$ . As we know, the condition  $\mathcal{E}_{lm}(k = 0; T) > 0$  is a condition for the stability of uniform thermodynamic states, a condition held for all temperatures  $T$  above the instability temperature  $T_s(\eta)$ . Thus, the instability (“orientational” spinodal) condition  $\mathcal{E}_{lm}(k = 0; T) = 0$  defines the threshold of thermodynamic instability of uni-

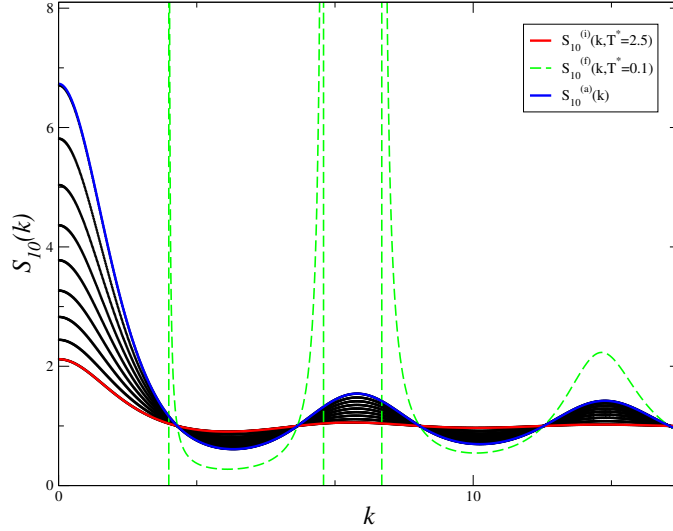


Figure 6.4: Time-evolution of the component  $(1, 0)$  of the structure factor for the system after the application of an instantaneous isochoric quench from the initial temperature  $T_i = 2.5$  (red line) to a final temperature  $T_f = 0.1$  (green dashed-line) that is inside the instability region of the arrest diagram, at the isochore  $\eta = 0.25$ . The blue line corresponds to the asymptotic long-time static structure factor  $S_{10}^a(k)$  of this quench.

form states, so that for all states with temperatures below  $T_s(\eta)$  we must have that  $\mathcal{E}_{lm}(k=0; T) < 0$  not only at  $k=0$ , but also at least within a finite interval  $0 \leq k \leq k_0$ . This means that the equilibrium static structure factor  $S_{10}^{eq}(k; \eta, T) = 1/n\mathcal{E}_{lm}(k; T)$  will attain unphysical negative values in this interval and will exhibit a singularity at  $k = k_0$ . This non-physical behavior, which is a manifestation of the non-existence of spatially uniform equilibrium states into the instability region, is illustrated in Fig. 6.4, which plots the state points  $[n\mathcal{E}_{lm}(k)]^{-1}$  (green and red curve) below the spinodal curve. As we can see in Fig. 6.4, in both cases the non-equilibrium stationary structure factor  $S_{10}^a(k)$  (blue curve) does not exhibit any singular or non-physical feature at any wave-vector. Of course, for the same reason, the non-equilibrium static structure factor  $S_{10}(k; t)$  will evolve smoothly from  $S_{10}^i(k)$  at  $t = 0$ , to  $S_{10}^f$  as  $t \rightarrow \infty$ , without exhibiting any hints of the singular behavior characteristic of the thermodynamic function  $[n\mathcal{E}_{lm}(k)]^{-1}$  below the ‘‘orientational’’ spinodal curve.

In terms of the non-equilibrium structural information, we analyze in detail the dependence of  $S_{10}^a(k)$  on the depth of the quench, i.e., on the final temperature  $T$ , as well as on the volume fraction  $\eta$ . With this intention, in Fig. 6.5

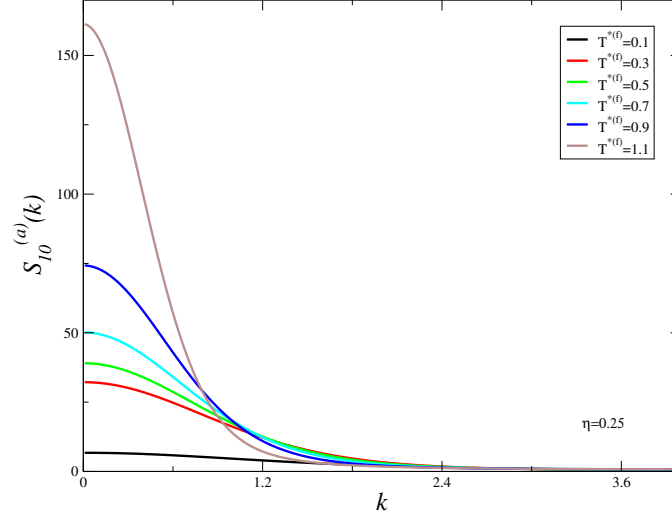


Figure 6.5: The asymptotic long-time static structure factors  $S_{10}^a(k)$  for different instantaneous quenches varying the final temperature  $T_f$ , from a swallow quench near to the instability borderline of the arrest diagram in Fig. 6.3 ( $T_f = 1.1$ ) to a profound quench inside the glass-glass type line.

we present a set of results for  $S_{10}^a(k)$  that illustrate the  $T$ -dependence of this asymptotic structural property for quenches along the isochore  $\eta = 0.25$ . All of these quenches start with the system equilibrated at the same initial temperature  $T_i = 2.5$ . Each quench ends at a different final temperature  $T_f$ , and the solid lines represent the resulting  $S_{10}^a(k; \eta = 0.25, T_f)$ . As we can observe, the magnitude in the value  $S_{10}^a(k = 0; \eta, T_f)$  changes dramatically depending on the deep of the quench, going to a greater value as the quench is nearing the "orientational" spinodal line. This feature in the spherical case for attractive potential [6] is the same except that it presents this growing value of a peak  $S^a(k_{max})$  in  $k > 0$  that is defined as a length scale which measure the size of the growing spatial heterogeneities. In our case, the projection  $S_{10}^a(k = 0; \eta, T_f)$  has not the same interpretation because it is attached not only for the translational but also the rotational structural properties, thus the spatial heterogeneities cannot being extracted only from one of the projections of  $S_{lm}^a(k = 0; \eta, T_f)$ . Further analysis can be made with the dynamical evolution, which is now in construction for the numerical calculations of the complete set of "non equilibrium" SCGLE equations.

# Conclusions

---

In summary, we have proposed the extension of the Self Consistent Generalized Langevin equation theory for systems of nonspherical interacting particles (NS-SCGLE), to consider general nonequilibrium conditions. The main contribution of this work consist in the general theoretical framework, developed in Chapter 3, able to describe the irreversible processes occurring in a given system after a sudden temperature quench, in which its spontaneous evolution in search of a thermodynamic equilibrium state could be interrupted by the appearance of conditions of dynamical arrest for translational or orientational (or both) degrees of freedom.

Our description consists essentially of the coarse-grained time-evolution equations for the spherical-harmonics-projections of the static structure factor of the fluid, which involves one translational and one orientational time-dependent mobility functions. These nonequilibrium mobilities, in turn, are determined from the solution of the nonequilibrium version of the SCGLE equations for the nonstationary dynamic properties (the spherical-harmonics-projections of the self-and collective intermediate scattering functions). The resulting theory is summarized by Eqs. (3.19)- (3.25), which describe the irreversible processes in model liquids of nonspherical particles, within the constraint that the system remains, on the average, spatially uniform. This theoretical framework is now ready to be applied for the description of such nonequilibrium phenomena.

The theoretical formalism derived in chapter 3 was applied in two simple but concise examples, which reveal interesting physical results. The first, described in chapter 4, reveals the two stationary states to which a system out of equilibrium can reach when it is subject to an instantaneous quench of temperature, that is, the process of equilibration and aging, which reveal a kinetic very different between one the other. In addition, it being a system with only orientational degrees of freedom, could be used as a simple model for the

understanding of the slow relaxation phenomena in glasses of spin particles, although the real characteristics of these systems are not within the scope of this thesis.

The second example that we wanted to approach has more relevance given one of the most important motivations of this work, being the simple model of particles with angle-dependent anisotropic interaction. The numerical methodology for the non-equilibrium structure factor is shown in chapter 5, and in chapter 6 this is used to obtain a non-equilibrium phase diagram of these systems, which are a simple model of "Janus"-like particles. It is observed in the phase diagram in the Fig 6.3 the existence of a thermodynamic instability in one of the components of the factor of structure that has the orientational degrees of freedom in a coupled state, which would indicate the formation of heterogeneities, giving rise to gels where the orientations play a very important role, as it happens in some cases of Janus particles. However, it is necessary to be able to calculate the kinetics of these systems, in such a way that a more forceful physical interpretation can be given. The theoretical formalism is now ready to be implemented in more complex systems, so future work is expected to reveal more information.

# Bibliography

- [1] C. A. Angell, K. L. Ngai, G. B. McKenna, P. F. McMillan, and S. W. Martin, “Relaxation in glassforming liquids and amorphous solids,” *Journal of Applied Physics*, vol. 88, no. 6, pp. 3113–3157, 2000. 1
- [2] K. L. Ngai, D. Prevosto, S. Capaccioli, and C. M. Roland, “Guides to solving the glass transition problem,” *Journal of Physics: Condensed Matter*, vol. 20, no. 24, p. 244125, 2008. 1
- [3] A. Walther and A. H. E. Muller, “Janus particles: Synthesis, self-assembly, physical properties, and applications,” *Chemical Reviews*, vol. 113, no. 7, pp. 5194–5261, 2013. PMID: 23557169. 1, 3
- [4] A. Goyal, C. K. Hall, and O. D. Velev, “Phase diagram for stimulus-responsive materials containing dipolar colloidal particles,” *Phys. Rev. E*, vol. 77, p. 031401, Mar 2008. 3
- [5] P. G. de Gennes, “Soft matter,” *Science*, vol. 256, no. 5056, pp. 495–497, 1992. 2
- [6] L. L.-F. José Manuel Olais-Govea and M. Medina-Noyola, “Non-equilibrium theory of arrested spinodal decomposition,” *The Journal of Chemical Physics*, vol. 143, no. 17, p. 174505, 2015. 4, 5, 34, 59, 61, 64, 66
- [7] L. Yeomans-Reyna and M. Medina-Noyola, “Self-consistent generalized langevin equation for colloid dynamics,” *Phys. Rev. E*, vol. 64, p. 066114, Nov 2001. 9
- [8] M. A. Chávez-Rojo and M. Medina-Noyola, “Self-consistent generalized langevin equation for colloidal mixtures,” *Phys. Rev. E*, vol. 72, p. 031107, Sep 2005. 9
- [9] L. Yeomans-Reyna, M. A. Chávez-Rojo, P. E. Ramírez-González, R. Juárez-Maldonado, M. Chávez-Páez, and M. Medina-Noyola, “Dynamic arrest within the self-consistent generalized langevin equation of colloid dynamics,” *Phys. Rev. E*, vol. 76, p. 041504, Oct 2007. 11
- [10] L. F. Elizondo-Aguilera, P. F. Zubieta Rico, H. Ruiz-Estrada, and O. Alarcón-Waess, “Self-consistent generalized langevin-equation theory for liquids of nonspherically interacting particles,” *Phys. Rev. E*, vol. 90, p. 052301, Nov 2014. 11, 13, 14, 15, 16, 18, 19, 20, 21, 36, 53, 60, 62

- 
- [11] M. Medina-Noyola and J. D. Rio-Correa, "The fluctuation-dissipation theorem for non-markov processes and their contractions: The role of the stationarity condition," *Physica A: Statistical Mechanics and its Applications*, vol. 146, no. 3, pp. 483 – 505, 1987. 12, 22
- [12] J. R. D. Copley and S. W. Lovesey, "The dynamic properties of monatomic liquids," *Reports on Progress in Physics*, vol. 38, no. 4, p. 461, 1975. 12
- [13] Y. S. Boon J.L., *Molecular Hydrodynamics*. Dover Publications Inc., 1980. 12, 22
- [14] R. Kubo, "The fluctuation-dissipation theorem," *Reports on Progress in Physics*, vol. 29, no. 1, p. 255, 1966. 12
- [15] R. Zwanzig, "Memory effects in irreversible thermodynamics," *Phys. Rev.*, vol. 124, pp. 983–992, Nov 1961. 12
- [16] H. Mori, "Transport, collective motion, and brownian motion," *Progress of Theoretical Physics*, vol. 33, no. 3, p. 423, 1965. 12
- [17] L. Onsager and S. Machlup, "Fluctuations and irreversible processes," *Phys. Rev.*, vol. 91, pp. 1505–1512, Sep 1953. 12, 22
- [18] S. Machlup and L. Onsager, "Fluctuations and irreversible process. ii. systems with kinetic energy," *Phys. Rev.*, vol. 91, pp. 1512–1515, Sep 1953. 12, 22
- [19] P. Langevin, "On the theory of brownian motion," *Comptes Rendus*, no. 146, p. 530, 1908. 12
- [20] J. w. O.-G. Luis Enrique Sánchez-Díaz, Edilio Lázaro-Lázaro and M. Medina-Noyola, "Non-equilibrium dynamics of glass-forming liquid mixtures," *The Journal of Chemical Physics*, vol. 140, no. 23, p. 234501, 2014. 15
- [21] H.-C. M. and M.-N. M., "Tracer diffusion of nonspherical colloidal particles," *Phys. Rev. E*, vol. 53, pp. R4306–R4309, May 1996. 16
- [22] R. Schilling and T. Scheidsteger, "Mode coupling approach to the ideal glass transition of molecular liquids: Linear molecules," *Phys. Rev. E*, vol. 56, pp. 2932–2949, Sep 1997. 17, 19, 33, 53
- [23] M. S. Wertheim, "Exact solution of the mean spherical model for fluids of hard spheres with permanent electric dipole moments," *The Journal of Chemical Physics*, vol. 55, no. 9, pp. 4291–4298, 1971. 18

- 
- [24] P. Ramírez-González and M. Medina-Noyola, “General nonequilibrium theory of colloid dynamics,” *Phys. Rev. E*, vol. 82, p. 061503, Dec 2010. 21, 22, 23, 25, 54
- [25] L. Onsager, “Reciprocal relations in irreversible processes. i.,” *Phys. Rev.*, vol. 37, pp. 405–426, Feb 1931. 22
- [26] L. Onsager, “Reciprocal relations in irreversible processes. ii.,” *Phys. Rev.*, vol. 38, pp. 2265–2279, Dec 1931. 22
- [27] H. Callen, *Thermodynamics*. John Wiley, 1960. 24, 25
- [28] A. Biltmo and P. Henelius, “Unreachable glass transition in dilute dipolar magnet,” *Nature Communications*, vol. 3, pp. 857 EP –, 05 2012. 31
- [29] S.-D. L. Enrique, R.-G. Pedro, Medina-Noyola, and M. Medina, “Equilibration and aging of dense soft-sphere glass-forming liquids,” *Phys. Rev. E*, vol. 87, p. 052306, May 2013. 34, 37, 40, 46
- [30] L. Fabbian, F. Sciortino, and P. Tartaglia, “Rotational dynamics in a simulated supercooled network-forming liquid,” *Journal of Non-Crystalline Solids*, vol. 235-237, pp. 325 – 330, 1998. 36



---

Theory of equilibration and aging in colloidal fluids of  
non-spherical interacting particles.

**Abstract:** We propose a first principles approach for the description of equilibration and aging phenomena in colloidal fluids constituted by non-spherical interacting particles. For this, we propose a formal extension of the so called non-equilibrium self consistent generalized Langevin equation theory, in order to describe the positional and orientational thermal fluctuations of the local concentration profile  $n(\mathbf{r}, \Omega; t)$  of a suddenly quenched colloidal liquid. The resulting theory provides, thus, the non-equilibrium time evolution of both, the static structure factor and the two-time correlation function of the density fluctuations after an instantaneous quench. The predictive capability of our theory is illustrated with several model system for which we discuss different physical properties. **Keywords:** glass-transition, non-spherical, Langevin.

---

# Equilibration and Aging of Liquids of Non-Spherically Interacting Particles

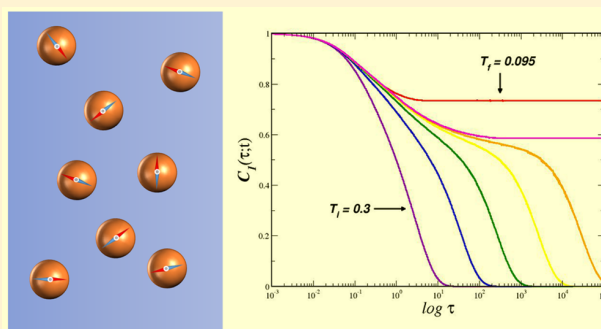
Ernesto C. Cortés-Morales,<sup>†</sup> L. F. Elizondo-Aguilera,<sup>\*,‡,§</sup> and M. Medina-Noyola<sup>†,‡</sup>

<sup>†</sup>Instituto de Física Manuel Sandoval Vallarta, Universidad Autónoma de San Luis Potosí, Alvaro Obregón 64, 78000 San Luis Potosí, SLP, México

<sup>‡</sup>Departamento de Ingeniería Física, División de Ciencias e Ingenierías, Universidad de Guanajuato, Loma del Bosque 103, 37150 León, México

<sup>§</sup>Institut für Materialphysik im Weltraum, Deutsches Zentrum für Luft- und Raumfahrt (DLR), 51170 Köln, Germany

**ABSTRACT:** The nonequilibrium self-consistent generalized Langevin equation theory of irreversible processes in liquids is extended to describe the positional and orientational thermal fluctuations of the instantaneous local concentration profile  $n(\mathbf{r}, \mathbf{\Omega}, t)$  of a suddenly quenched colloidal liquid of particles interacting through nonspherically symmetric pairwise interactions, whose mean value  $\overline{n(\mathbf{r}, \mathbf{\Omega}, t)}$  is constrained to remain uniform and isotropic,  $\overline{n}(\mathbf{r}, \mathbf{\Omega}, t) = \overline{n}(t)$ . Such self-consistent theory is cast in terms of the time-evolution equation of the covariance  $\sigma(t) = \overline{\delta n_{lm}(\mathbf{k}; t) \delta n_{lm}^\dagger(\mathbf{k}; t)}$  of the fluctuations  $\delta n_{lm}(\mathbf{k}; t) = n_{lm}(\mathbf{k}; t) - \overline{n_{lm}(\mathbf{k}; t)}$  of the spherical harmonics projections  $n_{lm}(\mathbf{k}; t)$  of the Fourier transform of  $n(\mathbf{r}, \mathbf{\Omega}, t)$ . The resulting theory describes the nonequilibrium evolution after a sudden temperature quench of both, the static structure factor projections  $S_{lm}(k, t)$  and the two-time correlation function  $F_{lm}(k, \tau; t) \equiv \overline{\delta n_{lm}(\mathbf{k}, t) \delta n_{lm}(\mathbf{k}, t + \tau)}$ , where  $\tau$  is the correlation delay time and  $t$  is the evolution or waiting time after the quench. As a concrete and illustrative application we use the resulting self-consistent equations to describe the irreversible processes of equilibration or aging of the orientational degrees of freedom of a system of strongly interacting classical dipoles with quenched positional disorder.



## I. INTRODUCTION

The fundamental description of dynamically arrested states of matter is a crucial step toward understanding the properties of very common amorphous solid materials such as glasses and gels,<sup>1–3</sup> and of more technologically specialized materials, such as spin glasses.<sup>4–6</sup> The main fundamental challenge posed by these materials derives from their inability to reach thermodynamic equilibrium within experimental times, and from the fact that their properties depend on the protocol of preparation, in obvious contrast with materials that have genuinely attained thermodynamic equilibrium. Understanding the origin of this behavior falls outside the realm of classical and statistical thermodynamics, and must unavoidably be addressed from the perspective of a nonequilibrium theory.<sup>7–9</sup> In fact, a major challenge for statistical physics is to develop a microscopic theory able to predict the properties of glasses and gels in terms not only of the intermolecular forces and applied external fields, but also in terms of the protocol of preparation of the material.

In addressing this challenge, one should start by identifying the most general principles that govern the irreversible evolution of nonequilibrium systems, and to choose the simplest but most fundamental theoretical perspective to be applied to our present context. There is abundant literature summarizing the rich history of the theory of irreversible

processes, which includes a considerable number of more or less general approaches devised to address one aspect or another of the phenomenology of nonequilibrium systems.<sup>7–9</sup> The present work will be based on a nonequilibrium extension of Onsager's theory of thermal fluctuations,<sup>10</sup> which in turn involves a nonequilibrium extension of the so-called generalized Langevin equation (GLE).

Nonequilibrium extensions of the generalized Langevin equation have already been successfully applied to the description of chemical reactions<sup>11,12</sup> and other fluctuation phenomena<sup>13</sup> in nonlinear nonequilibrium systems. Most of these applications, however, focus on the properties of systems with few degrees of freedom (e.g., the generalized position and velocity of a reactant molecule in a nonstationary reservoir<sup>14</sup>), and hence, must still be extended to describe the nonequilibrium kinetics of the collective variables of systems with many degrees of freedom, such as structural glass-forming liquids.

Although not based on nonequilibrium extensions of the GLE, let us also refer to the mean-field theory of the aging

Received: May 8, 2016

Revised: July 15, 2016

Published: July 26, 2016

dynamics of glassy spin systems,<sup>15</sup> which has also made relevant detailed predictions on the nonequilibrium behavior of glassy systems, some of them verified in experiments and simulations. Unfortunately, the models involved lack a geometric structure and hence cannot describe the spatial evolution of real glass formers.

In contrast, the mode coupling theory (MCT) of the glass transition<sup>16,17</sup> provides a *first-principles quantitative* description of the dynamic properties of structural glass forming liquids near their dynamical arrest transition. However, this theory, as well as the equilibrium version of the self-consistent generalized Langevin equation (SCGLE) theory of dynamical arrest,<sup>18,19</sup> are meant to describe the dynamics of *fully equilibrated* liquids. Hence, the phenomenology of the transient time-dependent processes, such as aging, occurring during the amorphous solidification of structural glass formers, falls completely out of the scope of these *equilibrium* theories. Thus, it is important to attempt their extension to describe these nonstationary nonequilibrium structural relaxation processes, which in the end constitute the most fundamental kinetic fingerprint of glassy behavior.

In an attempt to face this challenge, in 2000 Latz<sup>20</sup> proposed a formal nonequilibrium extension of MCT which, however, has not yet found a specific quantitative application. Meanwhile, the SCGLE theory has recently been extended to describe nonstationary nonequilibrium processes in glass-forming liquids.<sup>21,22</sup> The resulting nonequilibrium theory, referred to as the *nonequilibrium* self-consistent generalized Langevin equation (NE-SCGLE) theory, was derived within the fundamental framework provided by a nonstationary extension<sup>10</sup> of Onsager's theory of linear irreversible thermodynamics<sup>23,24</sup> and of time-dependent thermal fluctuations,<sup>25,26</sup> with an adequate extension<sup>27,28</sup> to allow for the description of memory effects.

The NE-SCGLE theory thus derived, aimed at describing nonequilibrium relaxation phenomena in general,<sup>21</sup> leads in particular<sup>22</sup> to a simple and intuitive but generic description of the essential behavior of the nonstationary and nonequilibrium structural relaxation of glass-forming liquids near and beyond its dynamical arrest transition. This was explained in detail in ref 29 in the context of a model liquid of soft-sphere particles. The recent comparison<sup>30</sup> of the predicted scenario with systematic simulation experiments of the equilibration and aging of dense hard-sphere liquids, indicates that the accuracy of these predictions go far beyond the purely qualitative level, thus demonstrating that the NE-SCGLE theory is a successful pioneering first-principles statistical mechanical approach to the description of these fully nonequilibrium phenomena.

As an additional confirmation, let us mention that for model liquids with hard-sphere plus attractive interactions, the NE-SCGLE theory predicts a still richer and more complex scenario, involving the formation of gels and porous glasses by arrested spinodal decomposition.<sup>31,32</sup> As we know, quenching a liquid from supercritical temperatures to a state point inside its gas–liquid spinodal region, normally leads to the full phase separation through a process that starts with the amplification of spatial density fluctuations of certain specific wavelengths.<sup>33–35</sup> Under some conditions, however, this process may be interrupted when the denser phase solidifies as an amorphous sponge-like nonequilibrium bicontinuous structure,<sup>36–40</sup> typical of physical gels.<sup>41</sup> This process is referred to as *arrested* spinodal decomposition, and has been observed in many colloidal systems, including colloid–polymer mixtures,<sup>36</sup>

mixtures of equally sized oppositely charged colloids,<sup>37</sup> lysozyme protein solutions,<sup>38</sup> mono- and bicomponent suspensions of colloids with DNA-mediated attractions,<sup>39</sup> and thermosensitive nanoemulsions.<sup>40</sup> From the theoretical side, it was not clear how to extend the classical theory of spinodal decomposition<sup>33–35</sup> to include the possibility of dynamic arrest, or how to incorporate the characteristic nonstationarity of spinodal decomposition, in existing theories of glassy behavior.<sup>42</sup> In refs 31 and 32 it has been shown that the NE-SCGLE theory provides precisely this missing unifying theoretical framework.

Recently, the NE-SCGLE theory was extended to multi-component systems,<sup>43</sup> thus opening the route to the description of more complex nonequilibrium amorphous states of matter. Until now, however, the NE-SCGLE theory faces the limitation of referring only to liquids of particles with radially symmetric pairwise interparticle forces, thus excluding its direct comparison with the results of important real and simulated experiments involving intrinsically nonspherical particles<sup>44,45</sup> and, in general, particles with nonradially symmetric interactions. The present work constitutes a first step in the direction of extending the NE-SCGLE theory to describe the irreversible evolution of the static and dynamic properties of a Brownian liquid constituted by particles with nonradially symmetric interactions, in which the orientational degrees of freedom are essential.

More concretely, the main purpose of the present paper is to describe the theoretical derivation of the NE-SCGLE time-evolution equations for the spherical harmonics projections  $S_{lm,lm}(k;t)$ ,  $F_{lm,lm}(k,\tau;t)$ , and  $F_{lm,lm}^S(k,\tau;t)$ , of the nonequilibrium and nonstationary static structure factor  $S(\mathbf{k},\Omega;t)$  and of the collective and self-intermediate scattering functions  $F(\mathbf{k},\Omega,\Omega',\tau;t)$  and  $F^S(\mathbf{k},\Omega,\Omega',\tau;t)$ . For this, we start from the same general and fundamental framework provided by the nonstationary extension of Onsager's theory, developed in ref 21 to discuss the spherical case. The result of the present application are eqs 40–46 below, in which  $\tau$  is the delay time, and  $t$  is the evolution (or “waiting”) time after the occurrence of the instantaneous temperature quench. The solution of these equations describe the nonequilibrium (translational and rotational) diffusive processes occurring in a colloidal dispersion after an instantaneous temperature quench, with the most interesting prediction being the aging processes that occur when full equilibration is prevented by conditions of dynamic arrest.

Although this paper only focuses on the theoretical derivation of the NE-SCGLE equations, as an illustration of the possible concrete applications of the extended nonequilibrium theory, here we also solve the resulting equations for one particular system and condition. We refer to a liquid of dipolar hard-spheres (DHS) with fixed positions and subjected to a sudden temperature quench. This is a simple model of the irreversible evolution of the collective orientational degrees of freedom of a system of strongly interacting magnetic dipoles with fixed but random positions. Although this particular application by itself has its own intrinsic relevance in the context of disordered magnetic materials, the main reason to choose it as the illustrative example is that eqs 40–46 describe coupled translational and rotational dynamics, whose particular case  $l = 0$  coincide with the radially symmetric case, already discussed in detail in refs 29, 31, and 43. Thus, the most novel features are to be expected in the nonequilibrium rotational dynamics illustrated in this exercise.

Just like in the case of liquids formed by spherical particles, the development of the NE-SCGLE theory for liquids of nonspherical particles requires the previous development of the *equilibrium* version of the corresponding SCGLE theory. Such an equilibrium SCGLE theory for nonspherical particles, however, was previously developed by Elizondo-Aguilera et al.,<sup>46</sup> following to a large extent the work of Schilling and collaborators<sup>47–49</sup> on the extension of mode coupling theory for this class of systems. Thus, we start our discussions in section II I.A with a brief review of the main elements of the non spherical *equilibrium* SCGLE theory and its application to dynamical arrest in systems formed by colloidal interacting particles with nonspherical potentials.

In section II I.B, we outline the conceptual basis and the main steps involved in the derivation of the nonequilibrium extension of the SCGLE theory for glass-forming liquids of nonspherical particles. In the same section, we summarize the resulting set of self-consistent equations, which constitutes this extended theory. In section III, we introduce a simplified model for interacting dipoles randomly distributed in space and apply our equations to investigate the slow orientational dynamics as well as the aging and equilibration processes of the system near its “spin glass”-like transitions. Finally in section IV we summarize our main conclusions.

## II. THEORETICAL FRAMEWORK

**II.A. Equilibrium SCGLE Theory of Brownian Liquids of Nonspherical Particles.** In this section we briefly describe the equilibrium SCGLE theory of the dynamics of liquids formed by nonspherical particles developed by Elizondo-Aguilera et al.<sup>46</sup> We first briefly review the generalized Langevin equation as a general and fundamental formalism, then define the main properties involved in the description of the dynamics of liquids formed by nonspherical particles, and finally summarize the time-evolution equations that result from this application of the GLE formalism, and which constitute the essence of the equilibrium SCGLE theory. After this review of the equilibrium theory, we shall proceed in the next section to develop its extension to nonequilibrium conditions.

**II.A.1. The Generalized Langevin Equation (GLE) Formalism.** The GLE formalism describes the dynamics of the thermal fluctuations  $\delta a_i(t) \equiv a_i(t) - a_i^{\text{eq}}$  of the instantaneous value of the macroscopic variables  $a_i(t)$  ( $i = 1, 2, \dots, \nu$ ), around their equilibrium value  $a_i^{\text{eq}}$ . It has the structure of a general linear stochastic equation with additive noise for the vector  $\delta \mathbf{a}(t) = [\delta a_1(t), \delta a_2(t), \dots, \delta a_\nu(t)]^\dagger$  (with the dagger indicating transpose), namely,

$$\frac{d\delta \mathbf{a}(t)}{dt} = -\omega \chi^{-1} \delta \mathbf{a}(t) - \int_0^t L(t-t') \chi^{-1} \delta \mathbf{a}(t') dt' + \mathbf{f}(t) \quad (1)$$

In this equation  $\chi$  is the matrix of static correlations,  $\chi_{ij} \equiv \langle \delta a_i(0) \delta a_j^*(0) \rangle$ ,  $\omega$  is an anti-Hermitian matrix,  $\omega_{ij} = -\omega_{ji}^* \equiv \langle \delta \dot{a}_i(0) \delta a_j^*(0) \rangle$  (with  $\langle \dots \rangle$  denoting the average over the initial values  $\delta \mathbf{a}(0)$ ). The matrix  $L(t)$  is determined by the fluctuation–dissipation relation  $L_{ij}(t) = \overline{f_i(t) f_j^*(0)}$ , where  $f_i(t)$  is the  $i$ th component of the vector of random forces  $\mathbf{f}(t)$ , and the overline denotes the average over the realizations of  $\mathbf{f}(t)$ . Besides the selection rules imposed by these symmetry properties of the matrices  $\chi$ ,  $\omega$ , and  $L(t)$ , other selection rules may be imposed by other symmetry conditions. For example,<sup>27</sup> if the variables  $a_i(t)$  have a definite parity upon time reversal,

$a_i(-t) = \lambda_i a_i(t)$  with  $\lambda_i = 1$  or  $-1$ , then  $\omega_{ij} = -\lambda_i \lambda_j \omega_{ji}$  and  $L_{ij}(t) = \lambda_i \lambda_j L_{ji}(t)$ .

Widely used in the early description of thermal fluctuations in simple liquids,<sup>50,51</sup> the GLE was strongly associated with the Zwanzig–Mori projection operator formalism.<sup>52–54</sup> This association, however, obscures the fact that in reality the mathematical structure of the GLE is not a consequence of the Hamiltonian basis of its Zwanzig–Mori’s derivation, nor its validity is restricted to the description of fluctuations around the thermodynamic equilibrium state (as Zwanzig–Mori’s derivation is). Instead, it is not difficult to discover<sup>27</sup> that the mathematical attribute of stationarity is a necessary and sufficient condition for the stochastic time-evolution equation of the fluctuations to have the structure of eq 1. Such an alternative point of view originates from Onsager and Machlup’s theory of thermal fluctuations<sup>25,26</sup> which, in its turn extends the fundamental (mathematical and physical) framework underlying Langevin’s proposal of his celebrated equation.<sup>55</sup>

Onsager and Machlup’s theory constitutes a general phenomenological model of equilibrium fluctuations. Including memory effects in this model is the phenomenological route to the generalized Langevin equation formalism.<sup>51</sup> One important feature of this phenomenological line of reasoning is its remarkable flexibility. Thus, since the essence of this formalism is the mathematical condition of stationarity,<sup>27</sup> and not necessarily the physical condition of thermodynamic equilibrium, it is in principle applicable to describe nonequilibrium stationary states (ss) of matter, as illustrated in the following section. In this section, however, we only consider its application to conventional equilibrium conditions.

**II.A.2. Collective Description of the Translational and Orientational Degrees of Freedom.** Let us start by considering a liquid formed by  $N$  identical nonspherical colloidal particles in a volume  $V$ ,<sup>46</sup> each having mass  $m$  and inertia tensor  $\mathbf{I}$ . The translational degrees of freedom are described by the vectors  $\mathbf{r}^N \equiv (\mathbf{r}_1, \dots, \mathbf{r}_N)$  and  $\mathbf{p}^N \equiv (\mathbf{p}_1, \dots, \mathbf{p}_N)$ , where  $\mathbf{r}_n$  denotes the center-of-mass position vector of the  $n$ th-particle and  $\mathbf{p}_n \equiv m d\mathbf{r}_n/dt = m\mathbf{v}_n(t)$  is the associated linear momentum. Similarly, the orientational degrees of freedom are described by the abstract vectors  $\boldsymbol{\Omega}^N \equiv (\boldsymbol{\Omega}_1, \dots, \boldsymbol{\Omega}_N)$  and  $\mathbf{L}^N \equiv (\mathbf{L}_1, \dots, \mathbf{L}_N)$ , where  $\boldsymbol{\Omega}_n$  denotes the Euler angles, which specify the orientation of the  $n$ th molecule, and  $\mathbf{L}_n = \mathbf{I}(\boldsymbol{\Omega}_n)\boldsymbol{\omega}_n$  is the corresponding angular momentum, so that  $\boldsymbol{\omega}_n$  denotes the angular velocity. Let us now assume that the potential energy  $U(\mathbf{r}^N, \boldsymbol{\Omega}^N)$  of the interparticle interactions is pairwise additivity, i.e., that

$$U(\mathbf{r}^N, \boldsymbol{\Omega}^N) = \sum_{n,n'=1}^N u(\mathbf{r}_n, \mathbf{r}_{n'}; \boldsymbol{\Omega}_n, \boldsymbol{\Omega}_{n'}) \quad (2)$$

where  $u(\mathbf{r}_n, \mathbf{r}_{n'}; \boldsymbol{\Omega}_n, \boldsymbol{\Omega}_{n'})$  is the interaction potential between particles  $n$  and  $n'$ . In the particular case of axially symmetric particles, which we shall have in mind here, the third Euler angle is actually redundant, and hence,  $\boldsymbol{\Omega}_n = \boldsymbol{\Omega}_n(\theta_n, \phi_n)$ .

The most basic observable in terms of which we want to describe the dynamical properties of a nonspherical colloidal system is the time-dependent microscopic one-particle density

$$n(\mathbf{r}, \boldsymbol{\Omega}; t) \equiv (1/\sqrt{N}) \sum_{n=1}^N \delta(\mathbf{r} - \mathbf{r}_n(t)) \delta(\boldsymbol{\Omega} - \boldsymbol{\Omega}_n(t)) \quad (3)$$

Given that  $\mathbf{\Omega} = \mathbf{\Omega}(\theta, \phi)$ , any function  $f(\mathbf{r}, \mathbf{\Omega})$  can be expanded with respect to plane waves and spherical harmonics as

$$f(\mathbf{r}, \mathbf{\Omega}) = \frac{1}{V} \frac{1}{\sqrt{4\pi}} \int d\mathbf{k} \sum_{lm} (i)^l f_{lm}(\mathbf{k}) e^{-i\mathbf{k}\cdot\mathbf{r}} Y_{lm}^*(\mathbf{\Omega}) \quad (4)$$

where

$$f_{lm}(\mathbf{k}) = \sqrt{4\pi} i^l \int_V d\mathbf{r} \int d\mathbf{\Omega} f(\mathbf{r}, \mathbf{\Omega}) e^{-i\mathbf{k}\cdot\mathbf{r}} Y_{lm}(\mathbf{\Omega}) \quad (5)$$

Thus, using eq 3 in eqs 4 and 5, we may define the so-called tensorial density modes

$$n_{lm}(\mathbf{k}, t) = \sqrt{\frac{4\pi}{N}} i^l \sum_{n=1}^N e^{i\mathbf{k}\cdot\mathbf{r}_n(t)} Y_{lm}(\mathbf{\Omega}_n(t)) \quad (6)$$

and hence, we can define the following two-time correlation functions,

$$\begin{aligned} F_{lm;l'm'}(\mathbf{k}, \tau; t) &\equiv \langle \delta n_{lm}^*(\mathbf{k}, t + \tau) \delta n_{l'm'}(\mathbf{k}, t) \rangle \\ &= \frac{4\pi}{N} i^{l-l'} \sum_{n \neq n'}^N \langle e^{i\mathbf{k}\cdot[\mathbf{r}_n(t+\tau) - \mathbf{r}_{n'}(t)]} Y_{lm}^*(\mathbf{\Omega}_n(t + \tau)) Y_{l'm'}(\mathbf{\Omega}_{n'}(t)) \rangle \end{aligned} \quad (7)$$

where  $\delta n_{lm}(\mathbf{k}, t) \equiv n_{lm}(\mathbf{k}, t) - \langle n_{lm}(\mathbf{k}, t) \rangle$ .

We also define for completeness the self-components

$$n_{lm}^S(\mathbf{k}, t) \equiv \sqrt{4\pi} i^l e^{i\mathbf{k}\cdot\mathbf{r}_T(t)} Y_{lm}(\mathbf{\Omega}_T(t)) \quad (8)$$

and the corresponding two-time correlation functions

$$\begin{aligned} F_{lm;l'm'}^S(\mathbf{k}, \tau; t) &\equiv \langle n_{lm}^S(\mathbf{k}, t + \tau) n_{l'm'}^S(\mathbf{k}, t) \rangle \\ &= 4\pi i^{l-l'} \langle e^{i\mathbf{k}\cdot[\mathbf{r}_T(t+\tau) - \mathbf{r}_T(t)]} Y_{lm}(\mathbf{\Omega}_T(t + \tau)) Y_{l'm'}(\mathbf{\Omega}_T(t)) \rangle \end{aligned} \quad (9)$$

where  $\mathbf{r}_T(t)$  denotes the position of the center of mass of any of the particles at time  $t$ , and  $\mathbf{\Omega}_T(t)$  describes its orientation. As indicated before, we will refer to  $\tau$  as the delay (or correlation) time, whereas for  $t$  we refer to the evolution time.

The equal-time value of these correlation functions are  $F_{lm;l'm'}(\mathbf{k}, \tau = 0; t) = S_{lm;l'm'}(\mathbf{k}; t)$  and  $F_{lm;l'm'}^S(\mathbf{k}, \tau = 0; t) = 1$  where  $S_{lm;l'm'}(\mathbf{k}; t)$  are the tensorial components of the static structure factor  $S(\mathbf{k}, \mathbf{\Omega}, \mathbf{\Omega}'; t)$ . Of course, the dependence of these quantities on the evolution time  $t$  is only relevant if the state of the system is not stationary. Under thermodynamic equilibrium,  $F_{lm;l'm'}(\mathbf{k}, \tau; t)$ ,  $F_{lm;l'm'}^S(\mathbf{k}, \tau; t)$ , and  $S_{lm;l'm'}(\mathbf{k}; t)$  cannot depend on  $t$ , and we should denote them as  $F_{lm;l'm'}^{(eq)}(\mathbf{k}, \tau)$ ,  $F_{lm;l'm'}^{S(eq)}(\mathbf{k}, \tau)$ , and  $S_{lm;l'm'}^{(eq)}(\mathbf{k})$ .

**3. Summary of the Equilibrium SCGLE Equations.** Applying the GLE formalism described in Subsection II.A.1, to the dynamical variables  $n_{lm}(\mathbf{k}, t)$  and  $n_{lm}^S(\mathbf{k}, t)$  defined in Subsection II.A.2, one can derive exact memory function equations for  $F_{lm;l'm'}^{(eq)}(\mathbf{k}, \tau)$  and  $F_{lm;l'm'}^{S(eq)}(\mathbf{k}, \tau)$ .<sup>46</sup> These memory function equations require independent determination of the corresponding self- and collective memory functions. In a manner similar to the spherical case, simple Vineyard-like approximate closure relations for these memory functions convert the originally exact equations into a closed self-consistent system of approximate equations for these dynamic properties.<sup>46</sup> The resulting approximate system of equations constitute the extension to liquids of particles interacting through non-spherical pair potentials, of the equilibrium SCGLE theory of the dynamic properties of liquids of spherical particles. These extended equations only involve as an external input the corresponding projections  $S_{lm;l'm'}^{(eq)}(\mathbf{k})$  of the equilibrium static

structure factor. Although for the rest of this section we shall only refer to these equilibrium structural properties, for notational convenience in what follows we shall not write the label (eq).

Let us thus summarize the set of self-consistent equations that constitute the equilibrium SCGLE theory for a Brownian liquid of axially symmetric non spherical particles. In the simplest version (we refer the reader to ref 46 for details), these equations involve only the diagonal elements  $F_{lm}(k, \tau) \equiv F_{lm;lm}(\mathbf{k}, \tau)$  and  $F_{lm}^S(k, \tau) \equiv F_{lm;lm}^S(\mathbf{k}, \tau)$ , and are written, in terms of the corresponding Laplace transforms  $F_{lm}(k, z)$  and  $F_{lm}^S(k, z)$ , as

$$F_{lm}(k, z) = \frac{S_{lm}(k)}{z + \frac{k^2 D_T^0 S_{lm}^{-1}(k)}{1 + \Delta \zeta_T^*(z) \lambda_T^{(lm)}(k)} + \frac{l(l+1) D_R^0 S_{lm}^{-1}(k)}{1 + \Delta \zeta_R^*(z) \lambda_R^{(lm)}(k)}} \quad (10)$$

and

$$F_{lm}^S(k, z) = \frac{1}{z + \frac{k^2 D_T^0}{1 + \Delta \zeta_T^*(z) \lambda_T^{(lm)}(k)} + \frac{l(l+1) D_R^0}{1 + \Delta \zeta_R^*(z) \lambda_R^{(lm)}(k)}} \quad (11)$$

In these equations,  $D_R^0$  is the rotational free-diffusion coefficient, and  $D_T^0$  is the center-of-mass translational free-diffusion coefficient, whereas the functions  $\lambda_T^{(lm)}(k)$  and  $\lambda_R^{(lm)}(k)$  are defined as  $\lambda_T^{(lm)}(k) = 1/[1 + (k/k_c)^2]$  and  $\lambda_R^{(lm)}(k) = 1$ , where  $k_c = \alpha \times k_{\max}$ , with  $k_{\max}$  being the position of the main peak of  $S_{00}(k)$  and  $\alpha = 1.305$ . This ensures that for radially symmetric interactions, we recover the original theory describing liquids of soft and hard spheres.<sup>43</sup>

On the other hand, within well-defined approximations discussed in appendix A of ref 46 the functions  $\Delta \zeta_\alpha^*(\tau)$  ( $\alpha = T, R$ ) may be written as

$$\begin{aligned} \Delta \zeta_T^*(\tau) &= \frac{1}{3} \frac{D_T^0}{(2\pi)^3 n} \int d\mathbf{k} k^2 \sum_l [2l+1] [1 - S_{l0}^{-1}(k)]^2 \\ &\times F_{l0}^S(k; \tau) F_{l0}(k; \tau) \end{aligned} \quad (12)$$

and

$$\begin{aligned} \Delta \zeta_R^*(\tau) &= \frac{1}{2} \frac{D_R^0}{(2\pi)^3} \frac{n}{4} \frac{1}{(4\pi)^2} \int d\mathbf{k} \sum_{l,m} [2l+1] h_{l0}^2(k) \\ &\times [A_{l,0m}]^2 [S_{lm}^{-1}(k)]^2 F_{lm}^S(k; \tau) F_{lm}(k; \tau) \end{aligned} \quad (13)$$

where  $h_{lm}(k)$  denotes the diagonal  $k$ -frame projections of the total correlation function  $h(\mathbf{k}, \mathbf{\Omega}, \mathbf{\Omega}')$ , i.e.,  $h_{lm}(k)$  is related to  $S_{lm}(k)$  by  $S_{lm}(k) = 1 + (n/4\pi) h_{lm}(k)$ , and  $n = N/V$  is the number density. Finally,  $A_{l,mm'} \equiv [C_{lm}^+ \delta_{m+1,m'} + C_{lm}^- \delta_{m-1,m'}]$  and  $C_{lm}^\pm \equiv \sqrt{(l \mp m)(l \pm m + 1)}$ .

Let us mention that, in order to obtain the closed set of eqs 10–13 involving the functions  $F_{lm}(k, \tau)$ ,  $F_{lm}^S(k, \tau)$ ,  $\Delta \zeta_T^*(\tau)$ , and  $\Delta \zeta_R^*(\tau)$ , we have introduced simple first-order Vineyard-like approximations, connecting the collective and self-memory kernels for both translational and rotational dynamics (see eq 42 in ref 46). On their turn, the functions  $\Delta \zeta_T^*(\tau)$  and  $\Delta \zeta_R^*(\tau)$  are, respectively, the translational and rotational memory kernels for the tracer diffusion, which can also be obtained within the GLE formalism.<sup>56</sup> For the main details in determining eqs 12 and 13, the reader is referred to the appendix of ref 46 and the references therein.

Thus, eqs 10–13 constitute the equilibrium non spherical version of the SCGLE theory, whose solution provides the full

time-evolution of the dynamic correlation functions  $F_{lm}(k; \tau)$  and  $F_{lm}^S(k; \tau)$  and of the memory functions  $\Delta\zeta_\alpha^*(\tau)$ . These equations may be numerically solved using standard methods once the projections  $S_{lm}(k)$  of the static structure factor are provided. Under some circumstances, however, one may only be interested in identifying and locating the regions in state space that correspond to the various possible ergodic or nonergodic phases involving the translational and orientational degrees of freedom of a given system. For this purpose, it is possible to derive from the full SCGLE equations the so-called bifurcation equations, i.e., the equations for the long-time stationary solutions of eqs 10–13. These are written in terms of the so-called nonergodicity parameters, defined as

$$f_{lm}(k) \equiv \lim_{\tau \rightarrow \infty} \frac{F_{lm}(k; \tau)}{S_{lm}(k)} \quad (14)$$

$$f_{lm}^S(k) \equiv \lim_{\tau \rightarrow \infty} F_{lm}^S(k; \tau) \quad (15)$$

and

$$\Delta\zeta_\alpha^{*(\infty)} \equiv \lim_{\tau \rightarrow \infty} \Delta\zeta_\alpha^*(\tau) \quad (16)$$

with  $\alpha = T, R$ . The simplest manner to determine these asymptotic solutions is to take the long-time limit of eqs 10–13, leading to a system of coupled equations for  $f_{lm}(k)$ ,  $f_{lm}^S(k)$ , and  $\Delta\zeta_\alpha^{*(\infty)}$ .

It is not difficult to show that the resulting equations can be written as

$$f_{lm}(k) = \frac{[S_{lm}(k)]\lambda_T^{(lm)}(k)\lambda_R^{(lm)}(k)}{S_{lm}(k)\lambda_T^{(lm)}(k)\lambda_R^{(lm)}(k) + k^2\gamma_T\lambda_R^{(lm)}(k) + l(l+1)\gamma_R\lambda_T^{(lm)}(k)} \quad (17)$$

and

$$f_{lm}^S(k) = \frac{\lambda_T^{(lm)}(k)\lambda_R^{(lm)}(k)}{\lambda_T^{(lm)}(k)\lambda_R^{(lm)}(k) + k^2\gamma_T\lambda_R^{(lm)}(k) + l(l+1)\gamma_R\lambda_T^{(lm)}(k)} \quad (18)$$

where the dynamic order parameters  $\gamma_T$  and  $\gamma_R$ , defined as

$$\gamma_\alpha \equiv \frac{D_\alpha^0}{\Delta\zeta_\alpha^{*(\infty)}} \quad (19)$$

are determined from the solution of

$$\frac{1}{\gamma_T} = \frac{1}{6\pi^2 n} \int_0^\infty dk k^4 \sum_l [2l+1][1 - S_{l0}^{-1}(k)]^2 S_{l0}(k) \times f_{l0}^S(k) f_{l0}(k) \quad (20)$$

and

$$\frac{1}{\gamma_R} = \frac{1}{16\pi^2 n} \int_0^\infty dk k^2 \sum_{lm} [2l+1][S_{l0}(k) - 1]^2 S_{lm}^{-1} \times (k) f_{lm}^S(k) f_{lm}(k) A_{l,0m}^2 \quad (21)$$

As discussed in ref 46 fully ergodic states are described by the condition that the nonergodicity parameters (i.e.,  $f_{lm}(k)$ ,  $f_{lm}^S(k)$ , and  $\Delta\zeta_\alpha^{*(\infty)}$ ) are all zero, and hence, the dynamic order parameters  $\gamma_T$  and  $\gamma_R$  are both infinite. Any other possible solution of these bifurcation equations indicate total or partial loss of ergodicity. Thus,  $\gamma_T$  and  $\gamma_R$  finite indicate full dynamic

arrest whereas  $\gamma_T$  finite and  $\gamma_R = \infty$  corresponds to the mixed state in which the translational degrees of freedom are dynamically arrested but not the orientational degrees of freedom.

**II.B. Nonequilibrium Extension.** The main reason for the previous brief review of the SCGLE theory for liquids with nonspherical interparticle interactions, is that this equilibrium theory contains the fundamental ingredients to develop a theoretical description of the genuine nonequilibrium nonstationary irreversible processes characteristic of glassy behavior, such as aging.<sup>21</sup> Let us now outline the conceptual basis and the main steps involved in the derivation of the nonequilibrium version of the SCGLE theory for glass-forming liquids of nonspherical particles, which we shall refer to as the *nonequilibrium* generalized Langevin equation (NE-SCGLE) theory.

**II.B.1. Nonstationary Onsager-Machlup Theory.** As mentioned before, including memory effects in Onsager and Machlup's general model of fluctuations is the phenomenological route to the generalized Langevin equation formalism.<sup>51</sup> One important feature of this phenomenological line of reasoning is its remarkable flexibility. Thus, since the essence of this formalism is the mathematical condition of stationarity,<sup>27</sup> and not necessarily the physical condition of thermodynamic equilibrium, it is in principle applicable to describe nonequilibrium stationary states (ss) of matter. In fact, by modeling a nonstationary stochastic process as a piecewise sequence of stationary processes, this phenomenological framework gave rise to the nonstationary version<sup>21</sup> of Onsager's theory of thermal fluctuations and irreversible processes.<sup>23–26</sup>

In summary, the nonequilibrium version of Onsager's formalism, which we take as our starting point, states that

- (I) the mean value  $\bar{\mathbf{a}}(t)$  of the vector  $\mathbf{a}(t) = [a_1(t), a_2(t), \dots, a_\nu(t)]^\dagger$  formed by the  $\nu$  macroscopic variables that describe the state of the system is the solution of some generally nonlinear equation, represented by

$$\frac{d\bar{\mathbf{a}}(t)}{dt} = \mathcal{R}[\bar{\mathbf{a}}(t)] \quad (22)$$

whose linear version in the vicinity of a stationary state  $\bar{\mathbf{a}}^{\text{ss}}$  (i.e.,  $\mathcal{R}[\bar{\mathbf{a}}^{\text{ss}}] = 0$ ) reads

$$\frac{d\Delta\bar{\mathbf{a}}(t)}{dt} = -\mathcal{L}[\bar{\mathbf{a}}^{\text{ss}}] \cdot \mathcal{E}[\bar{\mathbf{a}}^{\text{ss}}] \cdot \Delta\bar{\mathbf{a}}(t) \quad (23)$$

with  $\Delta\bar{\mathbf{a}}(t) \equiv \bar{\mathbf{a}}(t) - \bar{\mathbf{a}}^{\text{ss}}$ , and that

- (II) the relaxation equation for the  $\nu \times \nu$  covariance matrix  $\sigma(t) \equiv \overline{\delta\mathbf{a}(t)\delta\mathbf{a}^\dagger(t)}$  of the nonstationary fluctuations  $\delta\mathbf{a}(t) \equiv \mathbf{a}(t) - \bar{\mathbf{a}}(t)$  can be written as<sup>21</sup>

$$\frac{d\sigma(t)}{dt} = -\mathcal{L}[\bar{\mathbf{a}}(t)] \cdot \mathcal{E}[\bar{\mathbf{a}}(t)] \cdot \sigma(t) - \sigma(t) \cdot \mathcal{E}[\bar{\mathbf{a}}(t)] \cdot \mathcal{L}^\dagger[\bar{\mathbf{a}}(t)] + (\mathcal{L}[\bar{\mathbf{a}}(t)] + \mathcal{L}^\dagger[\bar{\mathbf{a}}(t)]) \quad (24)$$

In these equations  $\mathcal{L}[\mathbf{a}]$  is a  $\nu \times \nu$  "kinetic" matrix, defined in terms of  $\mathcal{R}[\mathbf{a}]$  as  $\mathcal{L}[\mathbf{a}] \equiv -(\partial\mathcal{R}[\mathbf{a}]/\partial\mathbf{a}) \cdot \mathcal{E}^{-1}[\mathbf{a}]$ , whereas  $\mathcal{E}[\mathbf{a}]$  is the  $\nu \times \nu$  thermodynamic ("stability") matrix, defined as

$$\mathcal{E}_{ij}[\mathbf{a}] \equiv -\frac{1}{k_B} \left( \frac{\partial^2 S[\mathbf{a}]}{\partial a_i \partial a_j} \right) = - \left( \frac{\partial F[\mathbf{a}]}{\partial a_j} \right) \quad (i, j = 1, 2, \dots, \nu) \quad (25)$$

with  $S[\mathbf{a}]$  being the entropy and  $F_j[\mathbf{a}] \equiv k_B^{-1} (\partial S[\mathbf{a}]/\partial a_j)$  the conjugate intensive variable associated with  $a_j$ . The function  $S = S[\mathbf{a}]$ , which assigns a value of the entropy  $S$  to any possible state point  $\mathbf{a}$  in the state space of the system, is thus the so-called fundamental thermodynamic relation,<sup>57</sup> and constitutes the most important and fundamental external input of the nonequilibrium theory. The previous equations, however, do not explicitly require the function  $S = S[\mathbf{a}]$ , but only its second derivatives defining the stability matrix  $\mathcal{E}[\mathbf{a}]$ . The most important property of the matrix  $\mathcal{E}[\mathbf{a}]$  is that its inverse is the covariance of the equilibrium fluctuations, i.e.,

$$\mathcal{E}[\bar{\mathbf{a}}^{\text{eq}}] \cdot \sigma^{\text{eq}} = I \quad (26)$$

with  $\sigma_{ij}^{\text{eq}} \equiv \overline{\delta a_i \delta a_j^{\text{eq}}}$ , where the average is taken with the probability distribution  $P^{\text{eq}}[\mathbf{a}]$  of the equilibrium ensemble.

In addition, the nonequilibrium version of Onsager's formalism introduces the globally nonstationary (but locally stationary) extension<sup>21</sup> of the generalized Langevin equation for the stochastic variables  $\delta a_i(t + \tau) \equiv a_i(t + \tau) - \bar{a}_i(t)$ ,<sup>21</sup>

$$\begin{aligned} \frac{\partial \delta \mathbf{a}(t + \tau)}{\partial \tau} &= -\omega[\bar{\mathbf{a}}(t)] \cdot \sigma^{-1}(t) \cdot \delta \mathbf{a}(t + \tau) \\ &- \int_0^\tau dt' \gamma[\tau - t'; \bar{\mathbf{a}}(t)] \cdot \sigma^{-1}(t) \cdot \delta \mathbf{a}(t + t') + \mathbf{f}(t + \tau) \end{aligned} \quad (27)$$

where the random term  $\mathbf{f}(t + \tau)$  has zero mean and two-time correlation function given by the fluctuation–dissipation relation  $\langle \mathbf{f}(t + \tau) \mathbf{f}(t + \tau') \rangle = \gamma[\tau - \tau'; \bar{\mathbf{a}}(t)]$ . From this equation one derives the time-evolution equation for the nonstationary time-correlation matrix  $C(\tau; t) \equiv \overline{\delta \mathbf{a}(t + \tau) \delta \mathbf{a}^\dagger(t)}$ , reading

$$\begin{aligned} \frac{\partial C(\tau; t)}{\partial \tau} &= -\omega[\bar{\mathbf{a}}(t)] \cdot \sigma^{-1}(t) \cdot C(\tau; t) \\ &- \int_0^\tau dt' \gamma[\tau - t'; \bar{\mathbf{a}}(t)] \cdot \sigma^{-1}(t) \cdot C(t'; t) \end{aligned} \quad (28)$$

whose initial condition is  $C(\tau = 0; t) = \sigma(t)$ . In these equations,  $\omega[\mathbf{a}]$  represents conservative (mechanical, geometrical, or streaming) relaxation processes, and is just the antisymmetric part of  $\mathcal{L}[\mathbf{a}]$ , i.e.,  $\omega[\mathbf{a}] = (\mathcal{L}[\mathbf{a}] - \mathcal{L}^\dagger[\mathbf{a}])/2$ . The memory function  $\gamma[\tau; \bar{\mathbf{a}}(t)]$ , on the other hand, summarizes the effects of all the complex dissipative irreversible processes taking place in the system.

Taking the Laplace transform (LT) of eq 28 to integrate out the variable  $\tau$  in favor of the variable  $z$ , rewrites this equation as

$$C(z; t) = \{z\mathbf{I} + \mathbf{L}[z; \bar{\mathbf{a}}(t)] \cdot \sigma^{-1}(t)\}^{-1} \cdot C(\tau = 0; t) \quad (29)$$

with  $\mathbf{L}[z; \bar{\mathbf{a}}(t)]$  being the LT of

$$\mathbf{L}[\tau; \bar{\mathbf{a}}(t)] \equiv 2\delta(\tau)\omega[\bar{\mathbf{a}}(t)] + \gamma[\tau; \bar{\mathbf{a}}(t)] \quad (30)$$

To avoid confusion, let us mention that  $\mathbf{L}[z; \bar{\mathbf{a}}(t)]$  thus defined is not, of course, an angular momentum. In terms of  $\mathbf{L}[z; \bar{\mathbf{a}}(t)]$ , the phenomenological “kinetic” matrix  $\mathcal{L}[\bar{\mathbf{a}}(t)]$  appearing in eq 24, is given by the following relation

$$\begin{aligned} \mathcal{L}[\bar{\mathbf{a}}(t)] &= \mathbf{L}[z = 0; \bar{\mathbf{a}}(t)] \equiv \omega[\bar{\mathbf{a}}(t)] \\ &+ \int_0^\infty dt' \gamma[\tau; \bar{\mathbf{a}}(t)] \end{aligned} \quad (31)$$

which extends to nonequilibrium conditions the well-known Kubo formula. The exact determination of  $\gamma[\tau; \bar{\mathbf{a}}]$  is perhaps

impossible except in specific cases or limits; otherwise one must resort to approximations. These may have the form of a closure relation expressing  $\gamma[\tau; \bar{\mathbf{a}}(t)]$  in terms of the two-time correlation matrix  $C(\tau; t)$  itself, giving rise to a self-consistent system of equations, as we illustrate in the application below.

**II.B.2. Application to the Derivation of the NE-SCGLE Equations for Nonspherical Particles.** These general and abstract concepts have specific and concrete manifestations, which we now discuss in the particular context of the description of nonequilibrium diffusive processes in colloidal dispersions. For this, let us identify the abstract state variables  $a_i$  with the number concentration  $a_{r,\Omega} \equiv N_{r,\Omega}/\Delta V$  of particles with orientation  $\Omega$  in the  $r$ th cell of an imaginary partitioning of the volume occupied by the liquid in  $C$  cells of volume  $\Delta V$ . In the continuum limit, the components of the state vector  $\mathbf{a}(t)$  then become the microscopic local concentration profile  $n(\mathbf{r}, \Omega; t)$  defined in eq 3 and the fundamental thermodynamic relation  $S = S[\mathbf{a}]$  (which assigns a value of the entropy  $S$  to any point  $\mathbf{a}$  of the thermodynamic state space<sup>57</sup>) becomes the functional dependence  $S = S[\mathbf{n}]$  of the entropy (or equivalently, of the free energy) on the local concentration profile  $n(\mathbf{r}, \Omega; t)$ .

Using this identification in eqs 22 and (24) leads to the time evolution equations for the mean value  $\bar{n}(\mathbf{r}, \Omega; t)$  and for the covariance  $\sigma(\mathbf{r}, \Omega; \mathbf{r}'\Omega'; t) \equiv \overline{\delta n(\mathbf{r}, \Omega; t) \delta n(\mathbf{r}', \Omega'; t)}$  of the fluctuations  $\delta n(\mathbf{r}, \Omega; t) = n(\mathbf{r}, \Omega; t) - \bar{n}(\mathbf{r}, \Omega; t)$  of the local concentration profile  $n(\mathbf{r}, \Omega; t)$ . These two equations are the nonspherical extensions of eqs 3.6 and 3.8 of ref 21, which are coupled between them through two (translational and rotational) local mobility functions,  $b^T(\mathbf{r}, \Omega; t)$  and  $b^R(\mathbf{r}, \Omega; t)$ , which in their turn, can be written approximately in terms of the two-time correlation function  $C(\mathbf{r}, \Omega; \mathbf{r}'\Omega'; t, t') \equiv \overline{\delta n(\mathbf{r}, \Omega; t) \delta n(\mathbf{r}', \Omega'; t')}$ . A set of well-defined approximations on the memory function of  $C(\mathbf{r}, \Omega; \mathbf{r}'\Omega'; t, t')$ , which extends to nonspherical particles those described in ref 21 in the context of spherical particles, results in the referred NE-SCGLE theory.

Rather than discussing these general NE-SCGLE equations, let us now write them explicitly as they apply to a more specific (but still generic) phenomenon, namely, to a glass-forming liquid of nonspherical particles subjected to a programmed cooling while constrained to remain spatially homogeneous and isotropic with fixed number density  $\bar{n}$ . Thus, rather than solving the time-evolution equation for  $\bar{n}(\mathbf{r}, \Omega; t)$ , we have that  $\bar{n}(\mathbf{r}, \Omega; t) = \bar{n}$  now becomes a control parameter. As a result, we only have to solve the time-evolution equation for the covariance  $\sigma(\mathbf{r}, \Omega; \mathbf{r}'\Omega'; t) = \sigma(\mathbf{r} - \mathbf{r}', \Omega, \Omega'; t)$ . Furthermore, let us only consider the simplest cooling protocol, namely, the instantaneous temperature quench at  $t = 0$  from an arbitrary initial temperature  $T_i$  to a final value  $T_f$ .

At this point, let us notice that it is actually more practical to identify the abstract vector  $\mathbf{a}(t) = [a_1(t), a_2(t), \dots, a_\nu(t)]^\dagger$  of state variables not with the local concentration  $n(\mathbf{r}, \Omega; t)$  itself, but with only one of its tensorial modes, so that  $\mathbf{a}(t) = [a_1(t)]$ , with  $a_1 \equiv n_{\text{lm}}(\mathbf{k}, t)$ , defined in eq 6. Under these conditions, the corresponding nonstationary covariance  $\sigma(t)$  is just a scalar, denoted by  $S_{\text{lm}}(k, t)$ , and defined as

$$\sigma(t) = S_{\text{lm}}(k, t) \equiv \overline{\delta n_{\text{lm}}^*(\mathbf{k}, t) \delta n_{\text{lm}}(\mathbf{k}, t)} \quad (32)$$

with  $\delta n_{\text{lm}}(\mathbf{k}, t) \equiv n_{\text{lm}}(\mathbf{k}, t) - \bar{n}_{\text{lm}}(\mathbf{k}, t)$ . In other words,  $S_{\text{lm}}(k, t)$  is a diagonal element of the matrix  $S_{\text{lm},l'm'}(k, t) \equiv \overline{\delta n_{\text{lm}}^*(\mathbf{k}, t) \delta n_{l'm'}(\mathbf{k}, t)}$ . The time-evolution equa-

tion of  $S_{lm}(k,t)$  then follows from identifying all the elements of eq 24.

The first of such elements is the thermodynamic matrix  $\mathcal{E}[\mathbf{a}]$ , which in this case is also a scalar, that we shall denote by  $\mathcal{E}_{lm}[n_{lm}(\mathbf{k})]$ . It is defined in terms of the second derivative of the entropy  $S[n_{lm}(\mathbf{k})]$  (in a contracted description in which the only explicit macroscopic variable is  $n_{lm}(\mathbf{k})$ ) as

$$\mathcal{E}_{lm}[n_{lm}(\mathbf{k})] \equiv -\frac{1}{k_B} \left( \frac{d^2 S[n_{lm}(\mathbf{k})]}{dn_{lm}^2(\mathbf{k})} \right) \quad (33)$$

According to eq 26, this thermodynamic property is just the inverse of the equilibrium value of  $S_{lm}^{\text{eq}}(k) \equiv \overline{\delta n_{lm}^*(\mathbf{k}) \delta n_{lm}(\mathbf{k})}^{\text{eq}}$  of  $S_{lm}(k,t)$ ,

$$\mathcal{E}_{lm}[n_{lm}(\mathbf{k})] = 1/S_{lm}^{\text{eq}}(k) \quad (34)$$

Let us notice, however, that  $\mathcal{E}_{lm}[n_{lm}(\mathbf{k})]$  is not just the diagonal element of the matrix  $\mathcal{E}_{lm,l'm'}[n]$ , defined in terms of the second partial derivative of the entropy  $S[n]$  (in a noncontracted description in which the explicit macroscopic variables are all the tensorial density modes  $n_{lm}(\mathbf{k})$  of the microscopic one-particle density  $n(\mathbf{r},\Omega;t)$ ) as

$$\mathcal{E}_{lm,l'm'}[n] \equiv -\frac{1}{k_B} \left( \frac{\partial^2 S[n]}{\partial n_{lm}(\mathbf{k}) \partial n_{l'm'}(\mathbf{k})} \right) \quad (35)$$

However, according again to eq 26, the inverse of this matrix yields the full equilibrium covariance  $S_{lm,l'm'}^{\text{eq}}(k) \equiv \overline{\delta n_{lm}^*(\mathbf{k}) \delta n_{l'm'}(\mathbf{k})}^{\text{eq}}$ , whose diagonal elements determine  $\mathcal{E}_{lm}[n_{lm}(\mathbf{k})]$ , according to eq 34. Let us mention, however, that in reality  $\mathcal{E}_{lm}[n_{lm}(\mathbf{k})]$  is also a functional of the spatially nonuniform local temperature field  $T(\mathbf{r})$ . To indicate this dependence more explicitly we shall denote the thermodynamic matrix as  $\mathcal{E}_{lm}[n_{lm}(\mathbf{k}); T]$ . Here, however, we shall impose the constraint that at any instant the system is thermally uniform,  $T(\mathbf{r}) = T$ , and instantaneously adjusted to the reservoir temperature  $T$ , which will then be a (possibly time-dependent) control parameter  $T(t)$ .

The second element of eq 24 that we must identify is the kinetic matrix  $\mathcal{L}[\mathbf{a}]$ . For this, let us first compare the equilibrium version of eq 29, namely,

$$C(z) = \{z\mathbf{I} + \mathbf{L}[z; \bar{\mathbf{a}}] \cdot \sigma^{-1}\}^{-1} \cdot \sigma \quad (36)$$

with its particular case in eq 10, in which the scalars  $F_{lm}(k,z)$  and  $S_{lm}(k)$  correspond, respectively, to  $C(z)$  and  $\sigma$ . This comparison allows us to identify  $\mathbf{L}[z; \bar{\mathbf{a}}]$  with the scalar

$$\left[ \frac{k^2 D_T^0}{1 + \Delta \zeta_T^*(z) \lambda_T^{(lm)}(k)} + \frac{l(l+1) D_R^0}{1 + \Delta \zeta_R^*(z) \lambda_R^{(lm)}(k)} \right] \quad (37)$$

Extending this identification to nonstationary conditions, we have that

$$\mathbf{L}[z; \bar{\mathbf{a}}(t)] = \left[ \frac{k^2 D_T^0}{1 + \Delta \zeta_T^*(z; t) \lambda_T^{(lm)}(k; t)} + \frac{l(l+1) D_R^0}{1 + \Delta \zeta_R^*(z; t) \lambda_R^{(lm)}(k; t)} \right] \quad (38)$$

where the functions  $\lambda_R^{(lm)}(k;t)$  are defined as unity and the functions  $\lambda_T^{(lm)}(k;t)$  as  $\lambda_T^{(lm)}(k;t) = 1/[1 + (k/k_c(t))^2]$ , where  $k_c = 1.305 \times k_{\text{max}}(t)$ , with  $k_{\text{max}}(t)$  being the position of the main

peak of  $S_{00}(k;t)$ . The functions  $\Delta \zeta_T^*(z;t)$  and  $\Delta \zeta_R^*(z;t)$ , to be defined below, are the nonstationary versions of the functions  $\Delta \zeta_T^*(z)$ , and  $\Delta \zeta_R^*(z)$ .

Since  $\mathcal{L}[\bar{\mathbf{a}}(t)] = \mathbf{L}[z = 0; \bar{\mathbf{a}}(t)]$  (see eq 31), the general and abstract time-evolution equation in eq 24 for the nonstationary covariance becomes

$$\begin{aligned} \frac{\partial S_{lm}(k; t)}{\partial t} = & -2 \left[ \frac{k^2 D_T^0}{1 + \Delta \zeta_T^*(z = 0; t) \lambda_T^{(lm)}(k = 0; t)} \right. \\ & \left. + \frac{l(l+1) D_R^0}{1 + \Delta \zeta_R^*(z = 0; t) \lambda_R^{(lm)}(k = 0; t)} \right] \\ & \times [\mathcal{E}_{lm}(k, t) S_{lm}(k; t) - 1] \end{aligned} \quad (39)$$

where  $\mathcal{E}_{lm}(k, t) = \mathcal{E}_{lm}[n_{lm}(\mathbf{k}); T(t)]$ . In the present application to the instantaneous isochoric quench at time  $t = 0$  to a final temperature  $T_f$  and fixed bulk density  $n$ , this property is a constant, i.e., for  $t > 0$  we have that  $\mathcal{E}_{lm}(k, t) = \mathcal{E}_{lm}[n_{lm}(\mathbf{k}); T_f] = \mathcal{E}_{lm}^{(f)}(k)$ . In addition, in consistency with the coarse-grained limit  $z = 0$  in  $\Delta \zeta_T^*(z = 0; t)$  and  $\Delta \zeta_R^*(z = 0; t)$ , we have also approximated  $\lambda_T^{(lm)}(k;t)$  and  $\lambda_R^{(lm)}(k;t)$  by its  $k \rightarrow 0$  limit  $\lambda_T^{(lm)}(k = 0;t)$  and  $\lambda_R^{(lm)}(k = 0;t)$ , which are actually unity. Thus, the previous equation reads

$$\begin{aligned} \frac{\partial S_{lm}(k; t)}{\partial t} = & -2 [k^2 D_0^T b^T(t) + l(l+1) D_0^R b^R(t)] \mathcal{E}_{lm}^{(f)}(k) \\ & \times [S_{lm}(k; t) - 1/\mathcal{E}_{lm}^{(f)}(k)] \end{aligned} \quad (40)$$

where the translational and rotational time-dependent mobilities  $b^T(t)$  and  $b^R(t)$  are defined as

$$b^T(t) = [1 + \int_0^\infty d\tau \Delta \zeta_T^*(\tau; t)]^{-1} \quad (41)$$

and

$$b^R(t) = [1 + \int_0^\infty d\tau \Delta \zeta_R^*(\tau; t)]^{-1} \quad (42)$$

in terms of the nonstationary  $\tau$ -dependent friction functions  $\Delta \zeta_T^*(\tau; t)$  and  $\Delta \zeta_R^*(\tau; t)$ .

In order to determine  $b^T(t)$  and  $b^R(t)$ , we adapt to nonequilibrium nonstationary conditions, the same approximations leading to eqs 12 and 13 for the equilibrium friction functions  $\Delta \zeta_T^*(\tau)$  and  $\Delta \zeta_R^*(\tau)$ , which in the present case lead to similar approximate expressions for  $\Delta \zeta_T^*(\tau; t)$  and  $\Delta \zeta_R^*(\tau; t)$ , namely,

$$\begin{aligned} \Delta \zeta_T^*(\tau; t) = & \frac{1}{3} \frac{D_T^0}{(2\pi)^3 n} \int d\mathbf{k} k^2 \sum_l [2l+1] \\ & \times [1 - S_{l0}^{-1}(k; t)]^2 F_{l0}^S(k, \tau; t) F_{l0}(k, \tau; t) \end{aligned} \quad (43)$$

and

$$\begin{aligned} \Delta \zeta_R^*(\tau; t) = & \frac{1}{2} \frac{D_R^0}{(2\pi)^3} \frac{n}{4} \frac{1}{(4\pi)^2} \int d\mathbf{k} \sum_{lm} [2l+1] h_{l0}^2(k; t) \\ & \times [A_{l,0m}]^2 [S_{lm}^{-1}(k; t)]^2 F_{lm}^S(k, \tau; t) F_{lm}(k, \tau; t) \end{aligned} \quad (44)$$

where  $F_{lm;l'm'}(\mathbf{k}, \tau; t)$  are the nonstationary,  $\tau$ -dependent correlation functions  $F_{lm;l'm'}(\mathbf{k}, \tau; t) \equiv \langle \delta n_{lm}^*(\mathbf{k}, t + \tau) \delta n_{l'm'}(\mathbf{k}, t) \rangle$ , with  $F_{lm;l'm'}^S(\mathbf{k}, \tau; t)$  being the corresponding self components.

In a similar manner, the time-evolution equations for  $F_{lm;l'm'}(k, \tau; t)$  and  $F_{lm;l'm'}^S(k, \tau; t)$  are written, in terms of the Laplace transforms  $F_{lm;l'm'}(k, z; t)$ ,  $F_{lm;l'm'}^S(k, z; t)$ ,  $\Delta\zeta_{\ddagger}^*(z; t)$ , and  $\Delta\zeta_{\ddagger}^R(z; t)$ , as

$$F_{lm}(k, z; t) = \frac{S_{lm}(k; t)}{z + \frac{k^2 D_T^0 S_{lm}^{-1}(k; t)}{1 + \Delta\zeta_{\ddagger}^*(z; t)\lambda_{\ddagger}^{(lm)}(k; t)} + \frac{l(l+1)D_R^0 S_{lm}^{-1}(k; t)}{1 + \Delta\zeta_{\ddagger}^R(z; t)\lambda_{\ddagger}^{(lm)}(k; t)}} \quad (45)$$

$$F_{lm}^S(k, z; t) = \frac{1}{z + \frac{k^2 D_T^0}{1 + \Delta\zeta_{\ddagger}^*(z; t)\lambda_{\ddagger}^{(lm)}(k; t)} + \frac{l(l+1)D_R^0}{1 + \Delta\zeta_{\ddagger}^R(z; t)\lambda_{\ddagger}^{(lm)}(k; t)}} \quad (46)$$

For given specific thermodynamic functions  $\mathcal{E}_{lm}[n_{lm}(\mathbf{k}); T_f]$ , eqs 40–46 constitute a closed set of equations for the nonequilibrium properties  $S_{lm}(k; t)$ ,  $F_{lm}(k, \tau; t)$ ,  $F_{lm}^S(k, \tau; t)$ , whose solution provides the NE-SCGLE description of the nonstationary and nonequilibrium structural relaxation of glass-forming liquids formed by nonspherical particles. In a concrete application, these equations only require as an input the specific form of  $\mathcal{E}_{lm}[n_{lm}(\mathbf{k}); T_f]$  and of the (arbitrary) initial static structure factor projections  $S_{lm}(k) \equiv S_{lm}(k; t = 0)$ . In the following section, we illustrate the concrete application of the theory with a simple but interesting application.

### III. RESULTS AND DISCUSSION

**Illustrative Application: Interacting Dipoles with Random Fixed Positions.** Equations 40–46 describe the coupled translational and rotational dynamics of a Brownian liquid of nonspherical particles in search of thermodynamic equilibrium after a sudden quench. A thorough application to a concrete system should then exhibit the full interplay of the translational and rotational degrees of freedom during this process. As mentioned in the introduction, however, carrying out such an exercise falls out of the scope of the present paper. Instead, as an illustrative application, here we discuss the solution of our resulting equations describing the irreversible evolution of the orientational dynamics of a system of strongly interacting dipoles with fixed but random positions subjected to a sudden temperature quench.

For this, let us recall that two important inputs of eqs 40–46, are the short-time self-diffusion coefficients  $D_T^0$  and  $D_R^0$ , which describe, respectively, the short-time Brownian motion of the center of mass and of the orientations of the particles. Hence, *arbitrarily* setting  $D_T^0 = 0$  implies that the particles are prevented from diffusing translationally in any time scale, thus remaining fixed in space. Within this simplification, eq 40 reduces to

$$\frac{\partial S_{lm}(k; t)}{\partial t} = -2l(l+1)D_R^0 b^R(t) \mathcal{E}_{lm}^{(f)}(k) [S_{lm}(k; t) - 1/\mathcal{E}_{lm}^{(f)}(k)] \quad (47)$$

whereas eqs 45 and (46) now read

$$F_{lm}(k, z; t) = \frac{S_{lm}(k; t)}{z + \frac{l(l+1)D_R^0 S_{lm}^{-1}(k; t)}{1 + \Delta\zeta_{\ddagger}^R(z; t)\lambda_{\ddagger}^{(lm)}(k; t)}} \quad (48)$$

and

$$F_{lm}^S(k, z; t) = \frac{1}{z + \frac{l(l+1)D_R^0}{1 + \Delta\zeta_{\ddagger}^R(z; t)\lambda_{\ddagger}^{(lm)}(k; t)}} \quad (49)$$

Also, the time-dependent translational mobility satisfies  $b^T(t) = 1$ . Hence, we only need to complement eqs 47, 48, and 49 with

$$b^R(t) = [1 + \int_0^\infty d\tau \Delta\zeta_{\ddagger}^R(\tau; t)]^{-1} \quad (50)$$

and

$$\Delta\zeta_{\ddagger}^R(\tau; t) = \frac{1}{2} \frac{D_R^0}{(2\pi)^3} \frac{n}{4} \frac{1}{(4\pi)^2} \int d\mathbf{k} \sum_{lm} [2l+1] h_{l0}^2(k; t) [A_{l,0m}]^2 [S_{lm}^{-1}(k; t)]^2 F_{lm}^S(k, \tau; t) F_{lm}(k, \tau; t) \quad (51)$$

where  $A_{l,0m} \equiv [C_{l0}^+ \delta_{l,m} + C_{l0}^- \delta_{-l,m}]$  and  $C_{l0}^\pm \equiv \sqrt{(l \mp 0)(l+1)}$ . In the following subsections, we report the simplest application of these equations.

**III.A. The Dipolar Hard-Sphere Liquid with Frozen Positions.** Let us consider a system formed by  $N$  identical dipolar hard spheres of diameter  $\sigma$  bearing a point dipole of magnitude  $\mu$  in their center, such that the dipolar moment of the  $n$ th particle ( $n = 1, 2, \dots, N$ ) can be written as  $\boldsymbol{\mu}_n = \mu \hat{\boldsymbol{\mu}}_n$  where the unitary vector  $\hat{\boldsymbol{\mu}}_n$  describes its orientation. Thus, the orientational degrees of freedom of the system,  $\boldsymbol{\Omega}^N$ , are described by the set of unitary vectors  $(\hat{\boldsymbol{\mu}}_1, \hat{\boldsymbol{\mu}}_2, \dots, \hat{\boldsymbol{\mu}}_N) = \boldsymbol{\Omega}^N$ , so that the pair potential  $u(\mathbf{r}_n, \mathbf{r}_{n'}; \boldsymbol{\Omega}_n, \boldsymbol{\Omega}_{n'})$  between particles  $n$  and  $n'$  is thus the sum of the radially symmetric hard-sphere potential  $u_{\text{HS}}(|\mathbf{r}_n - \mathbf{r}_{n'}|)$  plus the dipole–dipole interaction, given by

$$u_{\text{dip}}(\mathbf{r}_n, \mathbf{r}_{n'}; \boldsymbol{\Omega}_n, \boldsymbol{\Omega}_{n'}) = \mu^2 |\mathbf{r}_n - \mathbf{r}_{n'}|^{-5} [(\mathbf{r}_n - \mathbf{r}_{n'})^2 (\hat{\boldsymbol{\mu}}_n \cdot \hat{\boldsymbol{\mu}}_{n'}) - 3((\mathbf{r}_n - \mathbf{r}_{n'}) \cdot \hat{\boldsymbol{\mu}}_n)((\mathbf{r}_n - \mathbf{r}_{n'}) \cdot \hat{\boldsymbol{\mu}}_{n'})] \quad (52)$$

The state space of this system is spanned by the number density  $n$  and the temperature  $T$ , expressed in dimensionless form as  $[n\sigma^3]$  and  $[k_B T \sigma^3 / \mu^2]$  (with  $k_B$  being Boltzmann's constant). From now on, we shall denote  $[n\sigma^3]$  and  $[k_B T \sigma^3 / \mu^2]$  simply as  $n$  and  $T$ , i.e., we shall use  $\sigma$  as the unit of length, and  $\mu^2 / k_B \sigma^3$  as the unit of temperature; most frequently, however, we shall also refer to the hard-sphere volume fraction  $\phi \equiv \pi n / 6$ .

The application of the NE-SCGLE equations starts with the external determination of the thermodynamic function  $\mathcal{E}_{lm}^{(f)}(k) \equiv \mathcal{E}_{lm}(k; \phi, T_f)$ . At a given state point  $(\phi, T)$  the function  $\mathcal{E}_{lm}(k; \phi, T)$  can be determined using the fact that its inverse is identical to the projection  $S_{lm}^{\text{eq}}(k; \phi, T)$  of the equilibrium static structure factor  $S^{\text{eq}}(\mathbf{k}, \boldsymbol{\mu}, \boldsymbol{\mu}')$  at that state point. In the context of the present application, this equilibrium property will be approximated by the solution of the mean spherical approximation (MSA) for the dipolar hard sphere (DHS) fluid developed by Wertheim.<sup>58</sup> The details involved in the determination of the resulting equilibrium static structure factor, whose only nonzero projections are  $S_{00}^{\text{eq}}(k)$ ,  $S_{10}^{\text{eq}}(k)$  and  $S_{11}^{\text{eq}}(k) = S_{1-1}^{\text{eq}}(k)$ , can be consulted in ref.<sup>47</sup>

The equilibrium projections  $S_{lm}^{\text{eq}}(k; \phi, T)$  can also be used in the so-called bifurcation equations of the equilibrium theory. These are eqs 17–21 for the nonergodicity parameters  $\gamma_{\ddagger}^{\text{eq}}(\phi, T)$  and  $\gamma_{\ddagger}^{\text{eq}}(\phi, T)$ . According to eq 19, however,  $D_T^0 = 0$  implies  $\gamma_{\ddagger}^{\text{eq}}(\phi, T) = 0$ , so that in the present case we must only solve eq 21 for  $\gamma_{\ddagger}^{\text{eq}}(\phi, T)$ . If the solution is infinite, we say that the asymptotic stationary state is ergodic, and hence, that at the point  $(\phi, T)$  the system will be able to reach its thermodynamic equilibrium state. If, on the other hand,  $\gamma_{\ddagger}^{\text{eq}}(\phi, T)$  turns out to be finite, the system is predicted to become dynamically arrested

and thus, the long time limit of  $S_{lm}(k,t)$  will differ from the thermodynamic equilibrium value  $S_{lm}^{eq}(k;\phi,T)$ . The application of this criterion leads to the prediction that the system under consideration will equilibrate for temperatures  $T$  above a critical value  $T_c(\phi)$ , whereas the system will be dynamically arrested for temperatures below  $T_c$ . In this manner one can trace the dynamic arrest line  $T_c = T_c(\phi)$ , which for our illustrative example is presented in Figure 1. For example, along the isochore  $\phi = 0.2$ , this procedure determines that  $T_c = T_c(\phi = 0.2) = 0.116$ .

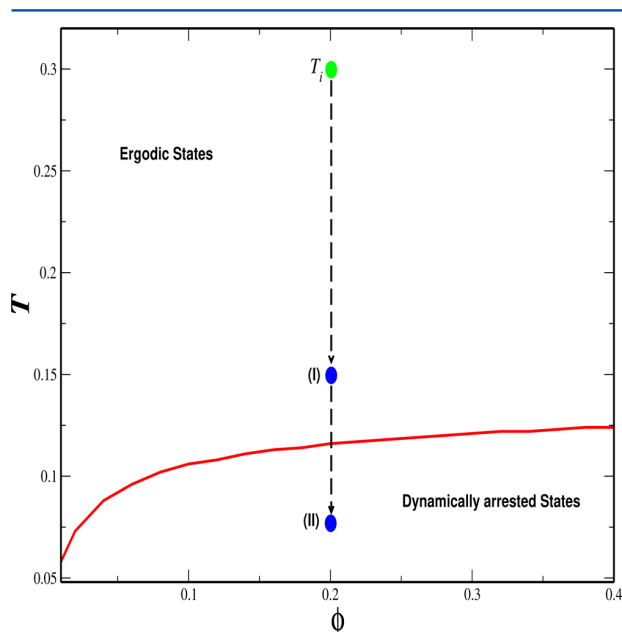


**Figure 1.** Dynamical arrest line (solid curve) in the  $(\phi, T)$  state space of the system of interacting dipoles with fixed positions. This line is the boundary between the region of ergodic states, at which the system is predicted to reach thermodynamic equilibrium, and the predicted region of dynamically arrested states. Each of the two superimposed vertical dashed arrows represent the quench of the system from an initial temperature  $T_i$  (green dot) to a final temperature  $T_f$  (blue dots), in one case above (I) and in the other case below (II) the dynamic arrest line.

We can now use the same thermodynamic function  $\mathcal{E}_{lm}^{(f)}(k) \equiv \mathcal{E}_{lm}(k; \phi, T_f)$  to go beyond the determination of the dynamic arrest line  $T_c = T_c(\phi)$  by solving the set of NE-SCGLE eqs 47–51 to describe the rotational diffusive relaxation of our system. For this, let us notice that these equations happen to have the same mathematical structure as the NE-SCGLE equations that describe the translational diffusion of spherical particles (see, e.g., eqs 2.1–2.6 of ref 31). Although the physical meaning of these two sets of equations is totally different, their mathematical similarity allows us to implement the same method of solution described in ref 29. Thus, we do not provide further details of the numerical protocol to solve eqs 47–51, but go directly to illustrate the resulting scenario.

At this point let us notice that there are two possible classes of stationary solutions of eq 47. The first class corresponds to the long-time asymptotic condition  $\lim_{t \rightarrow \infty} S_{lm}(k; t) = 1/\mathcal{E}_{lm}^{(f)}(k)$ , in which the system is able to reach the thermodynamic equilibrium condition

$S_{lm}^{eq}(k) = 1/\mathcal{E}_{lm}^{(f)}(k)$ . Equilibration is thus a sufficient condition for the stationarity of  $S_{lm}(k,t)$ . It is, however, not a necessary condition. Instead, according to eq 47, another sufficient condition for stationarity is that  $\lim_{t \rightarrow \infty} b_R(t) = 0$ . This is precisely the hallmark of dynamically arrested states. In what follows we discuss the phenomenology predicted by the solution of eqs 47–51 for each of these two mutually exclusive possibilities.

**III.B. Equilibration of the System of Interacting Dipoles with Random Fixed Positions.** Let us now discuss the solution of eqs 47–51 describing the nonequilibrium response of the system to an instantaneous temperature quench. For this, we assume that the system was prepared in an equilibrium state characterized by the initial value  $S_{lm}^{(i)}(k) = S_{lm}^{eq}(k; \phi, T_i) = S_{lm}(k, t = 0)$ , of  $S_{lm}(k, t)$ , and that at time  $t = 0$  the temperature is instantaneously quenched to a final value  $T_f$ . Normally one expects that, as a result, the system will eventually reach full thermodynamic equilibrium, so that the long time asymptotic limit of  $S_{lm}(k, t)$  will be the equilibrium projections  $S_{lm}^{eq}(k; \phi, T_f)$ . Such equilibration processes are illustrated in Figure 2a with an example in which the system was quenched from an initial equilibrium state at temperature  $T_i = 0.3$ ,  $S_{lm}(k, t = 0) = S_{lm}(k; \phi, T_i)$ , to a final temperature  $T_f = 0.15 > T_c = 0.116$ , keeping the volume fraction constant at  $\phi = 0.2$  (the first of the two quenches schematically indicated by the dashed vertical arrows of Figure 1).

Under these conditions, and from the physical scenario predicted in Figure 1, we should expect that the system will indeed equilibrate, so that  $S_{lm}(k, t \rightarrow \infty) = S_{lm}^{eq}(k; \phi, T_f)$ . This, however, will only be true for  $S_{10}(k, t)$  and  $S_{11}(k, t)$ , since, according to eq 47,  $S_{00}(k, t)$  must remain constant for  $t > 0$ , indicating that the artificially quenched spatial structure will not evolve as a result of the temperature quench. For the same reason, eqs 48 and 49 imply that the normalized intermediate scattering functions  $F_{00}(k, \tau; t)/S_{00}(k; t)$  and  $F_{00}^S(k, \tau; t)$  will be unity for all positive values of the correlation time  $\tau$  and waiting time  $t$ . For reference, the structure of the frozen positions represented by  $S_{00}(k, t) = S_{00}^{eq}(k, \phi, T_i)$ , is displayed in Figure 2a by the (magenta) dotted line, which clearly indicates that the fixed positions of the dipoles are strongly correlated, in contrast with a system of dipoles with purely random fixed positions, in which  $S_{00}(k, t)$  would be unity. In the same figure, the initial and final equilibrium static structure factor projections,  $S_{10}^{(i)}(k) = S_{10}^{eq}(k; \phi, T_i)$  and  $S_{10}^{(f)}(k) = S_{10}^{eq}(k; \phi, T_f)$ , are represented, respectively, by the (red) dashed and (blue) dot-dashed curves. The sequence of (brown) solid curves in between represents the evolution of  $S_{10}(k, t)$  with waiting time  $t$ , as a series of snapshots corresponding to the indicated values of  $t$ .

For each snapshot of the static structure factor projections  $S_{lm}(k, t)$ , the solution of eqs 47–51 also determines a snapshot of each of the dynamic correlation functions  $F_{lm}(k, \tau; t)$  and  $F_{lm}^S(k, \tau; t)$ . These functions are related with other more intuitive and experimentally accessible properties, such as the time-dependent autocorrelation function  $C_1(\tau; t) \equiv \langle \sum_{i=1}^N \hat{\mu}_i(t + \tau) \cdot \hat{\mu}_i(t) \rangle / \langle \sum_{i=1}^N \hat{\mu}_i(t) \cdot \hat{\mu}_i(t) \rangle$  of the normalized dipole vectors  $\hat{\mu}_i$ . In fact, since our dynamic correlators  $F_{lm}(k, \tau; t)$  and  $F_{lm}^S(k, \tau; t)$  were assumed to be described from the intermolecular  $k$ -frame,<sup>46</sup> one can relate them with the time-dependent autocorrelation function  $C_1(\tau; t)$  directly through the following expression,<sup>59</sup>

$$C_1(\tau; t) = \frac{1}{3} \lim_{k \rightarrow 0} \sum_{m=-1}^1 F_{1m}^S(k, \tau; t) \quad (53)$$

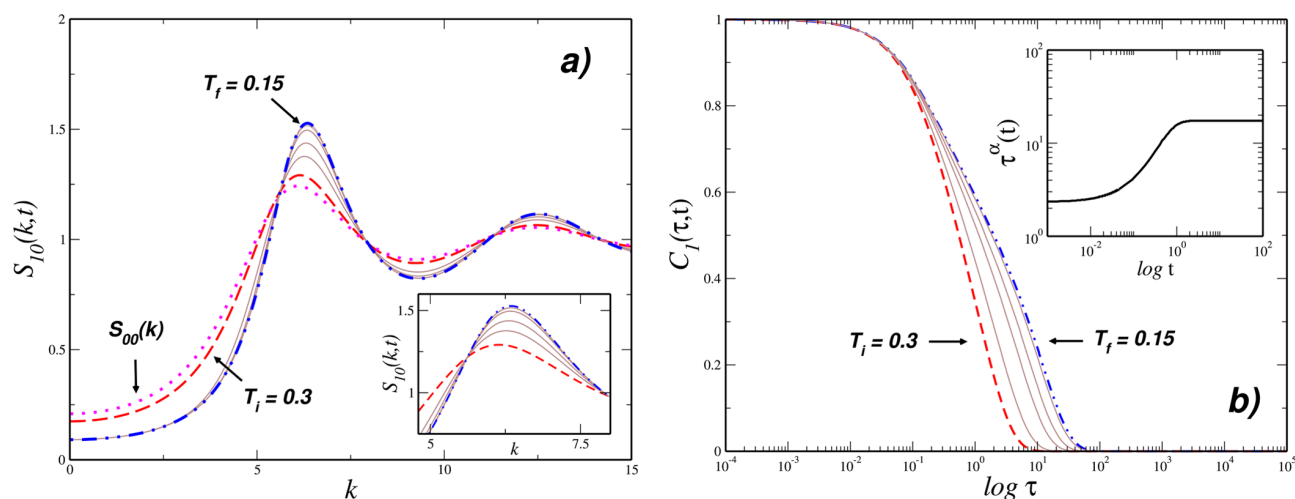


**Figure 2.** Illustration of an equilibration process. (a) Snapshots of the time evolution of the  $l = 1, m = 0$  static structure factor projection,  $S_{10}(k, t)$ , corresponding to the isochoric quench  $T_i \rightarrow T_f$  for  $\phi = 0.2$ , with  $T_i = 0.3$  and  $T_f = 0.15$ . The (red) dashed line is the initial structure factor  $S_{10}(k, t = 0) = S_{10}^{(i)}(k)$ . The (blue) dot-dashed line is the asymptotic limit  $S_{10}(k, t \rightarrow \infty) = S_{10}^{(f)}(k) = S_{10}^{(\text{eq})}(k)$ . The sequence of thinner (brown) solid lines in between represents  $S_{10}(k, t)$  for  $t = 0.3, 0.78, 1.42, 2.33$  and  $t \rightarrow \infty$ . For reference we also include the non-evolving component  $S_{00}(k, t) = S_{00}^{(e)}(k; \phi, T_i)$ , indicated by the dotted line. (b) Snapshots of the orientational autocorrelation function  $C_1(\tau; t)$  as a function of correlation time  $\tau$  (thin brown solid lines), corresponding to the same isochoric quench and same sequence of waiting times  $t$  as in panel a. The (red) dashed line represents the initial function  $C_1(\tau; t = 0) = C_1^{(\text{eq})}(\tau; \phi, T_i)$  and the (blue) dot-dashed line is the asymptotic limit  $C_1(\tau; t \rightarrow \infty) = C_1^{(\text{eq})}(\tau; \phi, T_f)$ . The inset plots the  $\alpha$ -relaxation time, defined as  $C_1(\tau_{\alpha}; t) = 1/e$ , as a function of waiting time  $t$ .

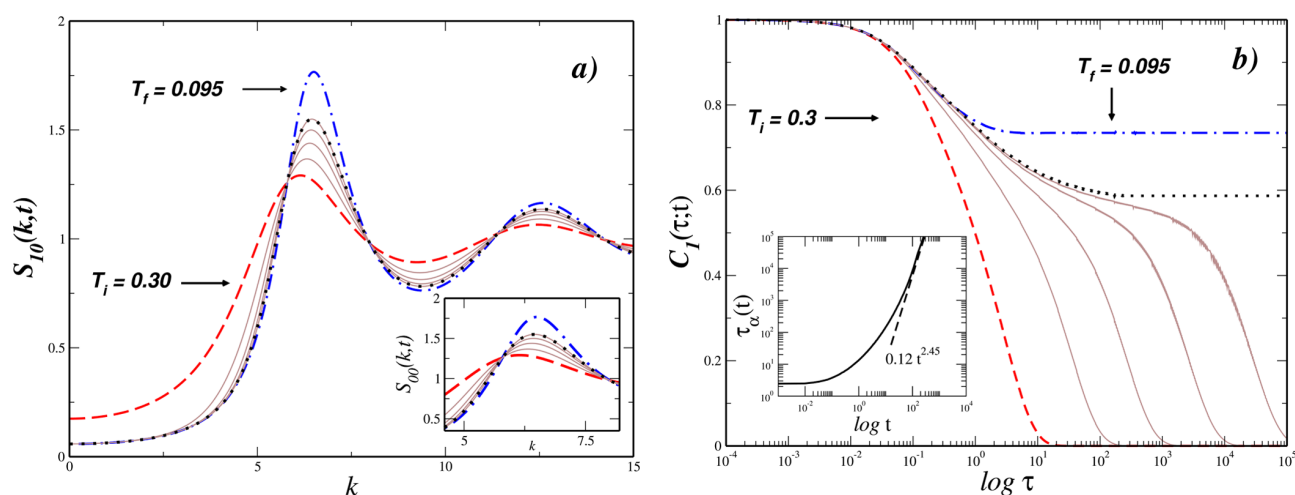


**Figure 3.** Illustration of an aging process. (a) Snapshots of the nonequilibrium time evolution of the  $l = 1, m = 0$  static structure factor projection,  $S_{10}(k, t)$ , corresponding to the isochoric quench  $T_i \rightarrow T_f$  for  $\phi = 0.2$ , with  $T_i = 0.3$  and  $T_f = 0.095$ . The (red) dashed line is the initial structure factor  $S_{10}(k, t = 0) = S_{10}^{(i)}(k)$ . The (blue) dot-dashed line is the (now inaccessible) equilibrium structure factor  $S_{10}^{(\text{eq})}(k; \phi, T_f)$ , whereas the (black) dotted line is the predicted asymptotic limit  $S_{10}(k, t \rightarrow \infty) = S_{10}^{(a)}(k)$ . The sequence of thinner (brown) solid lines in between represents  $S_{10}(k, t)$  for  $t = 1.16, 4.264, 14.056, \text{ and } 150.61$ . (b) Snapshots of the orientational autocorrelation function  $C_1(\tau; t)$  as a function of correlation time  $\tau$  (thin brown solid lines), corresponding to the same isochoric quench and same sequence of waiting times  $t$  as in panel a. The (red) dashed line represents the initial function  $C_1(\tau; t = 0) = C_1^{(\text{eq})}(\tau; \phi, T_i)$ , the (blue) dot-dashed line is the expected (but now inaccessible) equilibrium correlation  $C_1^{(\text{eq})}(\tau; \phi, T_f)$ , and the (black) dotted line is the predicted long- $t$  asymptotic limit,  $C_1(\tau; t \rightarrow \infty) = C_1^{(a)}(\tau)$ . The inset plots the corresponding  $\alpha$ -relaxation time as a function of waiting time  $t$ , with the (black) dashed line representing the asymptotic power law  $\tau_\alpha \propto t^{2.45}$ .

Let us notice that, according to eq 49, the three terms in the sum on the right-hand side of eq 53,  $F_{10}^S(k, \tau; t)$ ,  $F_{11}^S(k, \tau; t)$ , and  $F_{1-1}^S(k, \tau; t)$ , satisfy the same equation of motion (which only depends explicitly on  $l$ ) and thus, contribute exactly in the same manner to the  $\tau$  and  $t$  dependence of  $C_1(\tau; t)$ . Thus,  $C_1(\tau; t)$  summarizes the irreversible time evolution of the orientational dynamics, as illustrated in Figure 2b with the snapshots corresponding to the same set of evolution times  $t$  as the snapshots of  $S_{10}(k, t)$  in Figure 2a. We observe that  $C_1(\tau; t)$

starts from its initial equilibrium value,  $C_1(\tau; t = 0) = C_1^{(\text{eq})}(\tau; \phi, T_i)$  and quickly evolves with waiting time  $t$  toward  $C_1(\tau; t \rightarrow \infty) = C_1^{(\text{eq})}(k, \tau; \phi, T_f)$ . This indicates that the expected equilibrium state at  $(\phi = 0.2, T_f)$  is reached without impediment and that the orientational dynamics remains ergodic at that state point.

As mentioned before, the structure of eqs 47–51 is the same as that of the equations in ref 29 describing the spherical case. Thus, one should not be surprised that the general dynamic and

kinetic scenario predicted in both cases will exhibit quite similar patterns. For example, the nonequilibrium evolution described by the sequence of snapshots of  $C_1(\tau;t)$  can be summarized by the evolution of its  $\alpha$ -relaxation time  $\tau_\alpha(t)$ , defined through the condition  $C_1(\tau_\alpha;t) = 1/e$ . In the inset of Figure 2b we illustrate the saturation kinetics of the equilibration process in terms of the  $t$ -dependence of  $\tau_\alpha(t)$ , as determined from the sequence of snapshots of  $C_1(\tau_\alpha;t)$  displayed in the figure. Clearly, after a transient stage, in which  $\tau_\alpha(t)$  evolves from its initial value  $\tau_\alpha^{\text{eq}}(\phi, T_i)$ , it eventually saturates to its final equilibrium value  $\tau_\alpha^{\text{eq}}(\phi, T_f)$ .

**C. Aging of the System of Interacting Dipoles with Random Fixed Positions.** Let us now present the NE-SCGLE description of the second class of irreversible isochoric processes, in which the system starts in an ergodic state but ends in a dynamically arrested state. For this, let us consider now the case in which the system is subjected to a sudden isochoric cooling, at fixed volume fraction  $\phi = 0.2$ , and from the same initial state as before, but this time to the final state point  $(\phi, T_f = 0.095)$  lying inside the region of dynamically arrested states (the second of the two quenches schematically indicated by the dashed vertical arrows of Figure 1).

Under such conditions, the long-time asymptotic limit of  $S_m(k;t)$  will no longer be the expected equilibrium static structure factor  $S_m^{\text{eq}}(k; \phi, T_f)$ , but another, well-defined nonstationary structure factor  $S_m^{(a)}(k)$ . In Figure 3a, we illustrate this behavior with a sequence of snapshots of the nonequilibrium evolution of  $S_{10}(k;t)$  after this isochoric quench at  $\phi = 0.2$  from  $T^{(i)} = 0.3$  to  $T^{(f)} = 0.095$ . There we highlight the initial structure factor  $S_{10}^{(i)}(k) = S_{10}^{\text{eq}}(k; \phi, T_i)$ , represented by the (red) dashed line and the dynamically arrested long-time asymptotic limit,  $S_{10}^{(a)}(k)$ , of the nonequilibrium evolution of  $S_{10}(k;t)$ , described by the (black) dotted line. For reference, we also plot the expected, but inaccessible, equilibrium static structure factor  $S_{10}^{\text{eq}}(k; \phi, T_f) \neq S_{10}^{(a)}(k)$  (blue dot-dashed line).

Finally, let us illustrate how this scenario of dynamic arrest manifests itself in the nonequilibrium evolution of the dynamics. We recall that for each snapshot of the nonstationary structure factor  $S_m(k;t)$ , the solution of eqs 47–51 also determines a snapshot of all the dynamic properties at that waiting time  $t$ . For example, in Figure 3b we present the sequence of snapshots of  $C_1(\tau;t)$ , plotted as a function of correlation time  $\tau$ , that corresponds to the sequence of snapshots of  $S_{10}(k;t)$  in Figure 3a. In this figure we highlight in particular the initial value  $C_1(\tau; t = 0) = C_1^{\text{eq}}(\tau; \phi, T_i)$  (red dashed line), the predicted nonequilibrium asymptotic limit,  $C_1^{(a)}(\tau) \equiv \lim_{t \rightarrow \infty} C_1(k, \tau; t)$  (black dotted line) and the inaccessible equilibrium value of  $C_1^{\text{eq}}(\tau; \phi, T_f)$  (blue dot-dashed line). Notice that, in contrast with the equilibration process, in which the long-time asymptotic solution  $C_1^{\text{eq}}(\tau; \phi, T_f)$  decays to zero within a finite relaxation time  $\tau_\alpha^{\text{eq}}(\phi, T_f)$ , in the present case  $C_1^{\text{eq}}(\tau; \phi, T_f)$  does not decay to zero, but to a finite plateau. This arrested equilibrium correlation function, however, is completely inaccessible, since now the long- $t$  asymptotic limit of  $C_1(k, \tau; t)$  is  $C_1^{(a)}(\tau)$ , which is also a dynamically arrested function, but with a different plateau than  $C_1^{\text{eq}}(\tau; \phi, T_f)$ .

Just like in the equilibration process, which starts at the same initial state, here we also observe that at  $t = 0$ ,  $C_1(\tau;t)$  shows no trace of dynamic arrest, and that as the waiting time  $t$  increases, the relaxation time increases as well. We can summarize this irreversible evolution of  $C_1(\tau;t)$  by exhibiting the kinetics of the  $\alpha$ -relaxation time  $\tau_\alpha(t)$  extracted from the sequence of snapshots of  $C_1(\tau_\alpha;t)$  in the same figure. This is done in the

inset of Figure 3b. Clearly, after the initial transient stage, in which  $\tau_\alpha(t)$  increases from its initial value  $\tau_\alpha^{\text{eq}}(\phi, T_i)$  in a similar fashion as in the equilibration case,  $\tau_\alpha(t)$  no longer saturates to any finite stationary value. Instead, it increases with  $t$  without bound, and actually diverges as a power law,  $\tau_\alpha(t) \propto t^a$ , with  $a \approx 2.45$ .

Except for quantitative details, such as the specific value of this exponent, we find a remarkable general similarity between this predicted aging scenario of the dynamic arrest of our system of interacting dipoles, and the corresponding aging scenario of the structural relaxation of a soft-sphere glass-forming liquid described in ref 29 (compare, for example, our Figure 3b above, with Figure 12 of that reference). As said above, however, our intention in this paper is not to discuss the physics behind these similarities and these scenarios, but only to present the theoretical machinery that reveals it.

## IV. CONCLUSIONS

Thus, in summary, we have proposed the extension of the self-consistent generalized Langevin equation theory for systems of nonspherical interacting particles (NS-SCGLE), to consider general nonequilibrium conditions. The main contribution of this work consist thus in the general theoretical framework, developed in Section III.B, able to describe the irreversible processes occurring in a given system after a sudden temperature quench, in which its spontaneous evolution in search of a thermodynamic equilibrium state could be interrupted by the appearance of conditions of dynamical arrest for translational or orientational (or both) degrees of freedom.

Our description consists essentially of the coarse-grained time-evolution equations for the spherical-harmonics-projections of the static structure factor of the fluid, which involves one translational and one orientational time-dependent mobility functions. These nonequilibrium mobilities, in turn, are determined from the solution of the nonequilibrium version of the SCGLE equations for the nonstationary dynamic properties (the spherical-harmonics-projections of the self- and collective intermediate scattering functions). The resulting theory is summarized by eqs 40–46, which describe the irreversible processes in model liquids of nonspherical particles, within the constraint that the system remains, on the average, spatially uniform. This theoretical framework is now ready to be applied for the description of such nonequilibrium phenomena in many specific model systems.

Although in this paper we do not include a thorough discussion of any particular application, in section III we illustrated the predictive capability of our resulting equations by applying them to the description of the isochoric and uniform evolution of nonequilibrium process of a simple model, namely, a dipolar hard sphere liquid with fixed random positions, after being subjected to instantaneous temperature quench. Here we used this example mostly to illustrate some methodological aspects of the application of the theory, since this specific application allows us to easily implement the numerical methods described in detail in ref 29. The same illustrative example, however, also allows us to investigate the relevant features of the orientational dynamics during the equilibration and aging processes, but leaves open many relevant issues, such as the relationship between these predictions and the phenomenology of aging in spin-glass systems. Similarly, the nonequilibrium manifestations of the coupling between translational and rotational dynamics, involved in the complete

solution of eqs 40–46, will be the subject of future communications. Thus, we expect that the general results derived in this paper will be the basis of a rich program of research dealing with these problems.

## AUTHOR INFORMATION

### Corresponding Author

\*Electronic address: [luisfer.elizondo@gmail.com](mailto:luisfer.elizondo@gmail.com).

### Notes

The authors declare no competing financial interest.

## ACKNOWLEDGMENTS

This work was supported by the Consejo Nacional de Ciencia y Tecnología (CONACYT, México) through grants No. 242364, No. 182132, No. 237425 and No. 358254; and through the Red Temática del CONACYT: "Materia Condensada Blanda". M.M.N. acknowledge financial support from Proyecto Institucional de Excelencia Académica 2015 "Statistical Thermodynamics of Matter Out of Equilibrium". L.F.E.A. also acknowledge financial support from Secretaría de Educación Pública (SEP, México) through PRODEP (Postdoctoral Scholarship) and funding from the German Academic Exchange Service (DAAD) through the DLR-DAAD programme under grant No. 212.

## REFERENCES

- (1) Angell, C. A.; Ngai, K. L.; McKenna, G. B.; McMillan, P. F.; Martin, S. F. Relaxation in Glassforming Liquids and Amorphous Solids. *J. Appl. Phys.* **2000**, *88*, 3113–3157.
- (2) Ngai, K. L.; Prevosto, D.; Capaccioli, S.; Roland, C. M. Guides to Solving the Glass Transition Problem. *J. Phys.: Condens. Matter* **2008**, *20*, 244125.
- (3) Sciortino, F.; Tartaglia, P. Glassy Colloidal Systems. *Adv. Phys.* **2005**, *54*, 471–524.
- (4) Mydosh, J. A. *Spin Glasses: An Experimental Introduction*; Taylor & Francis: London, U.K., 1993.
- (5) Tam, K.-M.; Gingras, M. J. P. Spin-Glass Transition at Nonzero Temperature in a Disordered Dipolar Ising System: the Case of  $\text{LiHo}_x\text{Y}_{1-x}\text{F}_4$ . *Phys. Rev. Lett.* **2009**, *103*, 087202.
- (6) Biltmo, A.; Henelius, P. Unreachable Glass Transition in Dilute Dipolar Magnet. *Nat. Commun.* **2012**, *3*, 857.
- (7) de Groot, S. R.; Mazur, P. *Non-equilibrium Thermodynamics*; Dover: New York, 1984.
- (8) Keizer, J. *Statistical Thermodynamics of Nonequilibrium Processes*; Springer-Verlag: Berlin Heidelberg, 1987.
- (9) Lebon, G.; Jou, D.; Casas-Vázquez, J. *Understanding Non-equilibrium Thermodynamics Foundations, Applications, Frontiers*; Springer-Verlag: Berlin Heidelberg, 2008.
- (10) Ramírez-González, P. E.; Medina-Noyola, M. Glass Transition in Soft-Matter Dispersions. *J. Phys.: Condens. Matter* **2009**, *21*, 075101.
- (11) Hernandez, R.; Somer, F. L. Stochastic Dynamics in Irreversible Nonequilibrium Environments. I. The Fluctuation-Dissipation Relation. *J. Phys. Chem. B* **1999**, *103*, 1064–1069.
- (12) Kawai, S.; Komatsuzaki, T. Dynamic Reaction Coordinate in Thermally Fluctuating Environment in the Framework of the Multidimensional Generalized Langevin Equations. *Phys. Chem. Chem. Phys.* **2010**, *12*, 15382–15391.
- (13) Ghosh, P.; Chattopadhyay, S.; Chaudhuri, J. R. Enhancement of Current Commensurate with Mutual Noise-Noise Correlation in a Symmetric Periodic Substrate: the Benefits of Noise and Nonlinearity. *Chem. Phys.* **2012**, *402*, 48–55.
- (14) Popov, A.; Melvin, J.; Hernandez, R. Dynamics of Swelling/Contracting Hard Spheres Surmised by an Irreversible Langevin Equation. *J. Phys. Chem. A* **2006**, *110*, 1635–1644.
- (15) Cugliandolo, L. F.; Kurchan, J. Analytical Solution of the Off-Equilibrium Dynamics of a Long-Range Spin-Glass Model. *Phys. Rev. Lett.* **1993**, *71*, 173–176.
- (16) Götze, W. *Liquids, Freezing and the Glass Transition*; Hansen, J. P., Levesque, D., Zinn-Justin, J., Eds.; North-Holland: Amsterdam, 1991.
- (17) Götze, W.; Sjögren, L. Relaxation Processes in Supercooled Liquids. *Rep. Prog. Phys.* **1992**, *55*, 241–376.
- (18) Yeomans-Reyna, L.; Chávez-Rojo, M. A.; Ramírez-González, P. E.; Juárez-Maldonado, R.; Chavez-Páez, M.; Medina-Noyola, M. Dynamic Arrest within the Self-Consistent Generalized Langevin Equation of Colloid Dynamics. *Phys. Rev. E* **2007**, *76*, 041504.
- (19) Juárez-Maldonado, R.; Chávez-Rojo, M. A.; Ramírez-González, P. E.; Yeomans-Reyna, L.; Medina-Noyola, M. Simplified Self-Consistent Theory of Colloid Dynamics. *Phys. Rev. E* **2007**, *76*, 062502.
- (20) Latz, A. Non-Equilibrium Mode-Coupling Theory for Supercooled Liquids and Glasses. *J. Phys.: Condens. Matter* **2000**, *12*, 6353–6363.
- (21) Ramírez-González, P. E.; Medina-Noyola, M. General Non-equilibrium Theory of Colloidal Dynamics. *Phys. Rev. E* **2010**, *82*, 061503.
- (22) Ramírez-González, P. E.; Medina-Noyola, M. Aging of a Homogeneously Quenched Colloidal Glass-Forming Liquid. *Phys. Rev. E* **2010**, *82*, 061504.
- (23) Onsager, L. Reciprocal Relations in Irreversible Processes. I. *Phys. Rev.* **1931**, *37*, 405–426.
- (24) Onsager, L. Reciprocal Relations in Irreversible Processes. II. *Phys. Rev.* **1931**, *38*, 2265–2279.
- (25) Onsager, L.; Machlup, S. Fluctuations and Irreversible Processes. *Phys. Rev.* **1953**, *91*, 1505–1512.
- (26) Machlup, S.; Onsager, L. Fluctuations and Irreversible Processes. II. Systems with Kinetic Energy. *Phys. Rev.* **1953**, *91*, 1512–1515.
- (27) Medina-Noyola, M.; del Río-Correa, J. L. The Fluctuation-Dissipation Theorem for Non-Markov Processes and their Contractions: the Role of the Stationary Condition. *Phys. A* **1987**, *146*, 483–505.
- (28) Medina-Noyola, M. The Generalized Langevin Equation as a Contraction of the Description. An Approach to Tracer Diffusion. *Faraday Discuss. Chem. Soc.* **1987**, *83*, 21–31.
- (29) Sánchez-Díaz, L. E.; Ramírez-González, P. E.; Medina-Noyola, M. Equilibrium and Aging of Dense Soft-Sphere Glass-Forming Liquids. *Phys. Rev. E* **2013**, *87*, 052306.
- (30) Mendoza-Méndez, P.; Lázaro-Lázaro, E.; Sánchez-Díaz, L. E.; Ramírez-González, P. E.; Pérez-Angel, G.; Medina-Noyola, M. The Discontinuous Ideal Glass Transition, a Soft Crossover at Finite Waiting Times. 2016, arXiv:1404.1964. arXiv.org e-Print archive. <http://arxiv.org/abs/1404.1964> (accessed June 24, 2016).
- (31) Olais-Govea, J. M.; López-Flores, L.; Medina-Noyola, M. Non-Equilibrium Theory of Arrested Spinodal Decomposition. *J. Chem. Phys.* **2015**, *143*, 174505.
- (32) Olais-Govea, J. M.; López-Flores, L.; Medina-Noyola, M., Non-Equilibrium Theory of Arrested Spinodal Decomposition. 2016, arXiv:1505.00390. arXiv.org e-Print archive. <http://arxiv.org/abs/1505.00390> (accessed June 24, 2016).
- (33) Cahn, J. W.; Hilliard, J. E. Free Energy of a Nonuniform System. III. Nucleation in a Two-Component Incompressible Fluid. *J. Chem. Phys.* **1959**, *31*, 688–699.
- (34) Cook, H. E. Brownian Motion in Spinodal Decomposition. *Acta Metall.* **1970**, *18*, 297–306.
- (35) Furukawa, H. A Dynamic Scaling Assumption for Phase Separation. *Adv. Phys.* **1985**, *34*, 703–750.
- (36) Lu, P. J.; Zaccarelli, E.; Ciulla, F.; Schofield, A. B.; Sciortino, F.; Weitz, D. Gelation of Particles with Short-Range Attraction. *Nature* **2008**, *22*, 499–503.
- (37) Sanz, E.; Leunissen, M. E.; Fortini, A.; van Blaaderen, A.; Dijkstra, M. Gel Formation in Suspensions of Oppositely Charged

Colloids: Mechanism and Relation to the Equilibrium Phase Diagram. *J. Phys. Chem. B* **2008**, *112*, 10861–10872.

(38) Gibaud, T.; Schurtenberger, P. J. A Closer Look at Arrested Spinodal Decomposition in Proteins Solutions. *J. Phys.: Condens. Matter* **2009**, *21*, 322201.

(39) Di Michele, L.; Fiocco, D.; Varrato, F.; Sastry, S.; Eiser, E.; Foffi, G. Aggregation Dynamics, Structure, and Mechanical Properties of Bigels. *Soft Matter* **2014**, *10*, 3633–3648.

(40) Gao, Y.; Kim, J.; Helgeson, M. E. Microdynamics and Arrest of Coarsening During Spinodal Decomposition in Thermoreversible Colloidal Gels. *Soft Matter* **2015**, *11*, 6360–6370.

(41) Zaccarelli, E. Colloidal Gels: Equilibrium and Non-Equilibrium Routes. *J. Phys.: Condens. Matter* **2007**, *19*, 323101.

(42) Berthier, L.; Biroli, G. Theoretical Perspective on the Glass Transition and Amorphous Materials. *Rev. Mod. Phys.* **2011**, *83*, 587–645.

(43) Sánchez-Díaz, L. E.; Lázaro-Lázaro, E.; Olais-Govea, J. M.; Medina-Noyola, M. Non-Equilibrium Dynamics of Glass-Forming Liquid Mixtures. *J. Chem. Phys.* **2014**, *140*, 234501.

(44) Zheng, Z.; Wang, F.; Han, Y. Glass Transitions in Quasi-Two-Dimensional Suspensions of Colloidal Ellipsoids. *Phys. Rev. Lett.* **2011**, *107*, 065702.

(45) Edmond, K. V.; Elsesser, M. T.; Hunter, G. L.; Pine, D. J.; Weeks, E. R. Decoupling of Rotational and Translational Diffusion in Supercooled Colloidal Fluids. *Proc. Natl. Acad. Sci. U. S. A.* **2012**, *109*, 17891–17896.

(46) Elizondo-Aguilera, L. F.; Zubieta-Rico, P. F.; Ruíz Estrada, H.; Alarcón-Waess, O. Self-Consistent Generalized Langevin-Equation Theory for Liquids of Nonspherically Interacting Particles. *Phys. Rev. E* **2014**, *90*, 052301.

(47) Schilling, R.; Scheidsteger, T. Mode Coupling Approach to the Ideal Glass Transition of Molecular Liquids: Linear Molecules. *Phys. Rev. E: Stat. Phys., Plasmas, Fluids, Relat. Interdiscip. Top.* **1997**, *56*, 2932–2949.

(48) Fabbian, L.; Latz, A.; Schilling, R.; Sciortino, F.; Tartaglia, P.; Theis, C. Molecular Mode-Coupling Theory for Supercooled Liquids: Application to Water. *Phys. Rev. E: Stat. Phys., Plasmas, Fluids, Relat. Interdiscip. Top.* **1999**, *60*, 5768–5777.

(49) Letz, M.; Schilling, R.; Latz, A. Ideal Glass Transitions for Hard Ellipsoids. *Phys. Rev. E: Stat. Phys., Plasmas, Fluids, Relat. Interdiscip. Top.* **2000**, *62*, 5173–5178.

(50) Copley, J. R. D.; Lovesey, S. W. The Dynamic Properties of Monoatomic Liquids. *Rep. Prog. Phys.* **1975**, *38*, 461–563.

(51) Boon, J. L.; Yip, S. *Molecular Hydrodynamics*; Dover Publications, Inc.: New York, 1980.

(52) Kubo, R. The Fluctuation-Dissipation Theorem. *Rep. Prog. Phys.* **1966**, *29*, 255–284.

(53) Zwanzig, R. Memory Effects in Irreversible Thermodynamics. *Phys. Rev.* **1961**, *124*, 983–992.

(54) Mori, H. Transport, Collective Motion, and Brownian Motion. *Prog. Theor. Phys.* **1965**, *33*, 423–455.

(55) Langevin, P. On the Theory of Brownian Motion. *Comptes Rendus* **1908**, *146*, 530–533.

(56) Hernández-Contreras, M.; Medina-Noyola, M. Tracer Diffusion of Nonspherical Colloidal Particles. *Phys. Rev. E: Stat. Phys., Plasmas, Fluids, Relat. Interdiscip. Top.* **1996**, *53*, R4306–R4309.

(57) Callen, H. *Thermodynamics*; John Wiley: New York, 1960.

(58) Wertheim, M. S. Exact Solution of The Mean Spherical Model for Fluids of Hard Spheres with Permanent Electric Dipole Moments. *J. Chem. Phys.* **1971**, *55*, 4291–4298.

(59) Fabbian, L.; Sciortino, F.; Tartaglia, P. Rotational Dynamics in a Simulated Supercooled Network-Forming Liquid. *J. Non-Cryst. Solids* **1998**, *235–237*, 325–330.



A LETTERS JOURNAL EXPLORING  
THE FRONTIERS OF PHYSICS

OFFPRINT

## Dynamics of a suspension of interacting yolk-shell particles

L. E. SÁNCHEZ DÍAZ, E. C. CORTES-MORALES, X. LI, WEI-REN  
CHEN and M. MEDINA-NOYOLA

EPL, **108** (2014) 68007

Please visit the website  
[www.epljournal.org](http://www.epljournal.org)

**Note** that the author(s) has the following rights:

- immediately after publication, to use all or part of the article without revision or modification, **including the EPLA-formatted version**, for personal compilations and use only;
- no sooner than 12 months from the date of first publication, to include the accepted manuscript (all or part), **but not the EPLA-formatted version**, on institute repositories or third-party websites provided a link to the online EPL abstract or EPL homepage is included.

For complete copyright details see: <https://authors.eplletters.net/documents/copyright.pdf>.



A LETTERS JOURNAL EXPLORING  
THE FRONTIERS OF PHYSICS

**AN INVITATION TO  
SUBMIT YOUR WORK**

[www.epljournal.org](http://www.epljournal.org)

### **The Editorial Board invites you to submit your letters to EPL**

EPL is a leading international journal publishing original, innovative Letters in all areas of physics, ranging from condensed matter topics and interdisciplinary research to astrophysics, geophysics, plasma and fusion sciences, including those with application potential.

The high profile of the journal combined with the excellent scientific quality of the articles ensures that EPL is an essential resource for its worldwide audience. EPL offers authors global visibility and a great opportunity to share their work with others across the whole of the physics community.

### **Run by active scientists, for scientists**

EPL is reviewed by scientists for scientists, to serve and support the international scientific community. The Editorial Board is a team of active research scientists with an expert understanding of the needs of both authors and researchers.



[www.epljournal.org](http://www.epljournal.org)



OVER  
**560,000**  
full text downloads in 2013

**24 DAYS**  
average accept to online  
publication in 2013

**10,755**  
citations in 2013

*"We greatly appreciate  
the efficient, professional  
and rapid processing of  
our paper by your team."*

**Cong Lin**  
Shanghai University

### Six good reasons to publish with EPL

We want to work with you to gain recognition for your research through worldwide visibility and high citations. As an EPL author, you will benefit from:

- 1 Quality** – The 50+ Co-editors, who are experts in their field, oversee the entire peer-review process, from selection of the referees to making all final acceptance decisions.
- 2 Convenience** – Easy to access compilations of recent articles in specific narrow fields available on the website.
- 3 Speed of processing** – We aim to provide you with a quick and efficient service; the median time from submission to online publication is under 100 days.
- 4 High visibility** – Strong promotion and visibility through material available at over 300 events annually, distributed via e-mail, and targeted mailshot newsletters.
- 5 International reach** – Over 2600 institutions have access to EPL, enabling your work to be read by your peers in 90 countries.
- 6 Open access** – Articles are offered open access for a one-off author payment; green open access on all others with a 12-month embargo.

Details on preparing, submitting and tracking the progress of your manuscript from submission to acceptance are available on the EPL submission website [www.epletters.net](http://www.epletters.net).

If you would like further information about our author service or EPL in general, please visit [www.epjournal.org](http://www.epjournal.org) or e-mail us at [info@epjournal.org](mailto:info@epjournal.org).

EPL is published in partnership with:



European Physical Society



Società Italiana di Fisica

edp sciences IOP Publishing

EDP Sciences

IOP Publishing

# Dynamics of a suspension of interacting yolk-shell particles

L. E. SÁNCHEZ DÍAZ<sup>1</sup>, E. C. CORTES-MORALES<sup>2</sup>, X. LI<sup>1</sup>, WEI-REN CHEN<sup>1</sup> and M. MEDINA-NOYOLA<sup>2</sup>

<sup>1</sup> *Biology and Soft Matter Division, Oak Ridge National Laboratory - Oak Ridge, TN 37831, USA*

<sup>2</sup> *Instituto de Física “Manuel Sandoval Vallarta”, Universidad Autónoma de San Luis Potosí  
Álvaro Obregón 64, 78000 San Luis Potosí, SLP, México*

received 22 September 2014; accepted in final form 8 December 2014

published online 7 January 2015

PACS 82.70.Dd – Disperse systems; complex fluids: Colloids

PACS 61.20.Lc – Structure of liquids: Time-dependent properties; relaxation

**Abstract** – In this work we study the self-diffusion properties of a liquid of hollow spherical particles (shells) bearing a smaller solid sphere in their interior (yolks). We model this system using purely repulsive hard-body interactions between all (shell and yolk) particles, but assume the presence of a background ideal solvent such that all the particles execute free Brownian motion between collisions, characterized by short-time self-diffusion coefficients  $D_s^0$  for the shells and  $D_y^0$  for the yolks. Using a softened version of these interparticle potentials we perform Brownian dynamics simulations to determine the mean squared displacement and intermediate scattering function of the yolk-shell complex. These results can be understood in terms of a set of effective Langevin equations for the  $N$  interacting shell particles, pre-averaged over the yolks' degrees of freedom, from which an approximate self-consistent description of the simulated self-diffusion properties can be derived. Here we compare the theoretical and simulated results between them, and with the results for the same system in the absence of yolks. We find that the yolks, which have no effect on the shell-shell static structure, influence the dynamic properties in a predictable manner, fully captured by the theory.

Copyright © EPLA, 2014

In recent years, there has been a growing interest in designing and manufacturing new materials with nano- and micro-particles having specifically tailored morphologies [1–3], such as yolk-shell particles, in which a hollow shell carries a smaller particle in its interior [1,4]. These nanostructures can be synthesized by a variety of methods [5] for application in various fields such as nanoreactors [4], lithium-ion batteries [6], biomedical imaging [6], catalysis [7], and energy storage devices [6]. One can envision that current efforts to study individual yolk-shell entities with light or neutron scattering techniques [8] will soon be extended to consider liquids, and even crystals or glasses, of strongly interacting yolk-shell particles. Similarly, conventional preparation methods [9] could be employed to produce microemulsion droplets bearing a smaller solid particle inside, to study equilibrium and out-of-equilibrium condensed phases [10] made of such microemulsion yolk-shell droplets. To understand these phases and other self-assembled states [11], however, one needs to understand the dynamic properties of systems of strongly interacting yolk-shell particles in terms of the direct (*i.e.*, conservative) and hydrodynamic interactions among shells and between yolks and their confining shells.

The detailed and simultaneous description of such coupled effects is, of course, a highly involved problem. To make headway, however, we may profit from the ingenious manners to decouple them, developed in similar challenges in colloid science [12,13]. For example, at least for rigid shells, the complex effects of shell-shell hydrodynamic interactions can be taken into account through an effective self-diffusion coefficient  $D_s^0$  describing the shells' short-time Brownian motion [14,15]. For such purposes, the rich phenomenology of the hydrodynamic interactions of the captive yolk with its confining shell [16] could also be modelled as a simple effective free-diffusion process, characterized by another effective (short-time) self-diffusion coefficient  $D_y^0$ , also amenable to independent experimental determination [16].

Thus, the remaining task is to describe the effects of the direct interactions, for which we may develop or adapt to yolk-shell morphologies the well-established theories and methods proven effective in describing the effects of direct interactions on the structure and dynamics of conventional colloidal dispersions (with hydrodynamic interactions now entering only through the externally provided coefficients  $D_s^0$  and  $D_y^0$ ). We have launched a systematic program in

this direction, which starts with a series of Brownian dynamics (BD) simulations on simplified models built upon the assumptions above, and with the development of a self-consistent generalized Langevin equation (SCGLE) theory of yolk-shell colloid dynamics. The details of the simulations and of the derivation of this theory will be reported separately [17], but the present short communication illustrates the results with the simplest application of these methodologies.

Our simulations are based on the well-known Brownian dynamics algorithm of Ermak and McCammon [18] without hydrodynamic interactions (assumed to be contained only in  $D_s^0$  and  $D_y^0$ ). This algorithm consists essentially of the numerical solution of the *overdamped* version of the  $2N$  stochastic Langevin equations that govern the Brownian motion of the  $N$  shells and  $N$  yolks, written in terms of the position  $\mathbf{x}_i(t)$  and velocity  $\mathbf{v}_i(t)$  of the center of mass of the  $i$ -th shell particle, and of the position  $\mathbf{y}_i(t)$  and velocity  $\mathbf{w}_i(t)$  of the center of the  $i$ -th yolk particle, as

$$\begin{aligned} M_s \frac{d\mathbf{v}_i(t)}{dt} &= -\zeta_s^0 \mathbf{v}_i(t) + \mathbf{f}_i^0(t) \\ &\quad - \sum_{j \neq i} \nabla_i u_{ss}(|\mathbf{x}_i(t) - \mathbf{x}_j(t)|) \\ &\quad - \sum_j \nabla_i u_{sy}(|\mathbf{x}_i(t) - \mathbf{y}_j(t)|) \end{aligned} \quad (1)$$

and

$$\begin{aligned} M_y \frac{d\mathbf{w}_i(t)}{dt} &= -\zeta_y^0 \mathbf{w}_i(t) + \mathbf{g}_i^0(t) \\ &\quad - \sum_{j \neq i} \nabla_i u_{yy}(|\mathbf{y}_i(t) - \mathbf{y}_j(t)|) \\ &\quad - \sum_j \nabla_i u_{ys}(|\mathbf{y}_i(t) - \mathbf{x}_j(t)|), \end{aligned} \quad (2)$$

with  $i = 1, 2, \dots, N$ . In these equations  $\mathbf{f}_i^0(t)$  and  $\mathbf{g}_i^0(t)$  are Gaussian white random forces of zero mean, and variance is given by  $\langle \mathbf{f}_i^0(t) \mathbf{g}_j^0(0) \rangle = 0$ ,  $\langle \mathbf{f}_i^0(t) \mathbf{f}_j^0(0) \rangle = k_B T \zeta_s^0 2\delta(t) \delta_{ij} \overset{\leftrightarrow}{\mathbf{I}}$ , and  $\langle \mathbf{g}_i^0(t) \mathbf{g}_j^0(0) \rangle = k_B T \zeta_y^0 2\delta(t) \delta_{ij} \overset{\leftrightarrow}{\mathbf{I}}$ , with  $i, j = 1, 2, \dots, N$  and with  $\overset{\leftrightarrow}{\mathbf{I}}$  being the  $3 \times 3$  unit tensor. These equations are coupled together by the mutual direct forces between all the particles, assumed pairwise additive and determined by the radially symmetric pair potentials  $u_{ss}(r)$ ,  $u_{sy}(r) = u_{ys}(r)$ , and  $u_{yy}(r)$  describing, respectively, the shell-shell, shell-yolk, and yolk-yolk direct interactions. We have used this algorithm in the efficient, low-memory version proposed in ref. [19] to describe, for example, how the mean squared displacement (MSD)  $W(t) = \langle [\Delta \mathbf{R}(t)]^2 \rangle / 6$  and the self-intermediate scattering function (self-ISF)  $F_S(k, t) \equiv \langle \exp[i\mathbf{k} \cdot \Delta \mathbf{R}(t)] \rangle$  of tagged yolk-shell particles are influenced by the combined effect of these interactions.

To illustrate the results of this approach, below we shall consider as a first step a model monodisperse colloidal suspensions formed by  $N$  *rigid* spherical shell particles

of outer (inner) diameter  $\sigma_s$  ( $\sigma_{in}$ ) in a volume  $V$ , each of which bears one smaller (“yolk”) rigid particle of diameter  $\sigma_y$  ( $< \sigma_{in}$ ) diffusing in its interior. For simplicity, we assume purely repulsive hard-body interactions, such that the yolks only interact with their own shells,  $u_{yy}(r) = 0$ , and that  $u_{ss}(r)$  is infinite for  $r < \sigma_s$  and vanishes for  $r > \sigma_s$ , whereas  $u_{ys}(r)$  is infinite for  $r < \sigma_{ys}$  and vanishes for  $r > \sigma_{ys} \equiv (\sigma_{in} - \sigma_y)/2$ . In reality, the BD algorithm above is only defined for systems with continuous pair potentials. Thus, in practice we employ a softened version of these hard-body potentials, as explained in ref. [17].

Regarding our theoretical approach, let us first discuss the limit of infinite dilution, in which one isolated yolk-shell particle diffuses without interacting with other yolk-shell particles. A simple calculation to explain the effect of the yolk on the diffusivity of the shell may then be based on the so-called relaxation-effect method, first recognized by Debye and Hückel [20] and later employed by Onsager [21] in their treatment of ionic conductivity. In our case, the arguments start with Einstein’s relation,  $D_L = k_B T / \zeta_s$ , with the friction coefficient  $\zeta_s$  defined by the linear relation  $F = \zeta_s V$  for the drag force when the shell is pulled at constant velocity  $V$ . For an empty shell the friction is only caused by the solvent,  $F = \zeta_s^0 V$ , with  $\zeta_s^0$  determined by the well-known Stokes expression. The fact that it carries a yolk in its interior, however, generates an additional drag force on the shell,  $F = \zeta_s^0 V + \Delta \zeta_y V$ , so that determining the frictional effects embodied in  $\Delta \zeta_y$  becomes the crucial remaining problem. The determination of  $\Delta \zeta_y$  is analogous to Stokes calculation of  $\zeta_s^0$ . Stokes problem involved the solution of the Navier-Stokes equation to describe the hydrodynamic flow past a sphere moving at steady velocity  $V$  [22]. The present calculation of  $\Delta \zeta_y$  requires deriving and solving the equation of motion of the yolk inside the shell (or, more generally, of  $N_y$  yolks inside each shell), and then calculating the corresponding force on the shell.

For this we write the total drag force  $F = \zeta_s^0 V + \Delta \zeta_y V$  as  $\mathbf{F}(t) = \zeta_s^0 \mathbf{V}(t) - \nabla_{\mathbf{r}_s} \sum_{1 \leq i \leq N_y} u_{ys}(|\mathbf{r}_s(t) - \mathbf{r}_y^{(i)}(t)|)$ , where  $\mathbf{r}_s(t)$  and  $\mathbf{r}_y^{(i)}(t)$  are the instantaneous position of the centers of the shell and of the  $i$ -th yolk at time  $t$ , and  $u_{ys}(r)$  is the pair potential of the yolk-shell interaction. This expression can also be written as

$$\mathbf{F}(t) = \zeta_s^0 \mathbf{V}(t) + \int d^3 \mathbf{r} [\nabla u_{ys}(r)] n_y^*(\mathbf{r}, t), \quad (3)$$

where  $n_y^*(\mathbf{r}, t)$  is the local density of yolks at position  $\mathbf{r}$ , defined as  $n_y^*(\mathbf{r}, t) \equiv \sum_{1 \leq i \leq N_y} \delta(\mathbf{r} - (\mathbf{r}_y^{(i)}(t) - \mathbf{r}_s(t)))$ . The time evolution of  $n_y^*(\mathbf{r}, t)$  is determined by Fick’s law, which, if the multiple yolks do not interact among themselves (or, equivalently, if  $N_y = 1$ ), leads to

$$\begin{aligned} \frac{\partial n_y^*(\mathbf{r}, t)}{\partial t} &= [\nabla n_y^*(\mathbf{r}, t)] \cdot \mathbf{V}(t) \\ &\quad + D_y^0 \nabla \cdot n_y^*(\mathbf{r}, t) \nabla [\ln n_y^*(\mathbf{r}, t) + \beta u_{ys}(r)], \end{aligned} \quad (4)$$

where the first term on the r.h.s. is a streaming term due to the fact that the position vector  $\mathbf{r}$  has its origin in the center of the shell. Under equilibrium conditions  $\mathbf{V}(t) = \mathbf{V}^{eq} = 0$  and  $\nabla [\ln n_y^{eq}(\mathbf{r}) + \beta u_{ys}(r)] = 0$ , so that  $n_y^{eq}(\mathbf{r}) = n_y^{eq}(r) = N_y e^{-\beta u_{ys}(r)} / \int e^{-\beta u_{ys}(r)} d^3r$ , and  $\int d^3\mathbf{r} [\nabla u_{ys}(r)] n_y^{eq}(r) = 0$ .

In stationary-state conditions, not far from equilibrium,  $\mathbf{V}(t) = \mathbf{V}^{ss} \neq 0$  and  $n_y^*(\mathbf{r}, t) = n_y^{ss}(\mathbf{r})$ . We may thus write  $n_y^{ss}(\mathbf{r}) = n_y^{eq}(r) + \Delta n_y^{ss}(\mathbf{r})$  and linearize eq. (4) around  $n_y^{eq}(r)$ , to solve for  $\Delta n_y^{ss}(\mathbf{r})$ . Substituting this solution in eq. (3) allows us to write this equation as  $\mathbf{F}^{ss} = \zeta_s^0 \mathbf{V}^{ss} + \overset{\leftrightarrow}{\Delta} \zeta_y \cdot \mathbf{V}^{ss}$ , with the friction tensor  $\overset{\leftrightarrow}{\Delta} \zeta_y$  given by

$$\overset{\leftrightarrow}{\Delta} \zeta_y = \frac{1}{4\pi D_y^0} \int d^3\mathbf{r} \int d^3r' [\nabla u_{ys}(r)] \frac{1}{|\mathbf{r} - \mathbf{r}'|} [\nabla n_y^{eq}(r')]. \quad (5)$$

Using the fact that  $[\nabla u_{ys}(r)] = [\nabla n_y^{eq}(r)]/n_y^{eq}(r)$ , and approximating this equation as  $[\nabla u_{ys}(r)] \approx [\nabla n_y^{eq}(r)]/n_0$ , we can use Fourier transforms to write this expression as

$$\overset{\leftrightarrow}{\Delta} \zeta_y \approx \frac{\zeta_y^0}{(2\pi)^3 n_0} \int d^3\mathbf{k} \frac{[n_y^{eq}(k)]^2}{k^2} \mathbf{k}\mathbf{k}. \quad (6)$$

The friction tensor  $\overset{\leftrightarrow}{\Delta} \zeta_y$  is diagonal and isotropic, so that  $\overset{\leftrightarrow}{\Delta} \zeta_y = \overset{\leftrightarrow}{I} \Delta \zeta_y$ , with

$$\Delta \zeta_y \equiv \frac{\zeta_y^0}{3(2\pi)^3 n_0} \int d^3\mathbf{k} [n_y^{eq}(k)]^2. \quad (7)$$

This result for the scalar  $\Delta \zeta_y$  then allows us to determine the total friction coefficient as  $\zeta_s = \zeta_s^0 + \Delta \zeta_y$ , and the long-time self-diffusion coefficient as  $D_L = k_B T / [\zeta_s^0 + \Delta \zeta_y]$ . However, since the diffusive dynamics of the yolk does not relax instantaneously with respect to the motion of the shell, in the present case we may have to solve the dynamic version of this problem, thus determining a time-dependent friction function  $\Delta \zeta_y(t)$ , whose time integral is  $\Delta \zeta_y$ . The hydrodynamic analog is Boussinesq's calculation of a time-dependent hydrodynamic friction function  $\zeta_s^0(t)$  which incorporates the hydrodynamic memory effect deriving from the non-instantaneous response of the incompressible fluid [22].

The calculation of the time-dependent friction function  $\Delta \zeta_y(t)$  not only in the infinite dilution limit is the next task of our theoretical methods. For this, however, a more robust version of the relaxation method must be employed. One possibility is to resort to the well-known dynamical formalism referred to as mode coupling theory (MCT), whose multicomponent version writes the dynamic properties (such as  $W(t)$  and  $F_S(k, t)$ ) in terms of the short-time parameters  $D_s^0$  and  $D_y^0$  only, and of the static structural properties of the system (*i.e.*, the radial distribution functions or partial static structure factors). In our general program we proceed along these lines, but we employ an alternative (but essentially equivalent)

formalism, namely, the SCGLE theory of colloid dynamics [23–28]. This choice originates in the enormous flexibility of this formalism, which has allowed, for example, the development of a quantitative non-equilibrium molecular theory of aging in glass-forming liquids [29].

The application of the SCGLE formalism to the present problem is discussed in detail in ref. [17]. Thus, here we only write the final results of those derivations needed to describe the dynamics of the simulated system above, namely, the following set of four coupled approximate equations. Two of them express  $F_S(k, t)$  and  $F(k, t) \equiv (1/N) \langle \sum_{i,j=1}^N e^{i\mathbf{k} \cdot (\mathbf{r}_i(t) - \mathbf{r}_j(0))} \rangle$  (the shell intermediate scattering function) in terms of the time-dependent friction functions  $\Delta \zeta_y^*(t)$  and  $\Delta \zeta_s^*(t)$ , which represent the friction effects on a tracer shell particle due to its direct interactions with its own yolk and with the other shells, respectively. In Laplace space these two expressions read

$$F(k, z) = \frac{S(k)}{z + \frac{k^2 S^{-1}(k) D_s^0}{1 + \Delta \zeta_y^*(z) + \lambda(k) \Delta \zeta_s^*(z)}} \quad (8)$$

$$F_S(k, z) = \frac{1}{z + \frac{k^2 D_s^0}{1 + \Delta \zeta_y^*(z) + \lambda(k) \Delta \zeta_s^*(z)}}. \quad (9)$$

The other two equations are the self-consistent closure relations for  $\Delta \zeta_y^*(t)$  and  $\Delta \zeta_s^*(t)$ , namely,

$$\Delta \zeta_y^*(t) = \frac{D_y^0 n_0}{3(2\pi)^3} \int d^3\mathbf{k} [k g_{ys}(k)]^2 e^{-k^2 D_y^0 t} F_S(k, t) \quad (10)$$

and

$$\Delta \zeta_s^*(t) = \frac{D_s^0}{3(2\pi)^3 n} \int d\mathbf{k} \left[ \frac{k[S(k) - 1]}{S(k)} \right]^2 F(k, t) F_S(k, t). \quad (11)$$

In these equations  $S(k)$  is the (shell-shell) static structure factor,  $g_{ys}(k)$  is the Fourier transform of  $g_{ys}(r) \equiv \exp[-\beta u_{ys}(r)]$ ,  $n_0 \equiv 1 / \int \exp[-\beta u_{ys}(r)] d^3r$ , and  $n \equiv N/V$ . The function  $\lambda(k)$  is given by [28]

$$\lambda_\alpha(k) = 1 / [1 + (k/k_c)]^2 \quad (12)$$

with  $k_c = 1.305(2\pi/\sigma)$  being an empirically chosen cutoff wave vector [30].

We have solved eqs. (8)–(11) for our yolk-shell model above, for given static structural properties  $g_{ys}(k)$  and  $S(k)$ , with  $S(k)$  provided by the Percus-Yevick [31] approximation with its Verlet-Weis correction [32]. From this solution, all the collective and self-dynamic properties are determined, including the MSD  $W(t)$  (see details in ref. [17]). In what follows we illustrate the solution with the theoretical results for  $W(t)$  and  $F_S(k, t)$ , which are compared with the BD simulation data. Let us mention that all the results discussed in this paper correspond to a fixed yolk-shell geometry, in which the thickness ( $\sigma_s - \sigma_{in}$ ) of the shell is 5% of the shell's outer diameter,  $\sigma_{in}/\sigma_s = 0.9$ , and in which the yolk's diameter is 0.2

in units of  $\sigma_s$ , *i.e.*,  $\sigma_y/\sigma_s = 0.2$ . The results reported below will be expressed using  $\sigma_s$  and  $\sigma_s^2/D_s^0$  as the units of length and time, respectively.

We begin by analyzing the results in fig. 1 of our BD simulations for the MSD  $W(t; \phi, \delta)$  of tagged yolk-shell particles, varying the shell volume fraction  $\phi \equiv \pi n \sigma_s^3/6$  and the dynamic asymmetry parameter  $\delta \equiv D_y^0/D_s^0$ . These results will be compared with the MSD  $W^{(HS)}(t; \phi)$  of the corresponding system of *empty* shells, equivalent in our model to the MSD of a Brownian hard-sphere liquid at volume fraction  $\phi$  [33,34]. Figures 1(a) and (b) contain, respectively, the results for  $W(t; \phi, \delta)$  at  $\phi = 0$  (freely diffusing yolk-shells) and  $\phi = 0.4$  (strongly interacting yolk-shells). Figure 1(a) is intended to illustrate two effects in a simple manner. The first is the effect of yolk-shell interactions, which is illustrated by the comparison of the circles, representing the MSD  $W(t; \phi = 0, \delta = 1)$  of freely diffusing yolk-shell particles, and the dotted line, representing the MSD  $W_0(t) \equiv D_s^0 t$  of freely diffusing *empty* shells. The deviation of the simulation data from  $W_0(t)$  is a measure of the additional friction effects upon the displacement of the yolk-shell complex due to the yolk-shell interaction. The solid line that lies near the circles represents the prediction of our SCGLE theory. The first conclusion that we can draw from this comparison is that the SCGLE-predicted deviation of  $W(t; \phi = 0, \delta = 1)$  from  $W_0(t)$ , coincides very satisfactorily with the deviation observed in the BD data.

The second effect illustrated by fig. 1(a) involves the dynamic asymmetry parameter. The next conclusion to draw from the results in this figure is that the deviation of  $W(t; \phi = 0, \delta)$  from  $W_0(t)$  increases when the dynamic contrast parameter  $\delta$  decreases. This is illustrated by the comparison of the BD simulations corresponding to  $\delta = 0.2$  (triangles) with the BD data corresponding to  $\delta = 1.0$  (circles). This means, for example, that if the interior of the shell becomes more viscous, so that the ratio  $\delta$  decreases, then also the overall diffusivity of the yolk-shell particle will decrease. As evidenced by the solid and dashed lines in fig. 1(a), this trend is also predicted by the SCGLE theory and shows good qualitative agreement with the simulation data. In fact, our theory predicts, and the simulations corroborate, that this trend is reversed when one considers the opposite limit, in which  $\delta$  is now larger than 1. This trend is best illustrated in the inset of fig. 1(a), which exhibits the measured (circles) and predicted (solid line) dependence on  $\delta$  of the scaled long-time self-diffusion coefficient  $D^*(\phi, \delta) \equiv D_L/D_s^0$ , obtained as  $D^*(\phi, \delta) = \lim_{t \rightarrow \infty} W(t; \phi, \delta)/D_s^0 t$ . There we can see that the reduction of the mobility  $D^*(\phi = 0, \delta)$  from its unit value  $D_{HS}^*(\phi = 0) = 1$ , in the absence of yolks, may be considerable. For example, for  $\delta = 0.2$  we have that  $D^*(\phi = 0, \delta) \approx 0.17$ . As a reference, a reduction in  $D_{HS}^*(\phi)$  of a similar magnitude can also be produced as a result of pure shell-shell interactions, but only at shell volume fractions above 40%, as gathered from the results

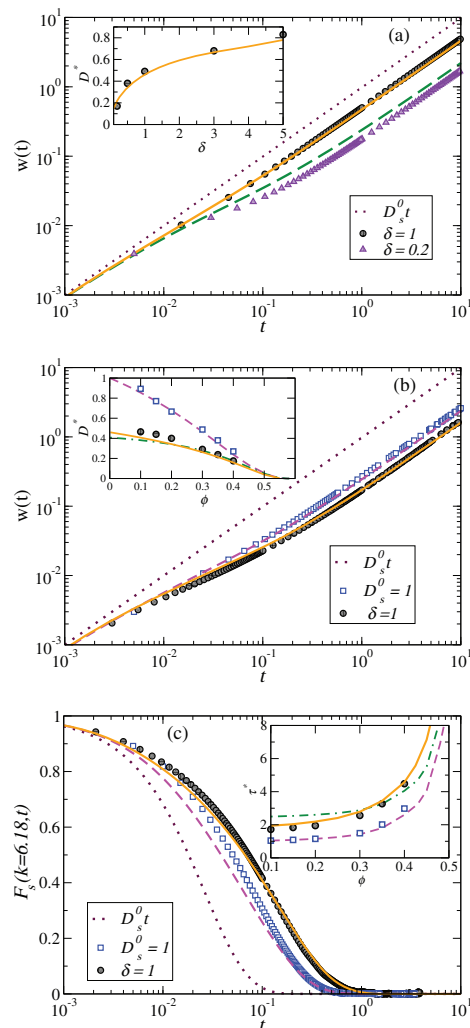


Fig. 1: (Colour on-line) (a) Mean square displacement  $W(t; \phi = 0)$  of non-interacting yolk-shell particles, (b) the MSD  $W(t; \phi = 0.4)$ , and (c) the self-intermediate scattering function  $F_s(k = 6.18, t; \phi = 0.4)$  at volume fraction  $\phi = 0.4$ . For all figures, shell thickness  $(\sigma_s - \sigma_{in})/2 = 0.05$  (or  $\sigma_{in} = 0.9$ ) and yolk diameter  $\sigma_y = 0.2$ . Recall that we take  $\sigma_s$  as the units of length and  $\sigma_s^2/D_s^0$  as the time unit. For each figure, circles plot the Brownian dynamics data for the yolk-shell particles, whereas the solid line is the corresponding theoretical prediction of the SCGLE theory with a dynamic asymmetry parameter of  $\delta \equiv D_y^0/D_s^0 = 1$ . In panels (a) and (b) the dotted line represents the MSD  $W_0(t; \phi = 0) = D_s^0 t$  of a freely diffusing empty shell, and in (c) it represents the self-ISF  $F_s^0(k, t; \phi = 0) = \exp(-k^2 D_s^0 t)$  for the same. In (a), the triangles plot the Brownian dynamics data and the dashed line plots the theoretical prediction, both corresponding to  $\delta = 0.2$ . In the case of (b) and (c), the squares are the simulation data for the empty-shell particles, and the dashed line is the corresponding theoretical prediction of the SCGLE theory with short-time diffusion coefficient  $D_s^0 = 1$ . The inset in (a) shows the long-time self-diffusion coefficient  $D^*$  as function of  $\phi$ . The insets in panels (b) and (c) are the long-time self-diffusion  $D^*$  and  $\tau^*(\equiv k^2 D_s^0 \tau_\alpha)$ , respectively, both as a function of  $\phi$ . Symbols and lines for these insets are the same as described in their own main panels. The dot-dashed line in inset (b) is the prediction for  $D^*$  using eq. (13), and (c) shows the same prediction for the value of  $\tau^*$ .

of the inset in fig. 1(b), which discusses the effects of shell-shell interactions.

Let us now study the effects of shell-shell interactions, suppressed in the previous discussion, by analyzing the results of our simulations in fig. 1(b), in which we now fix the dynamic asymmetry parameter at the value  $\delta = 1$ . The circles in this figure represent the BD results for the MSD  $W(t; \phi = 0.4, \delta)$  of yolk-shell particles at a volume fraction  $\phi = 0.4$ . These results are to be compared with the squares, which correspond to the BD results for the MSD  $W^{(HS)}(t; \phi = 0.4)$  of a liquid of empty shells (or solid hard spheres) at the same volume fraction and same short-time self-diffusion coefficient  $D_s^0$ . The MSD  $W_0(t) = D_s^0 t$  of freely diffusing empty shells is also plotted for reference as a dotted line. We observe that the deviation of  $W(t; \phi = 0.4, \delta)$  from  $W^{(HS)}(t; \phi = 0.4)$  remains rather similar to the corresponding deviation observed at  $\phi = 0$  in fig. 1(a) (where  $W^{(HS)}(t; \phi = 0) = D_s^0 t$ ), but now both  $W(t; \phi = 0.4, \delta)$  and  $W^{(HS)}(t; \phi = 0.4)$  deviate dramatically from this free-diffusion limit. This means that for this concentration, the mutual friction effects due to shell-shell interactions overwhelm the “internal” friction effects caused by yolk-shell interactions.

From the long-time BD data for  $W(t; \phi = 0.4, \delta)$  and  $W^{(HS)}(t; \phi = 0.4)$  in fig. 1(b), we can extract the value of  $D^*(\phi, \delta)$  and  $D_{HS}^*(\phi)$ , which represent the mobility of a tracer yolk-shell particle and of an empty shell, respectively. In the inset of fig. 1(b), we plot the values of  $D^*(\phi, \delta)$  and  $D_{HS}^*(\phi)$  (circles and squares, respectively) determined from the corresponding BD results at a few volume fractions. This inset thus summarizes the main trends illustrated by the results in figs. 1(a) and (b), by evidencing that at low volume fractions, the difference between the mobility of a yolk-shell complex and the mobility of an empty shell is determined only by the yolk-shell friction, whereas at higher concentrations it is dominated by the shell-shell interactions. The solid lines in fig. 1(b) represent again the predictions of the SCGLE theory for the properties of the yolk-shell system, whereas the dashed lines are the corresponding predictions for the empty-shell (or hard-sphere) suspension. Once again, the agreement with the simulation results is also quite reasonable for a theory with no adjustable parameters.

Beyond this quantitative observation, however, the theoretical description provides additional insights on the interpretation of the qualitative trends exhibited by the simulation data of the long-time self-diffusion coefficients  $D^*(\phi, \delta)$  and  $D_{HS}^*(\phi)$ . For example, it is not difficult to demonstrate that if the shell-shell mutual friction  $\int_0^\infty dt \Delta\zeta_s^*(t; \phi, \delta)$  does not depend strongly on the presence or absence of the yolk (which one expects to be the case at high concentrations), then an approximate relationship between  $D^*(\phi, \delta)$  and  $D_{HS}^*(\phi)$  can be derived, namely,

$$D^*(\phi, \delta) = \frac{D_0^*(\delta) \times D_{HS}^*(\phi)}{D_{HS}^*(\phi) + D_0^*(\delta)[1 - D_{HS}^*(\phi)]}. \quad (13)$$

where  $D_0^*(\delta) \equiv D^*(\phi = 0, \delta) = [1 + \Delta\zeta_y^*(\delta)]^{-1}$ , with  $\Delta\zeta_y^*(\delta) \equiv \int_0^\infty dt \Delta\zeta_y^*(t; \phi = 0, \delta)$ . This expression interpolates  $D^*(\phi, \delta)$  between its exact low- and high-concentration limits  $D_0^*(\delta)$  and  $D_{HS}^*(\phi)$ , and the dot-dashed line in the inset of fig. 1(b) is the result of using this approximate expression.

The BD simulations and the SCGLE theory provide other relevant collective and self-diffusion dynamic properties, such as the intermediate scattering functions, specially amenable to determination by dynamic light scattering techniques and adequate index-matching methods. To close this illustrative presentation, let us discuss the BD results in fig. 1(c) for the self-ISF  $F_S(k = 6.18, t; \phi = 0.4, \delta = 1)$  (circles), which we compare with the self-ISF  $F_S^{HS}(k = 6.18, t; \phi = 0.4)$  of a liquid of empty shells at the same volume fraction (squares). For reference, we also plot as a dotted line the self-ISF  $F_S^0(k, t) \equiv F_S^{HS}(k, t; \phi = 0) = \exp(-k^2 D_s^0 t)$  of freely diffusing empty shells. Here too, the solid and dashed lines correspond to the solution of eqs. (8)–(12) with and without the shell friction term  $\Delta\zeta_y^*(t)$ , and comparison again indicates very reasonable agreement with the simulation data.

In this case, the difference between the yolk-shell and empty-shell results can also be expressed more economically in terms of the corresponding  $\alpha$  relaxation times  $\tau_\alpha$ , defined by the condition  $F_S(k, \tau_\alpha) = 1/e$  and scaled as  $\tau^* \equiv k^2 D_s^0 \tau_\alpha$ . The inset of fig. 1(c) exhibits the theoretical (solid line) and simulated (circles) results for the yolk-shell  $\tau^*(k; \phi, \delta)$  evaluated at  $k = 6.18$  for  $\delta = 1$  as a function of  $\phi$ . These results may be compared with the theoretical (dashed line) and simulated (squares) results for  $\tau_{HS}^*(k = 6.18; \phi = 0.4)$ , corresponding to the empty-shell suspension, with similar conclusions as in fig. 1(b). In analogy with the relationship in eq. (13), from the SCGLE equations one can also derive an approximate relationship between  $\tau^*(k; \phi, \delta)$  and  $\tau_{HS}^*(k; \phi)$ , namely,  $\tau^*(k; \phi, \delta) \approx \tau_{HS}^*(k; \phi) + \Delta\zeta_y^*(\delta)$ . This prediction of the value of  $\tau^*(k; \phi, \delta)$  has a rather modest quantitative accuracy, as indicated by the dot-dashed line in the inset. Still, it contributes to a simple and correct qualitative understanding of the main features of the properties of the yolk-shell system being studied.

In summary, in this work we have carried out BD simulations and have proposed a statistical mechanical approach for describing the dynamic properties of a complex system, namely, a concentrated suspension of yolk-shell particles. Here we have discussed the simplest illustrative model representation, in which each shell carries only a single yolk, and in which the yolk-shell and shell-shell forces are modeled as purely repulsive, hard-body interactions. This implied an additional simplification, namely, the absence of yolk-yolk direct interactions. These simplifications allowed us to reach a reasonable understanding of the differences between a yolk-shell system and a suspension of empty shell, and of the main trends observed upon the variation of relevant parameters, such as the

short-time dynamic asymmetry parameter  $\delta$  or the shell volume fraction  $\phi$ . The message, however, is that the theoretical approach presented here can be extended to consider other, more complex conditions, such as including more than one yolks per shell and studying the effects of yolk-shell and shell-shell interactions beyond the purely repulsive, hard-core-like interactions considered here.

We close this communication with a reminder that the effects of hydrodynamic interactions must always be taken into account in any practical use of the methodology introduced here. As explained in the introduction, however, this information will be contained in the short-time self-diffusion coefficients  $D_s^0$  and  $D_y^0(\phi)$ , which are considered here external inputs. A simple illustration of the accuracy of this procedure is provided by the excellent comparison between the experimental data for the ratio  $D_L/D_y^0$  of a hard-sphere suspension, which involves strong hydrodynamic interactions particularly at high concentrations, and its simulated counterpart, which does not involve hydrodynamic interactions (see, for example, fig. 3 of ref. [35]).

\* \* \*

This work was supported by the U.S. Department of Energy, Office of Basic Energy Sciences, Materials Sciences and Engineering Division. This research at the SNS at Oak Ridge National Laboratory was sponsored by the Scientific User Facilities Division, Office of Basic Energy Sciences, U.S. Department of Energy. This work was also supported by the Consejo Nacional de Ciencia y Tecnología (CONACYT, Mexico), through Grants No. 132540 and No. 182132.

## REFERENCES

- [1] LOU X. W., ARCHER L. A. and YANG Z., *Adv. Mater.*, **20** (2008) 3987.
- [2] JOO S. H., PARK J. Y., TSUNG C. K., YAMADA Y., YANG P. D. and SOMORJAI G. A., *Nat. Mater.*, **8** (2009) 126.
- [3] YIN D., RIOUX R. M., ERDONMEZ C. K., HUGHES S., SOMORJAI G. A. and ALIVISATOS A. P., *Science*, **304** (2004) 711.
- [4] KAMATA K., LU Y. and XIA Y. N., *J. Am. Chem. Soc.*, **125** (2003) 2384.
- [5] ZHAO Y. and JIANG L., *Adv. Mater.*, **21** (2009) 3621.
- [6] LIU J., XIA H., XUE D. F. and LU L., *J. Am. Chem. Soc.*, **131** (2009) 12086.
- [7] LI H. X., BIAN Z. F., ZHU J., HUO Y. N., LI H. X. and LU Y. F., *J. Am. Chem. Soc.*, **129** (2007) 8406.
- [8] LI X., LIU K.-H., WU B., SANCHEZ-DIAZ L. E., SMITH G. S. and CHEN W.-R., *J. Appl. Crystallogr.*, **46** (2013) 1551.
- [9] TEECE L. J. *et al.*, *Soft Matter*, **7** (2011) 1341.
- [10] BARTLETT P. *et al.*, *Phys. Rev. E*, **85** (2012) 021404.
- [11] OKADA A., NAGAO D., UENO T., ISHII H. and KONNO M., *Langmuir*, **29** (2013) 9004.
- [12] PUSEY P. N., in *Liquids, Freezing and Glass Transition*, edited by HANSEN J. P., LEVESQUE D. and ZINN-JUSTIN J. (Elsevier, Amsterdam) 1991, Chapt. 10.
- [13] BRADER J., *J. Phys.: Condens. Matter*, **22** (2010) 363101.
- [14] MEDINA-NOYOLA M., *Phys. Rev. Lett.*, **60** (1988) 2705.
- [15] BRADY J. F., *J. Fluid Mech.*, **272** (2006) 109.
- [16] CERVANTES-MARTÍNEZ A. E., RAMÍREZ-SAITO A., ARMENTA-CALDERÓN R., OJEDA-LÓPEZ M. A. and ARAUZ-LARA J. L., *Phys. Rev. E*, **83** (2011) 030402(R).
- [17] SÁNCHEZ-DÍAZ L. E., CORTÉS-MORALES E. C., LI X., CHEN W.-R. and MEDINA-NOYOLA M., in preparation (2014).
- [18] ERMAK D. L. and MCCAMMON J. A., *J. Chem. Phys.*, **69** (1978) 1352.
- [19] DUBBELDAM D., FORD D. C., ELLIS D. E. and SNURR R. Q., *Mol. Simul.*, **35** (2009) 1084.
- [20] DEBYE P. and HÜCKEL E., *Phys. Z.*, **24** (1923) 305.
- [21] ONSAGER L., *Phys. Z.*, **28** (1927) 277.
- [22] LANDAU L. D. and LIFSHITZ E. M., *Fluid Mechanics* (Pergamon Press, Oxford) 1959.
- [23] YEOMANS-REYNA L. and MEDINA-NOYOLA M., *Phys. Rev. E*, **62** (2000) 3382.
- [24] YEOMANS-REYNA L. and MEDINA-NOYOLA M., *Phys. Rev. E*, **64** (2001) 066114.
- [25] YEOMANS-REYNA L., ACUÑA-CAMPA H., GUEVARA-RODRÍGUEZ F. and MEDINA-NOYOLA M., *Phys. Rev. E*, **67** (2003) 021108.
- [26] RAMÍREZ-GONZÁLEZ P. E. *et al.*, *Rev. Mex. Fís.*, **53** (2007) 327.
- [27] YEOMANS-REYNA L., CHAVEZ-ROJO M., RAMÍREZ-GONZÁLEZ P. E., JUÁREZ-MALDONADO R., CHAVEZ-PAEZ M. and MEDINA-NOYOLA M., *Phys. Rev. E*, **76** (2007) 041504.
- [28] JUÁREZ-MALDONADO R., CHAVEZ-ROJO M., RAMÍREZ-GONZÁLEZ P. E., YEOMANS-REYNA L. and MEDINA-NOYOLA M., *Phys. Rev. E*, **76** (2007) 062502.
- [29] SÁNCHEZ-DÍAZ L. E., RAMÍREZ-GONZÁLEZ P. E. and MEDINA-NOYOLA M., *Phys. Rev. E*, **87** (2013) 052306.
- [30] LÓPEZ-FLORES L., YEOMANS-REYNA L. L. and MEDINA-NOYOLA M., *J. Phys.: Condens. Matter*, **24** (2012) 375107.
- [31] PERCUS J. K. and YEVICK G. J., *Phys. Rev.*, **110** (1957) 1.
- [32] VERLET L. and WEIS J.-J., *Phys. Rev. A*, **5** (1972) 939.
- [33] DE J. GUEVARA-RODRÍGUEZ F. and MEDINA-NOYOLA M., *Phys. Rev. E*, **68** (2003) 011405.
- [34] LOPEZ-FLORES L., RUIZ-ESTRADA H., CHÁVEZ-PÁEZ M. and MEDINA-NOYOLA M., *Phys. Rev. E*, **88** (2013) 042301.
- [35] PÉREZ-ÁNGEL G. *et al.*, *Phys. Rev. E*, **83** (2011) 060501(R).

